Finanziato dall'Unione europea
NextGenerationEU

Ministero dell'Università e della Ricerca

Italiadomani
PIANO NAZIONALE DI RIPRESA E RESILIENZA

INAF
ISTITUTO NAZIONALE DI ASTROFISICA

Looking for a multi-wavelength counterpart for FRBs

Maura Pilia

Overview

- Why?
- How?
- What have we learned so far?
- What next?

Why look for multi-wavelength emission?

For a review see e.g. Nicastro et al. 2021


Merging Black Holes
Supernovae
Magnetars
Evaporating Black Holes
Super-giant Pulses
The Unknown
extra-Galactic
Implied rate of 1000s per day, per sky... but what are they?
Gamma-ray Bursts
Micro-quasars
Flare stars
Galactic
SETI
Pernicious RFI
Atmospheric effects
"Blitzars"
Magnetars
We are here
Pulsars
Credit: Jason Hessels

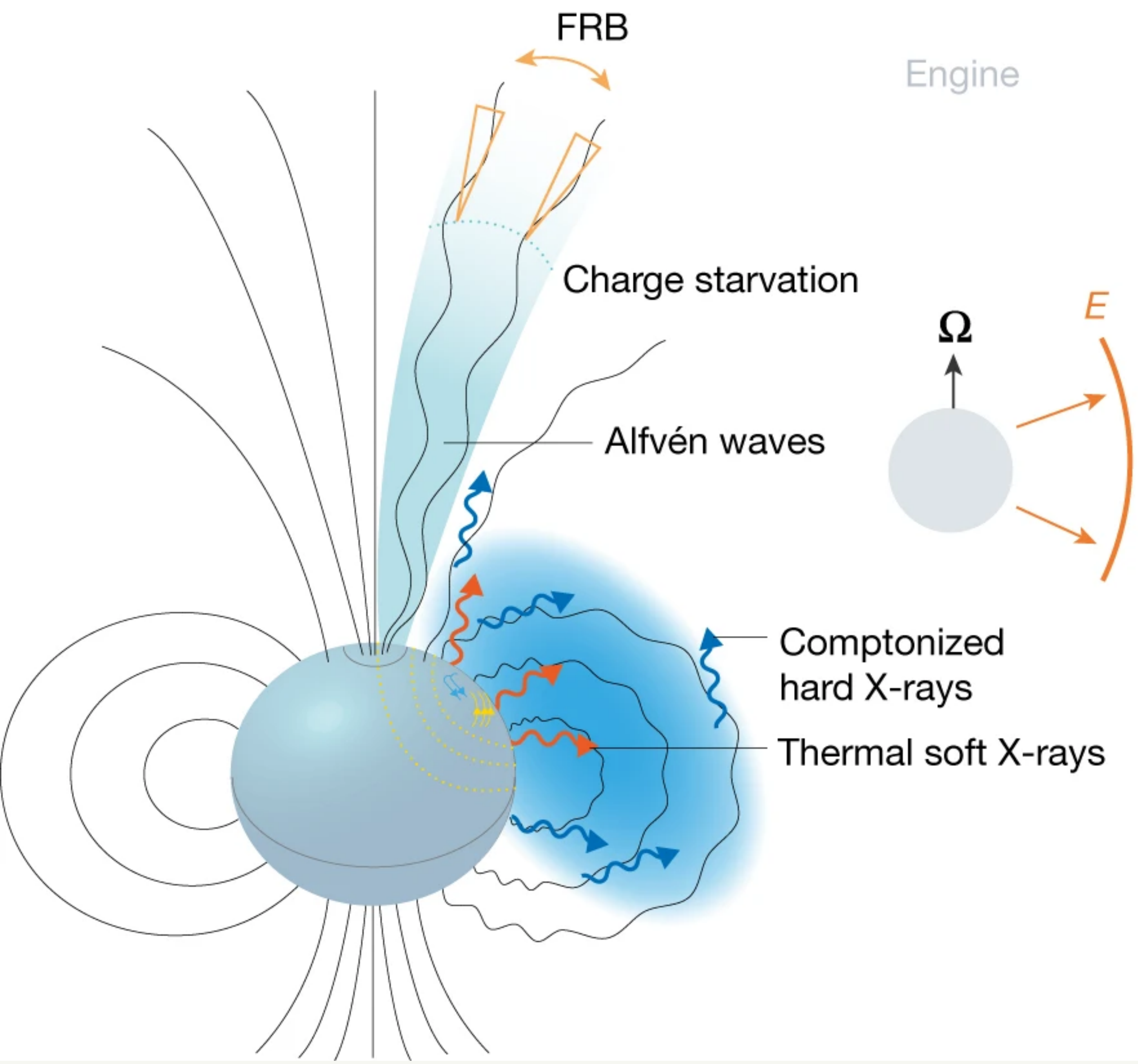

Lu et al. 2020

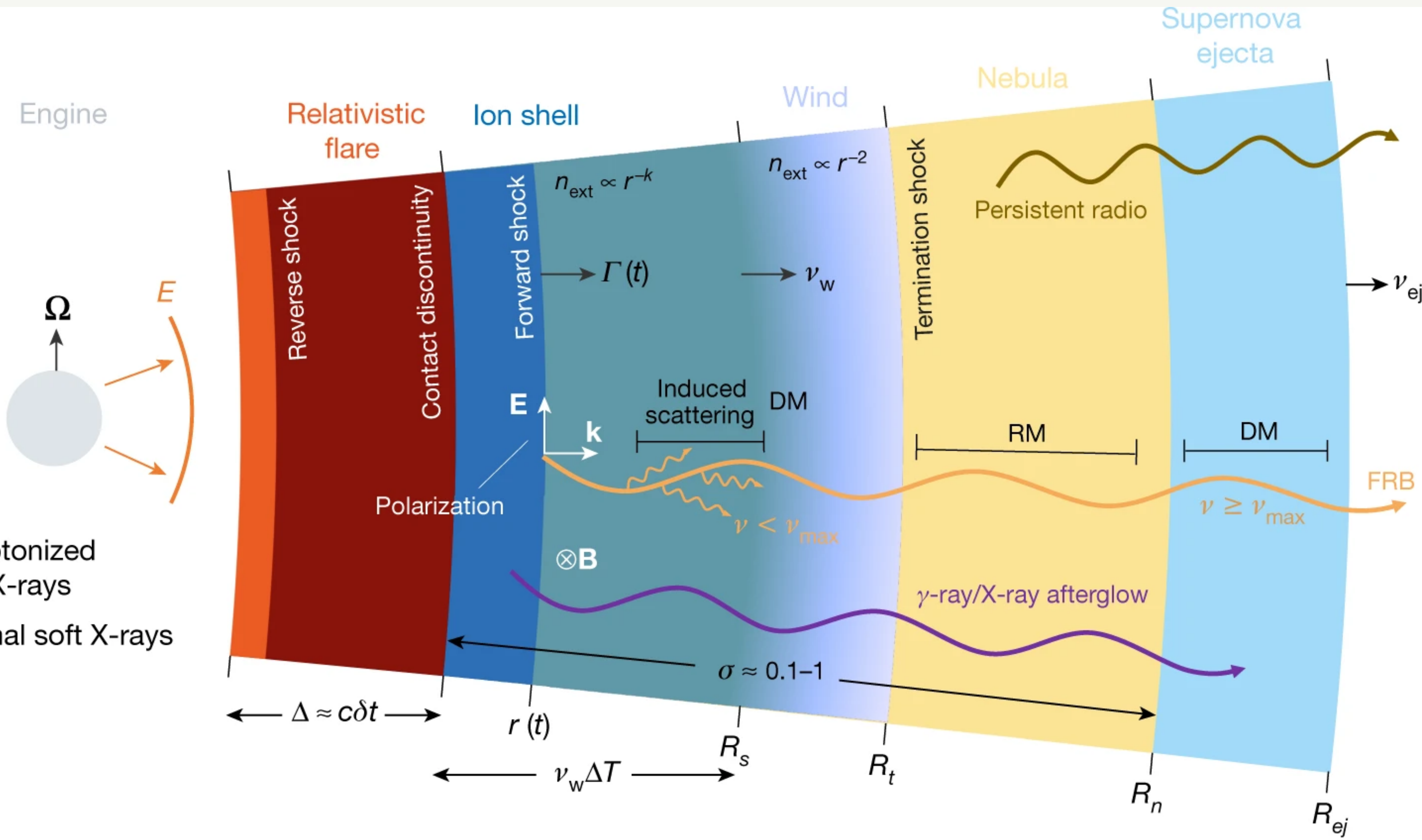

Metzger et al. 2020

Not all models

Predict high energy emission

- Coherent curvature radiation is possible if the geometry of the magnetic field and the emitting region is well ordered. Curvature photons are produced along the same direction of the particle velocities, much depressing the possibility to scatter. *Therefore the model predicts an absent or very weak inverse Compton emission at high energies.*

- **This makes the ~GHz-millimeter band the preferred band where FRBs can be observed. The weakness of the produced emission at high (X and γ-ray) energies is a strong prediction of the model.**

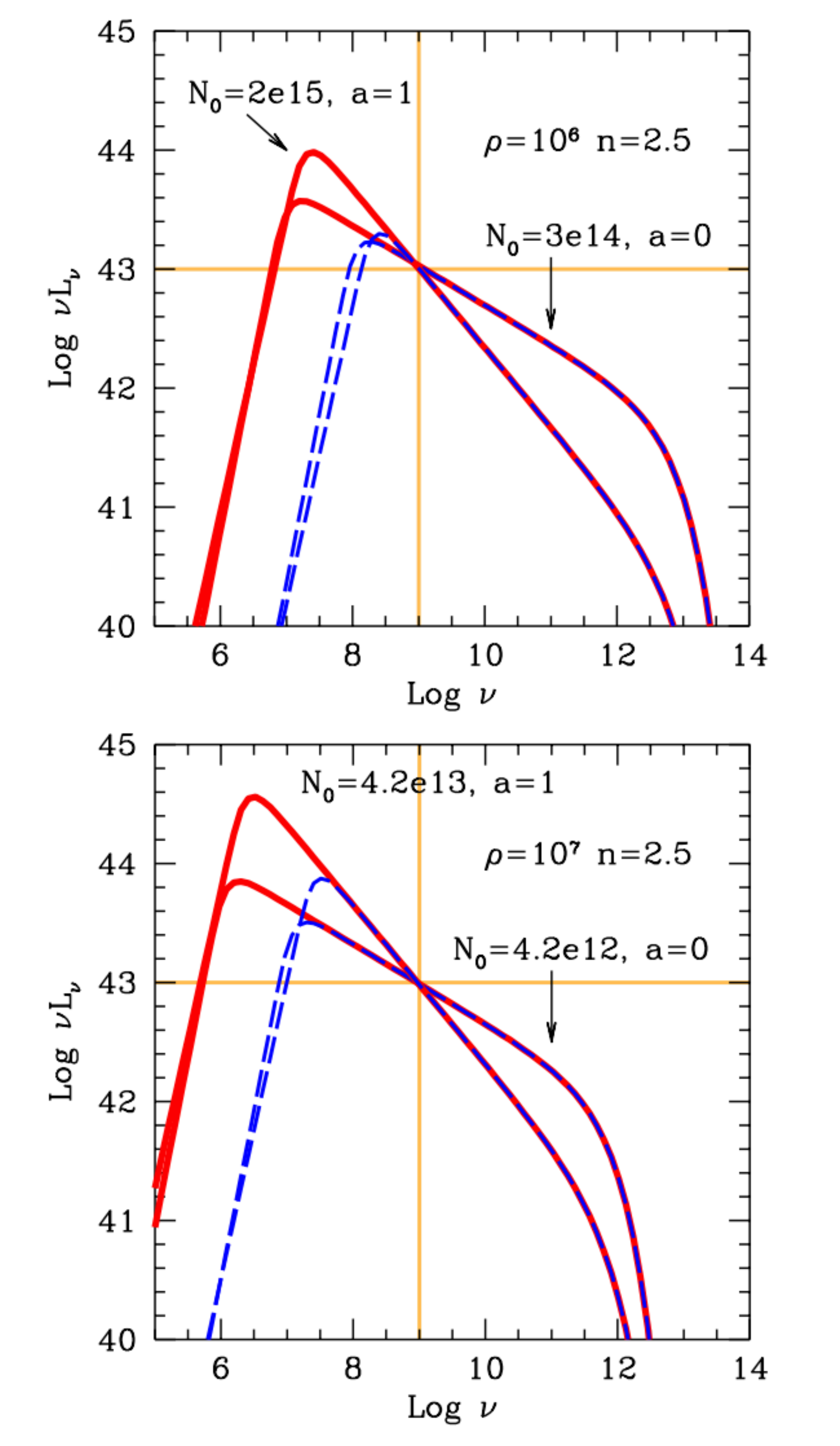

Ghisellini & Locatelli 2018

How have we gone at it?

First attempts

FRB 140514

We report here on an FRB discovered in real-time at 1.4 GHz at the Parkes radio telescope.

We coordinated the fastest and largest follow-up effort ever undertaken for an FRB, with data from 12 telescopes. No associated slow transient, progenitor, or host galaxy was identified, effectively ruling out any association between this FRB and an SN at $z < 0.3$ or long GRB.

A tighter constraint on FRB origins in the future will require not only robust and immediate triggering or commensal observing at multiple observatories, but also improved sky localization of radio pulses within FRB and pulsar surveys.

Petroff et al. 2015

Table 1. Observed properties of FRB 140514.

Event date UTC	14 May 2014
Event time UTC, $\nu_{1.4\,\mathrm{GHz}}$	17:14:11.06
Event time, ν_{∞}	17:14:09.83
Local date AEST	15 May 2014
Local time AEST	03:14:11.06
RA	22:34:06.2
Dec.	−12:18:46.5
(ℓ, b)	$(50^\circ\!.8, -54^\circ\!.6)$
Beam diameter	14.4 arcmin
$\mathrm{DM}_{\mathrm{FRB}}$ (pc cm^{-3})	562.7(6)
$\mathrm{DM}_{\mathrm{MW}}$ (pc cm^{-3})	34.9
Detection S/N	16(1)
Observed width, Δt (ms)	$2.8^{+3.5}_{-0.7}$
Scattering time-scale, $\tau_{1\,\mathrm{GHz}}$ (ms)	5.4(1)
Dispersion index, α	−2.000(4)
Peak flux density, $S_{\nu,\,1400\,\mathrm{MHz}}$ (Jy)	$0.47^{+0.11}_{-0.08}$
Fluence, $\mathcal{F}$ (Jy ms)	$1.3^{+2.3}_{-0.5}$

Table 2. Derived cosmological properties of FRB 140514.

z	$< 0.44(1)$
Comoving distance (Gpc)	$< 1.71(3)$
Luminosity distance (Gpc)	$< 2.46^{+0.04}_{-0.06}$
Energy (erg)	$< 3.7^{+4.7}_{-2.0} \times 10^{38}$
Distance modulus (mag)	< 42.2

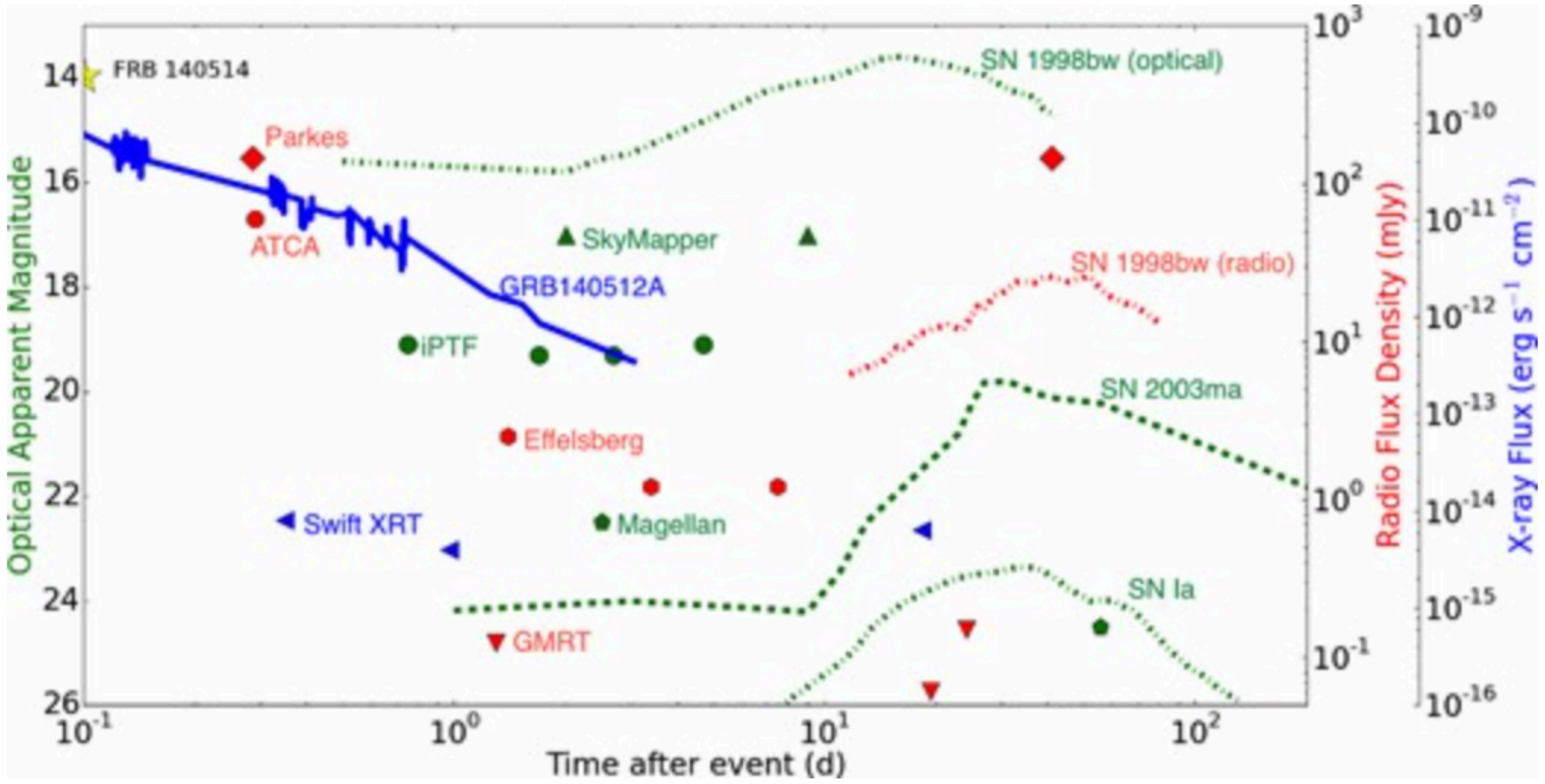

FRB 121102

aka R1

We have utilized the fast read-out capabilities of ULTRASPEC to search for optical burst counterparts to the repeating fast radio burst FRB 121102. Our observations, conducted simultaneously with the Effelsberg 100-m radio telescope, provide a 5σ upper limit to the optical burst fluence of 0.046 Jy ms. We are only able to place weak limits on the broad-band spectral index, in that it is steeper than $\alpha = -0.2$. Deeper searches for optical bursts would provide further constraints to this index, but this would only be possible with a larger telescope and an instrument that can run at a higher cadence. The upcoming HiPERCAM instrument, when mounted on the 10.4-m Gran Telescopio Canarias (Dhillon et al. 2016), will be capable of reaching a fluence detection limit of 0.0004 Jy ms, approximately 115 times deeper than the limit presented in this work, and 1500 times fainter than the median radio burst fluence.

Table 1. Observations conducted with ULTRASPEC on the TNT. The $i' + z'$ filter is a custom-made broad-band filter comprising the SDSS i' and z' passbands.

Date	Start time (UTC)	End time (UTC)	t_{exp} (ms)	Filter	No. of coincident radio bursts	Conditions
2017-01-16	15:50:00	19:45:12	70.7	$i' + z'$	3	Clear, 3 arcsec seeing
2017-01-19	15:35:14	18:46:45	70.7	$i' + z'$	5	Clear, 1 arcsec seeing
2017-01-25	13:29:54	14:31:15	70.7	$i' + z'$	0	Clear, 3 arcsec seeing
2017-01-25	15:15:20	19:00:22	70.7	$i' + z'$	3	Clear, 3 arcsec seeing
2017-02-16	12:43:21	17:32:27	70.7	i'	0	Intermittent clouds, 1 arcsec seeing
2017-02-19	14:34:38	17:32:24	70.7	i'	1	Intermittent clouds, 1.5 arcsec seeing

TOA (BMJD)	Flux density (Jy)	Pulse width (ms)	Fluence (Jy ms)
57769.6881141561(4)	0.7(1)	3.56(9)	2.6(4)
57769.702301263(2)	0.17(3)	3.4(4)	0.6(1)
57769.7639680761(3)	0.8(1)	2.05(6)	1.7(3)
57772.6649755688(7)	0.36(5)	2.1(1)	0.7(1)
57772.688014045(3)	0.11(2)	3.2(7)	0.35(9)
57772.758495566(1)	0.25(4)	5.1(3)	1.3(2)
57772.762396326(1)	0.22(3)	1.8(2)	0.40(7)
57772.784720292(1)	0.21(3)	1.9(3)	0.40(9)
57778.6885027615(7)	0.39(6)	2.6(1)	1.0(2)
57778.756270766(2)	0.11(2)	2.1(4)	0.23(6)
57778.756271161(2)	0.18(3)	2.9(3)	0.5(1)
57778.799193770(1)	0.21(3)	1.8(2)	0.38(7)
57803.692917989(2)	0.21(3)	3.5(3)	0.7(1)

Hardy et al. 2017

FRB 121102

R1

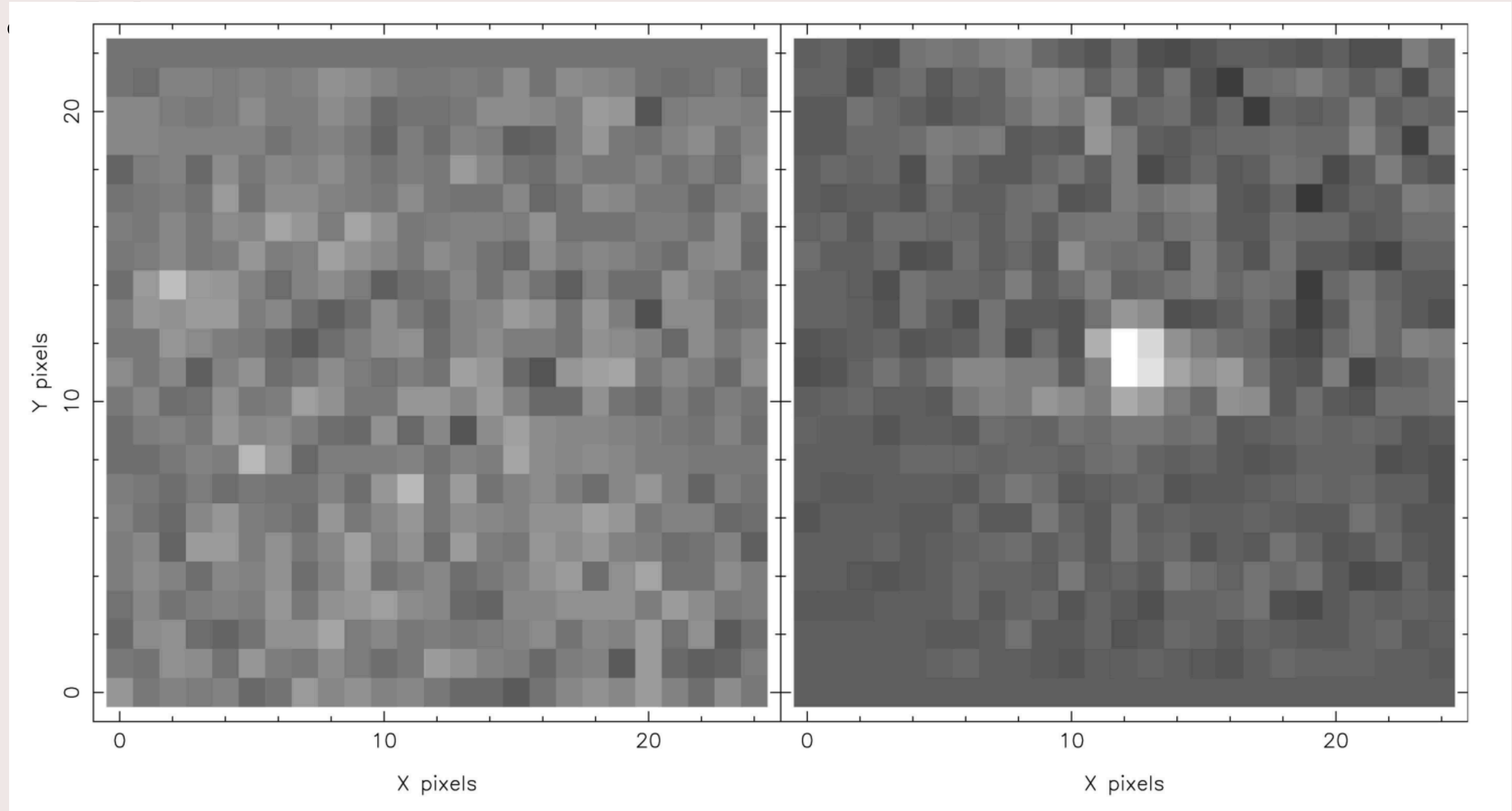

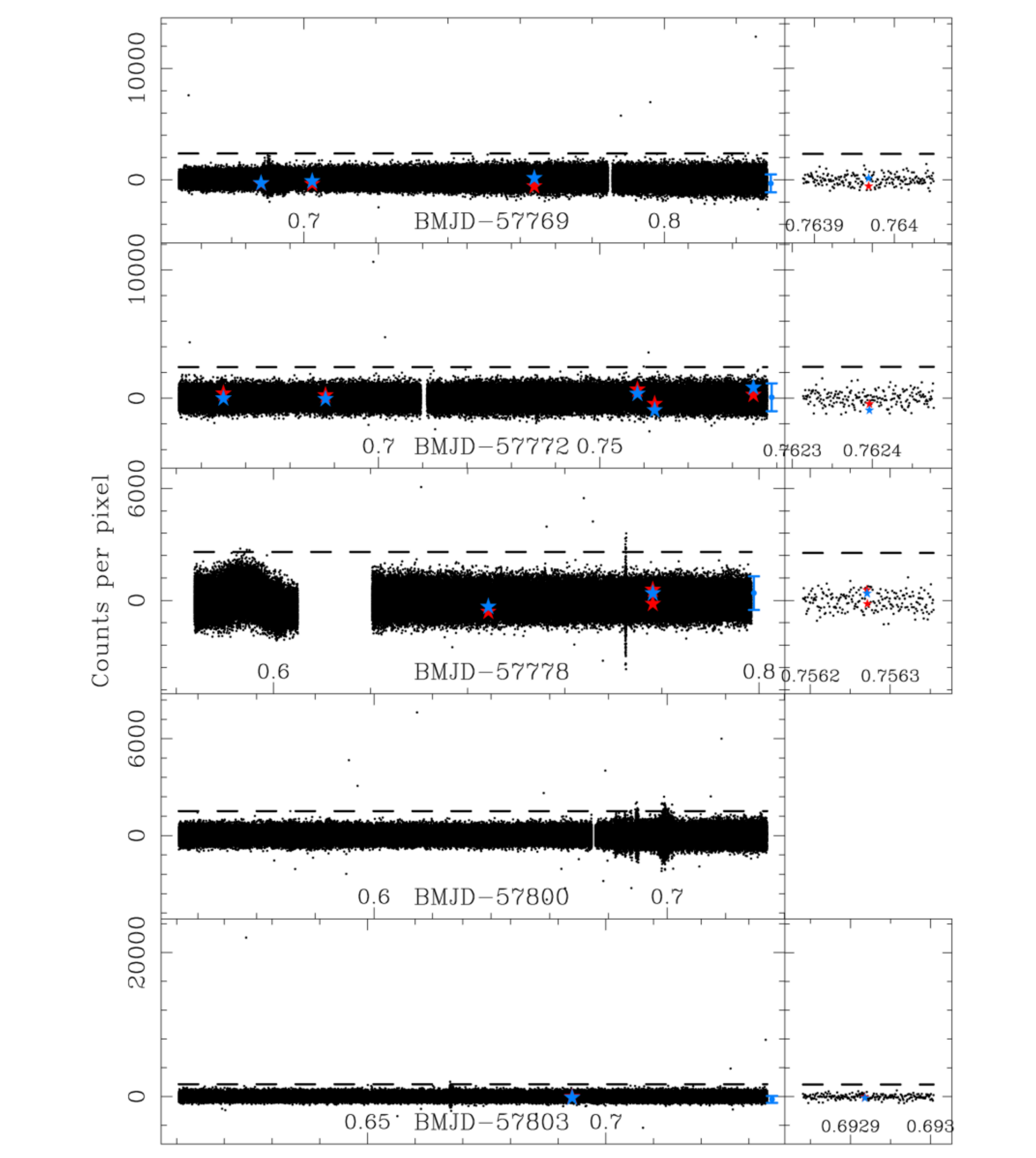

Hardy et al. 2017

FRB 121102

R1

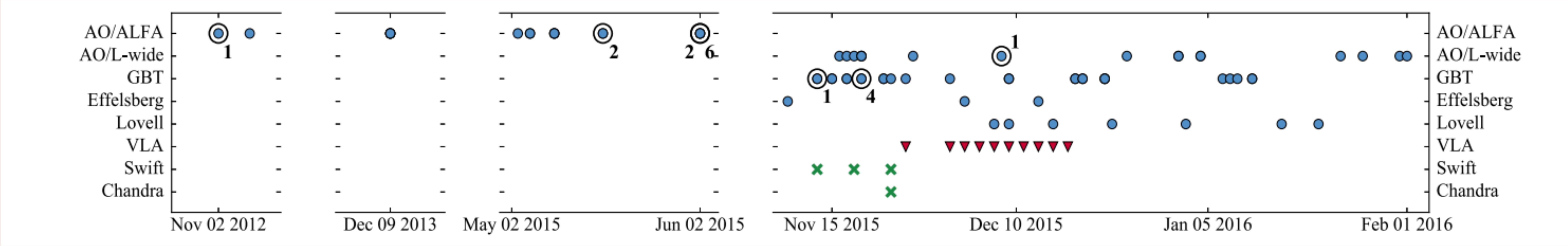

Table 3
Burst Properties

Peak Time (MJD)	Peak Flux Density (Jy)	Fluence (Jy ms)	DM (pc cm^{-3})
57339.356046005567	0.04	0.2	559.9 ± 3.4 ± 3.7
57345.447691250090	0.06	0.4	565.1 ± 1.8 ± 3.4
57345.452487925162	0.04	0.2	568.8 ± 3.2 ± 3.4
57345.457595303807	0.02	0.08	⋯
57345.462413106565	0.09	0.6	560.0 ± 3.1 ± 3.3
57364.204632665605	0.03	0.09	558.6 ± 0.3 ± 1.4

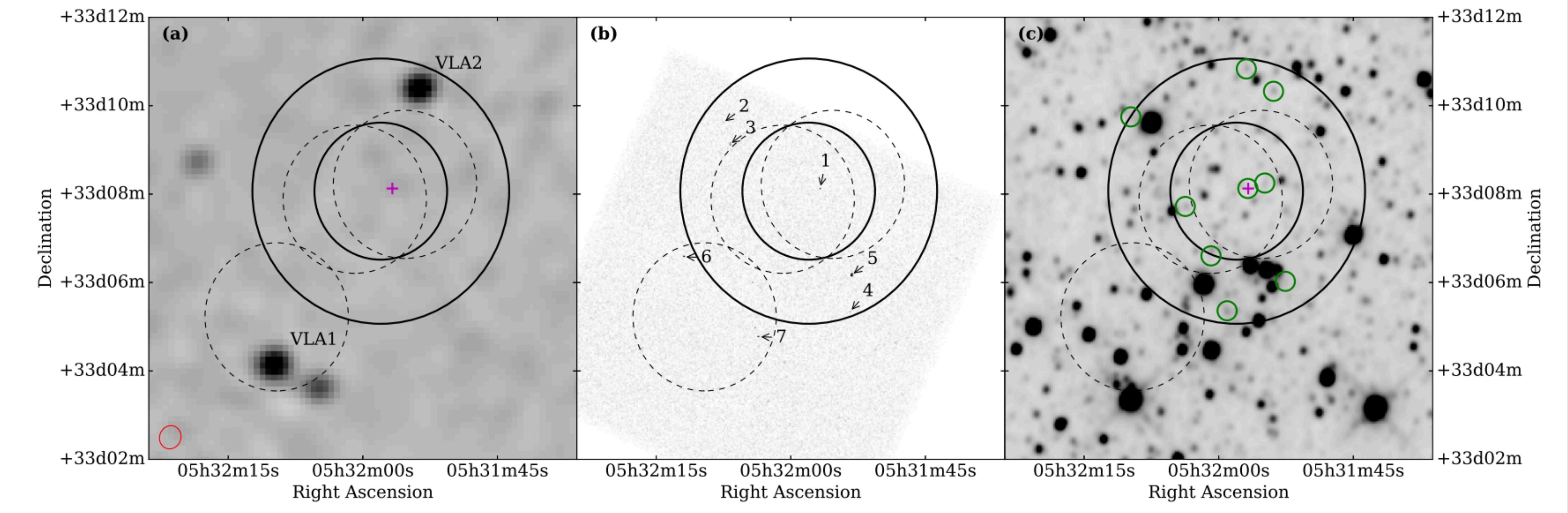

Scholz et al. 2017

New repeaters!

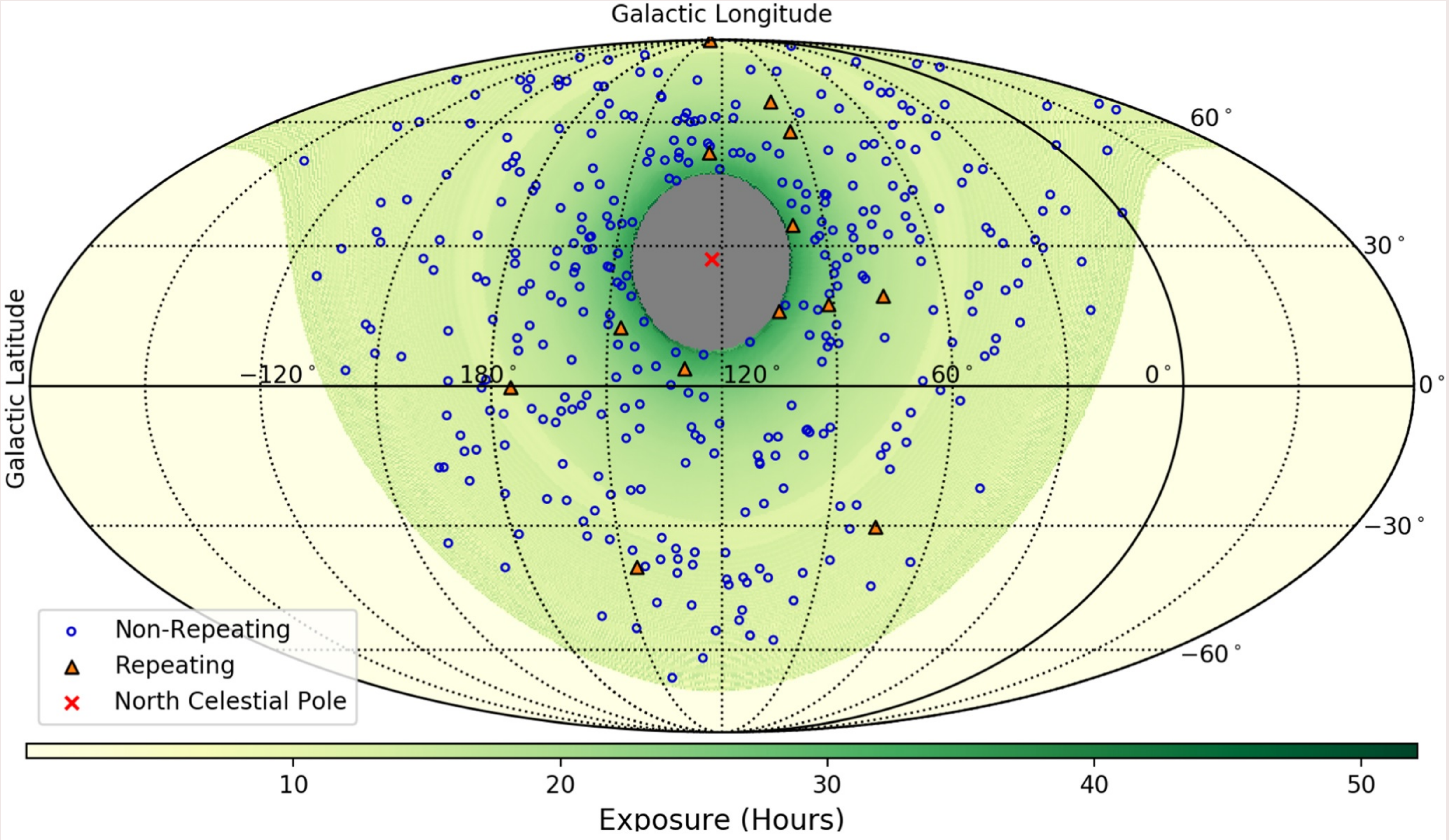

CHIME/FRB Collaboration 2021

A periodic repeater!

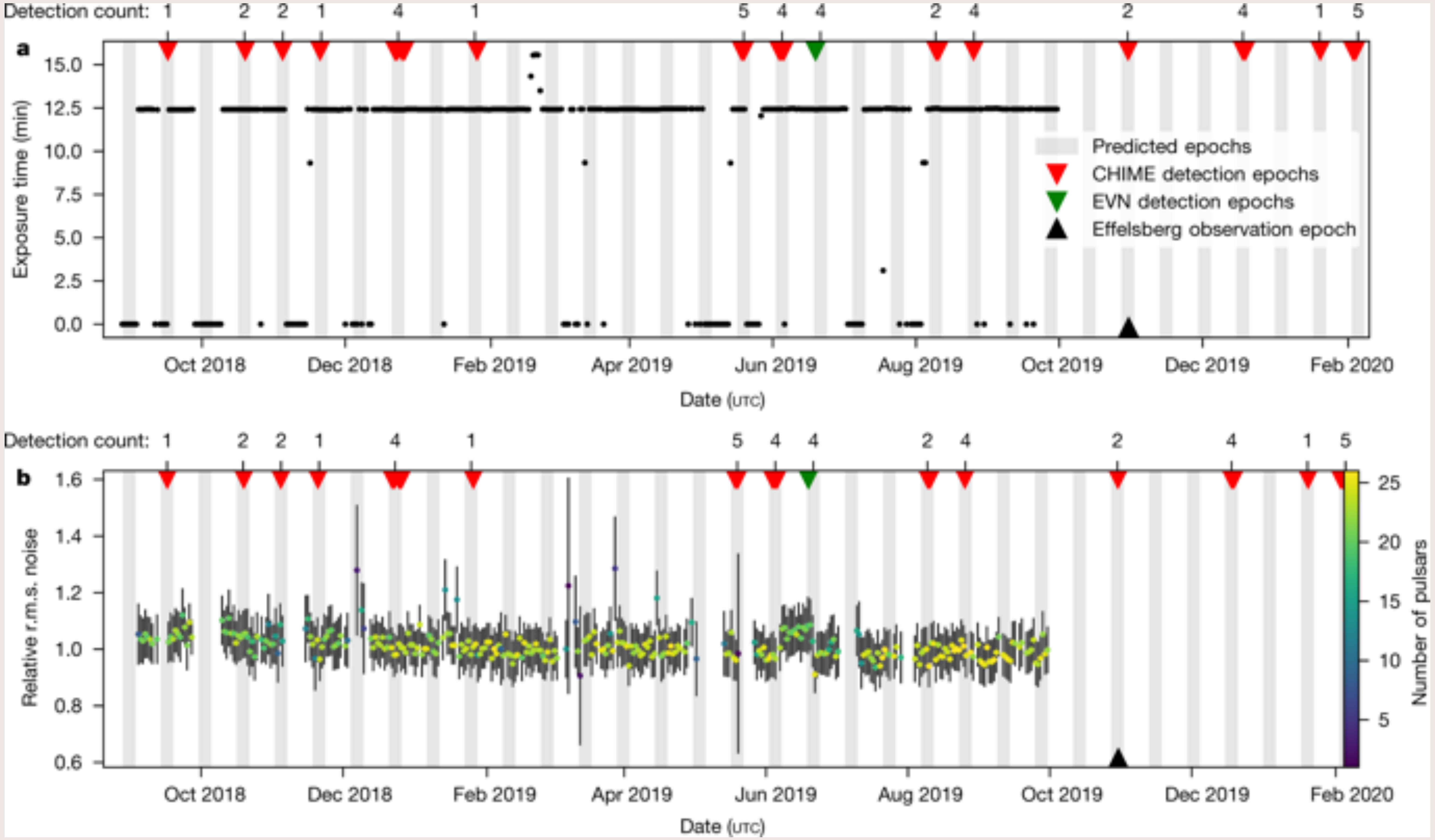

Chime/FRB Collaboration, Nature, 2020

MWL campaigns on FRB20180916B (R3)

- Periodicity announced in January 2020
- First campaign by CHIME/FRB group simultaneously with the confirmation of periodicity (Scholz et al. 2020)
- First successful campaign by our group in February (*)
- Parallel campaigns (both targeted and archival) by other collaborators, see e.g. Guidorzi et al. 2020, Casentini et al. 2020, Tavani et al. 2020

Our contribution

The three bursts

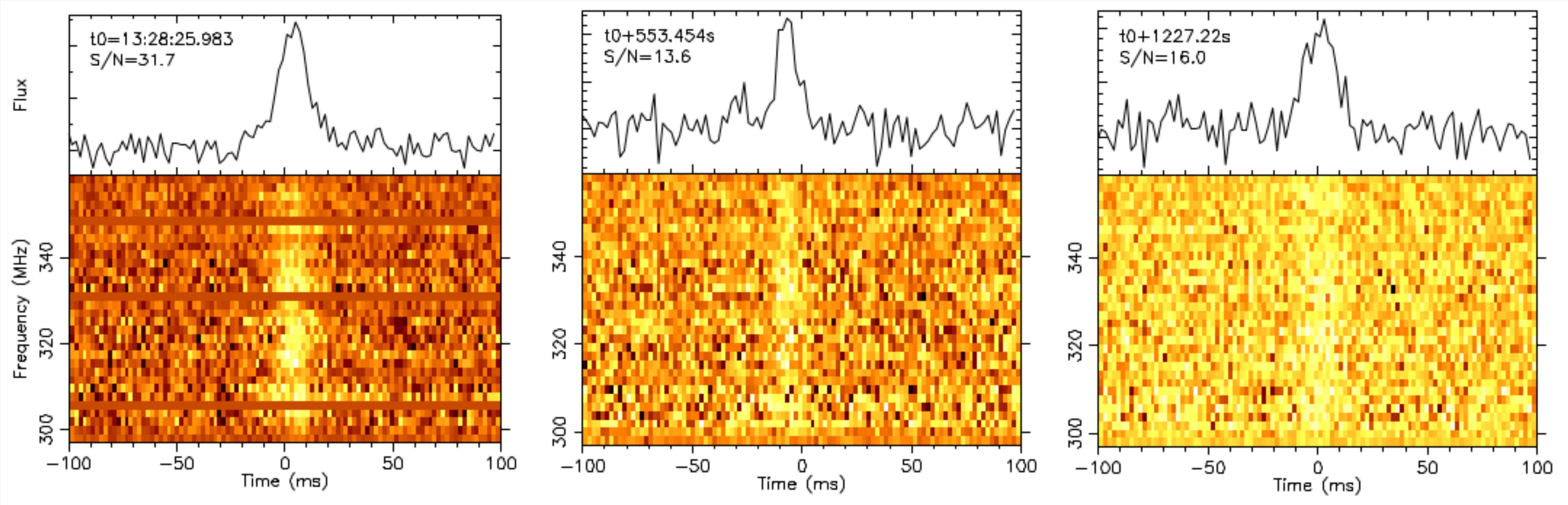

Time (UT)	Time (MJD)	Width (ms)	S/N (-)	Peak flux (Jy)	Fluence (Jy ms)	DM (pc cm^{-3})
13:28:25.983(8)	58899.56141184	13(4)	31.7	2.8(9)	37(16)	349.8(1)
13:37:39.437(7)	58899.56781756	9(4)	13.6	1.5(7)	13(8)	349.4(1)
13:48:53.20(1)	58899.57561573	14(4)	16.0	1.4(4)	19(8)	350.1(1)

Pilia et al. 2020, ApJL

Multiwavelength campaign

$S_{\nu,Jy} = 2.8\text{Jy}$

$\delta t = 0.03s$

$\Delta\nu = 0.064\text{GHz}$

$d_{150} = d/150\text{Mpc}$

$E_{r,i} = 6.3 \times 10^{37}\text{erg}$

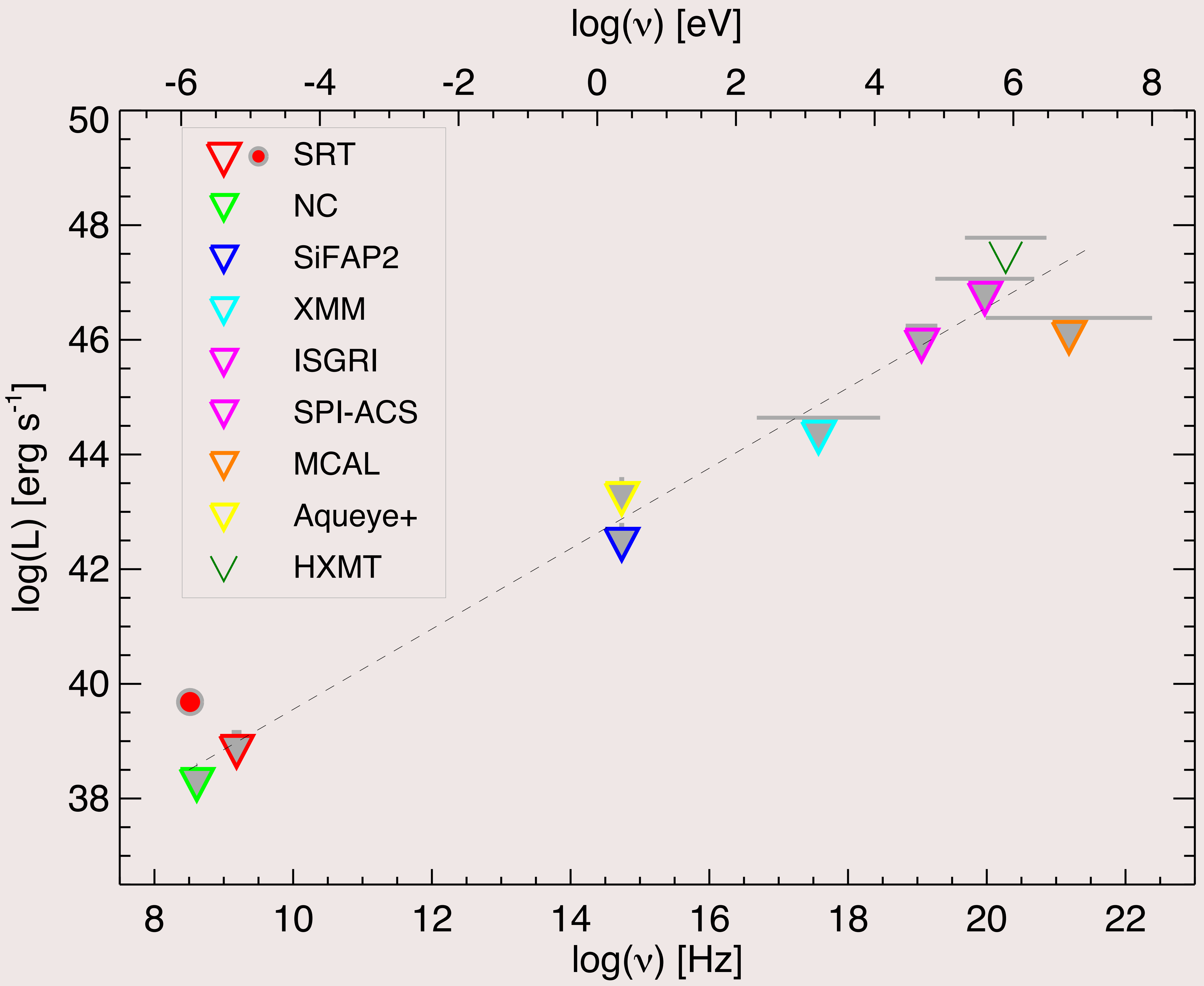

Pilia et al. 2020, ApJL

Simultaneous multi-wavelength coverage

XMM-Newton and AGILE

- **XMM-Newton**
- 0.3 - 10 keV
- BB kT = 0.5 keV
- PL $\Gamma = 3$
- N_H = 4.3e21 cm^{-1}
- Persistent L = 10^{41} erg/s
- Burst L = 10^{45} erg/s
- $\frac{E_X}{E_{radio}} \sim 7 \times 10^6$

- **AGILE - MCAL**
- 0.4 - 100 MeV
- Triggers: 330µs - 8s
- Burst 1
- Isotropic E = 2.2×10^{46} erg
- $\frac{E_X}{E_{radio}} \sim 5 \times 10^8$

SGR 1806-20

Here we report that SGR 1806–20 emitted a giant flare on 27 December 2004. The total (isotropic) flare energy is 2×10^{46} erg, which is about a hundred times higher than the other two previously observed giant flares. The energy release probably occurred during a catastrophic reconfiguration of the neutron star's magnetic field. If the event had occurred at a larger distance, but within 40 megaparsecs, it would have resembled a short, hard γ-ray burst, suggesting that flares from extragalactic SGRs may form a subclass of such bursts.

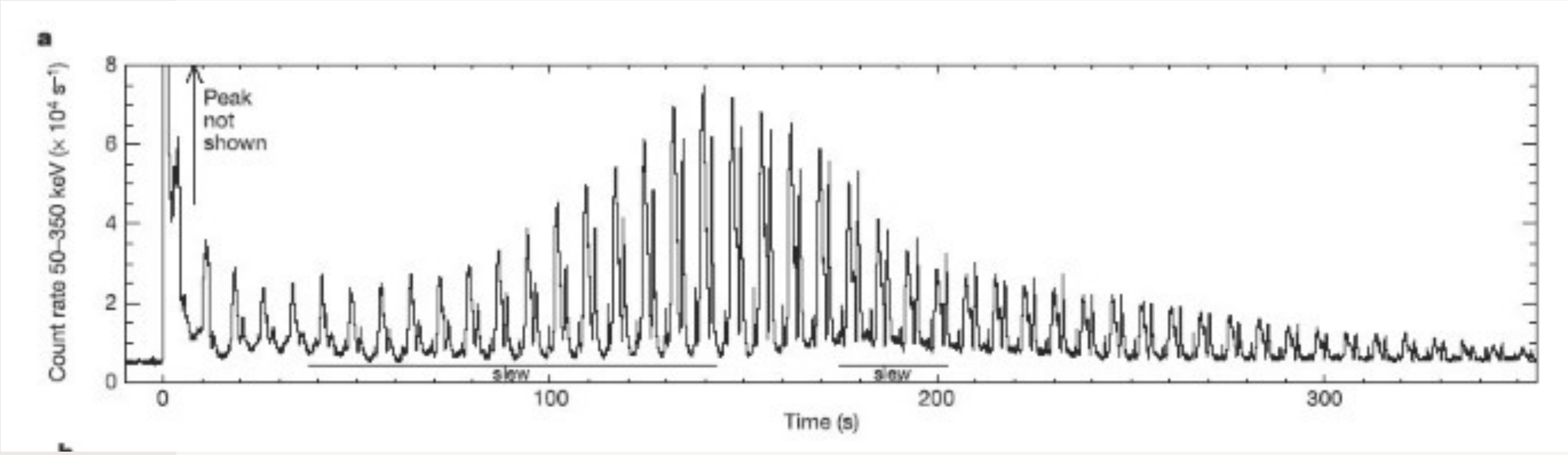

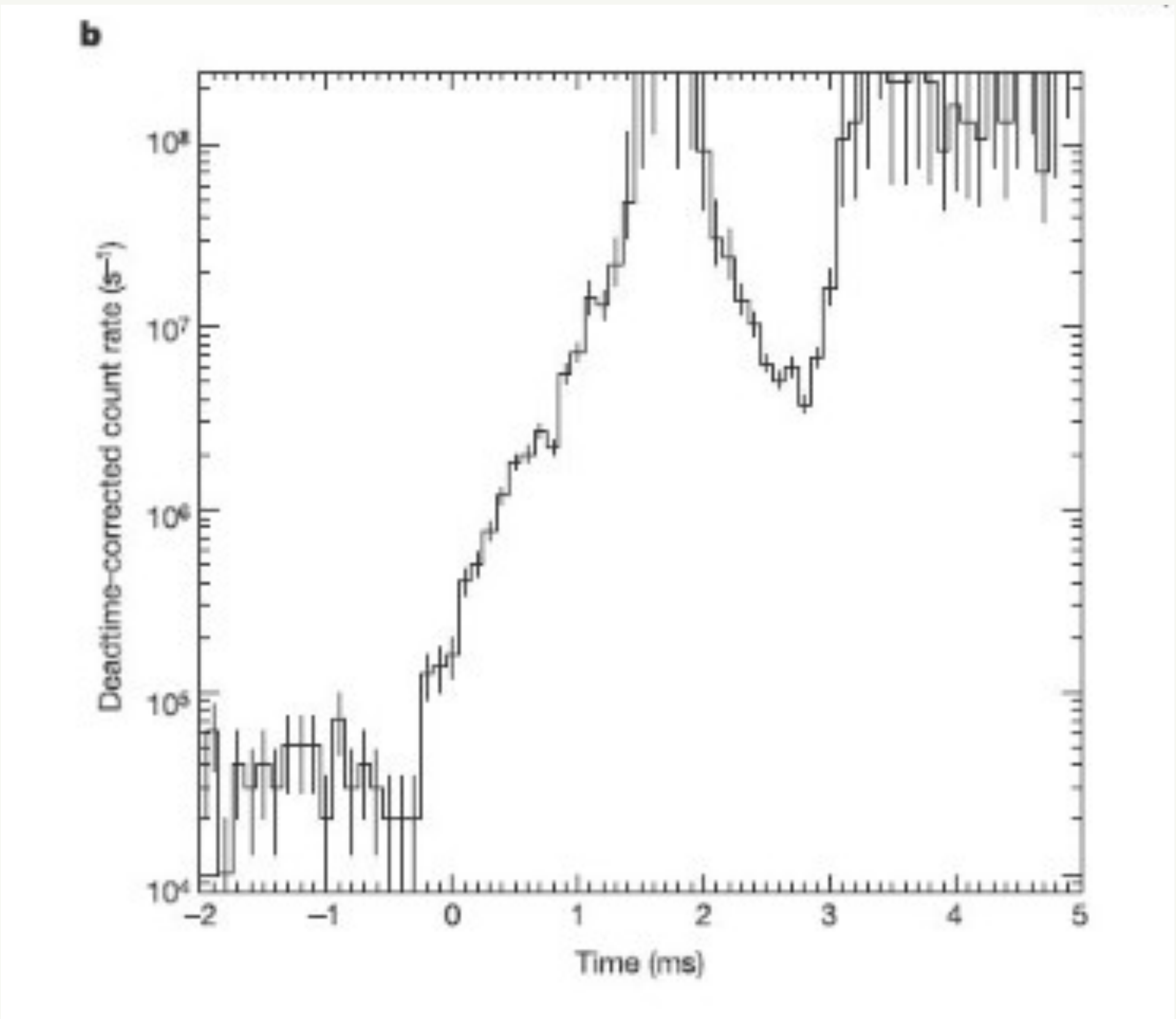

Palmer et al. 2005

SGR 1935+2154

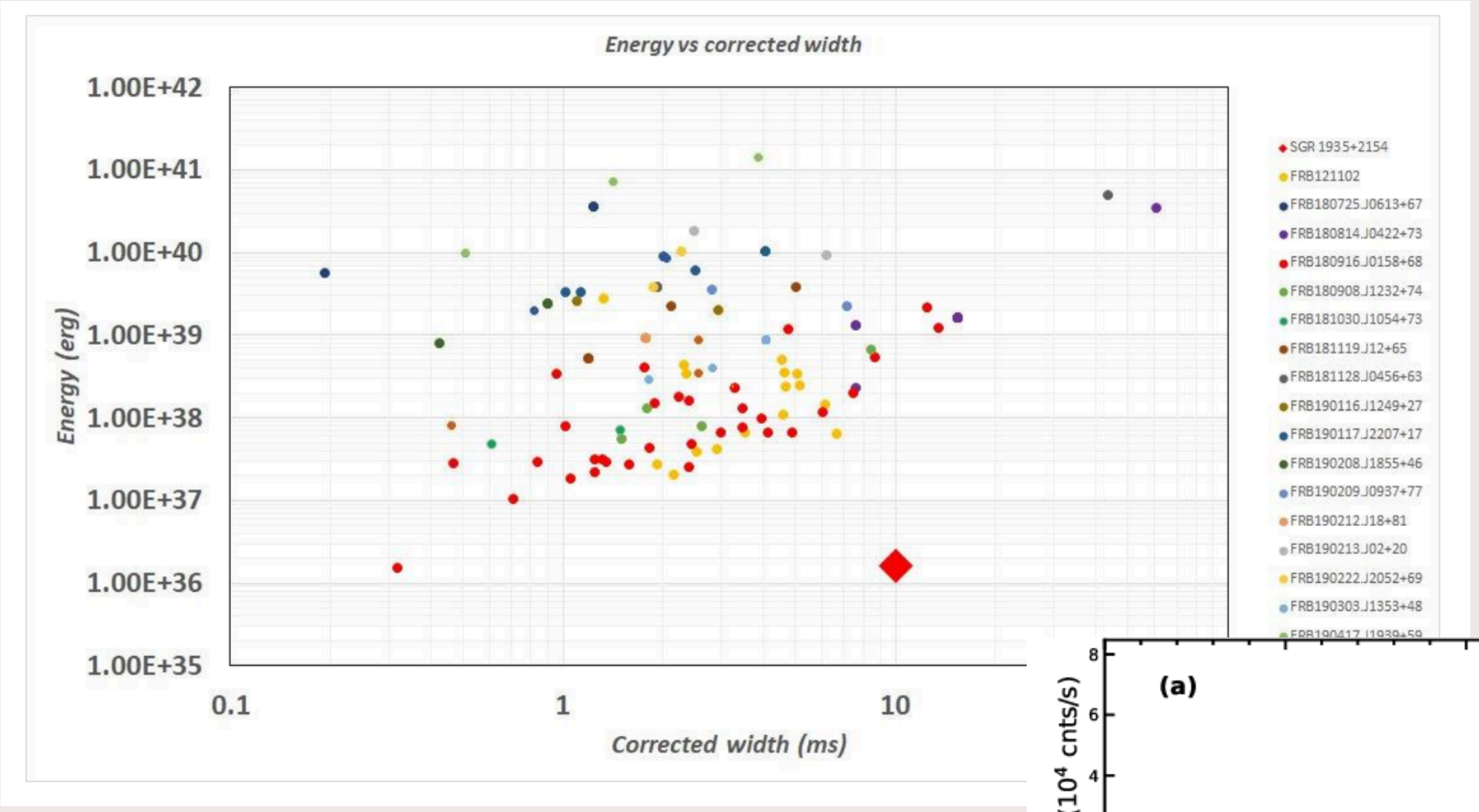

Tavani et al. 2020, NatAstro

Mereghetti et al. 2020, ApJ

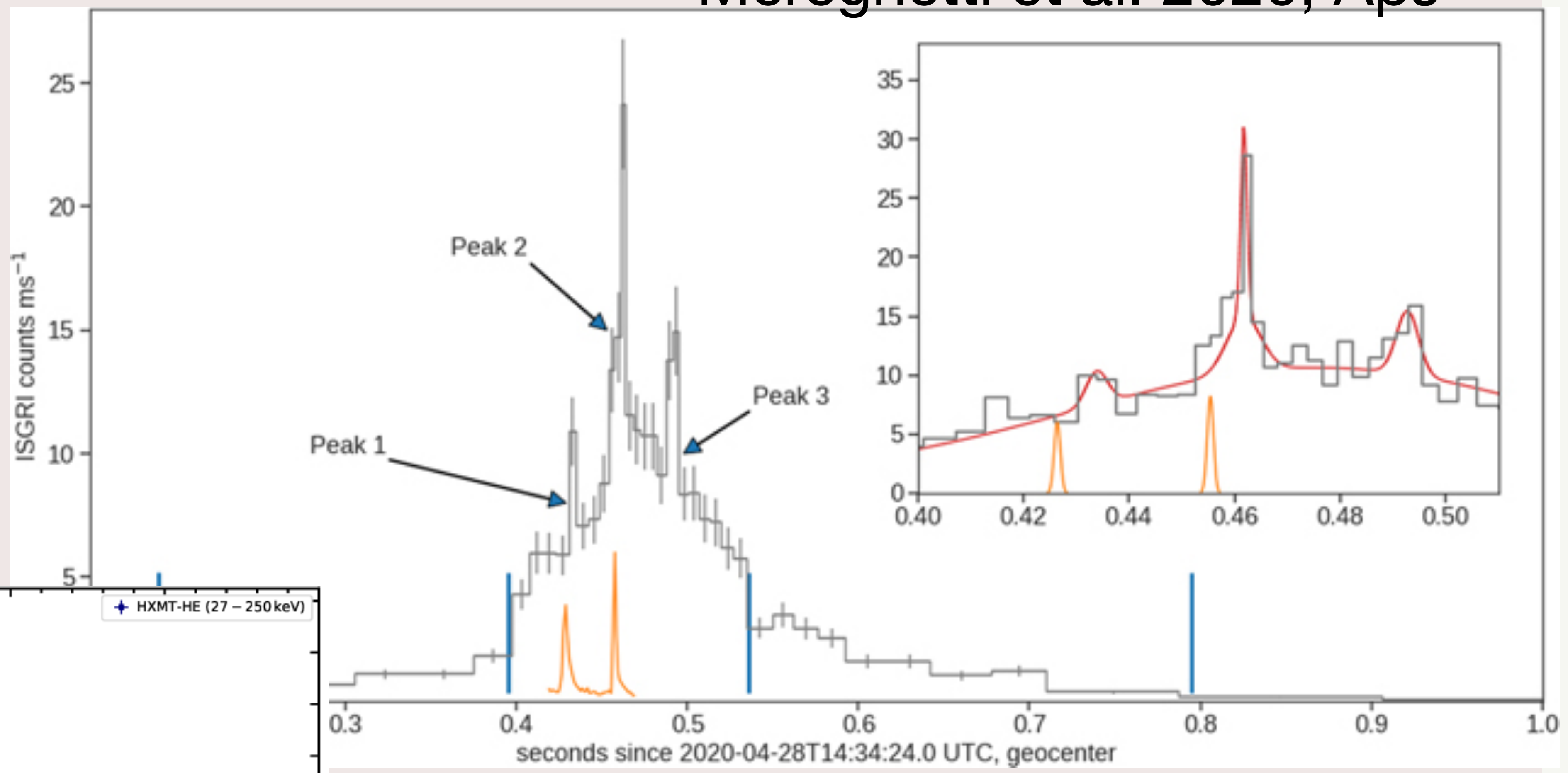

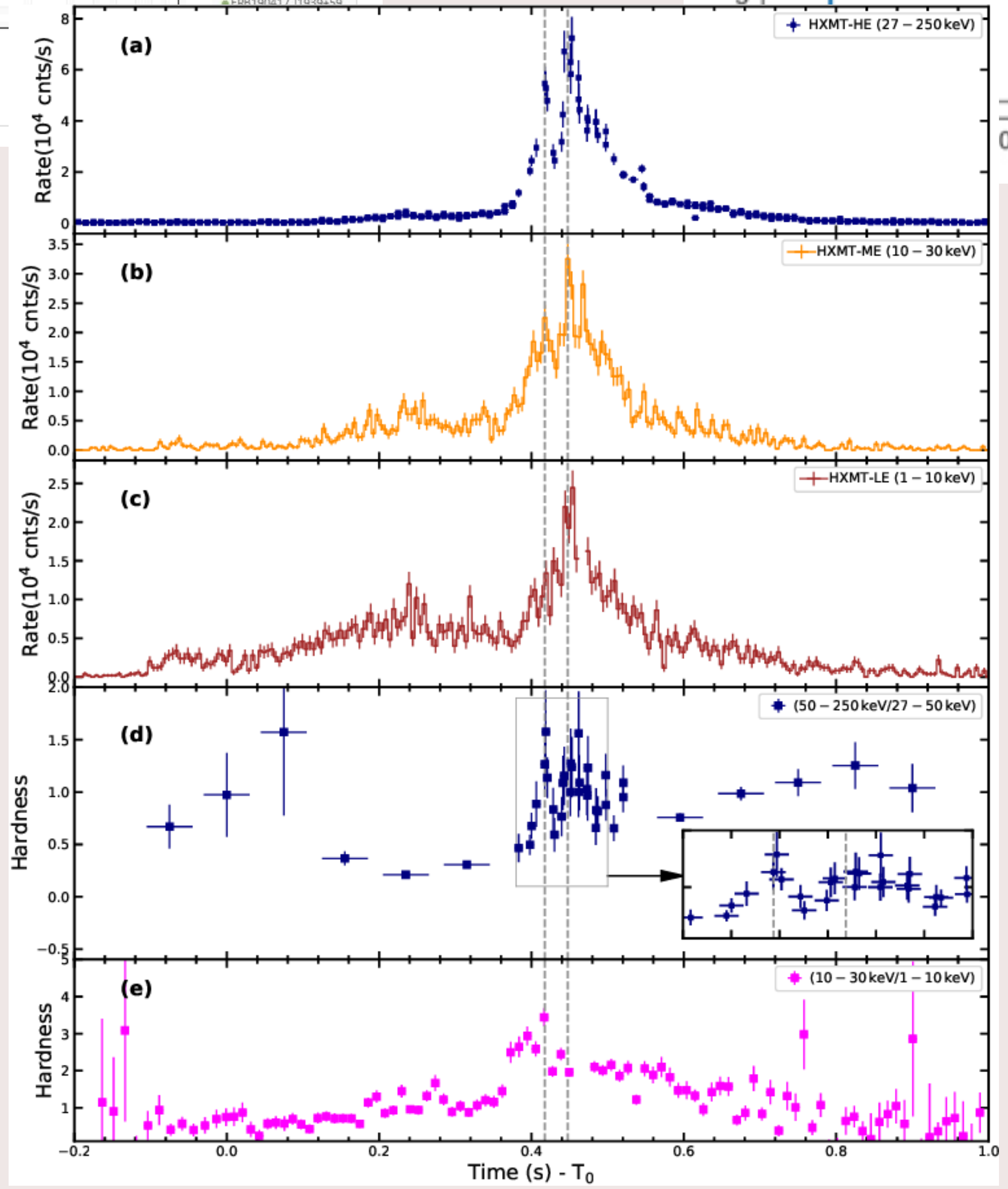

HXMT Coll. 2020, NatAstro

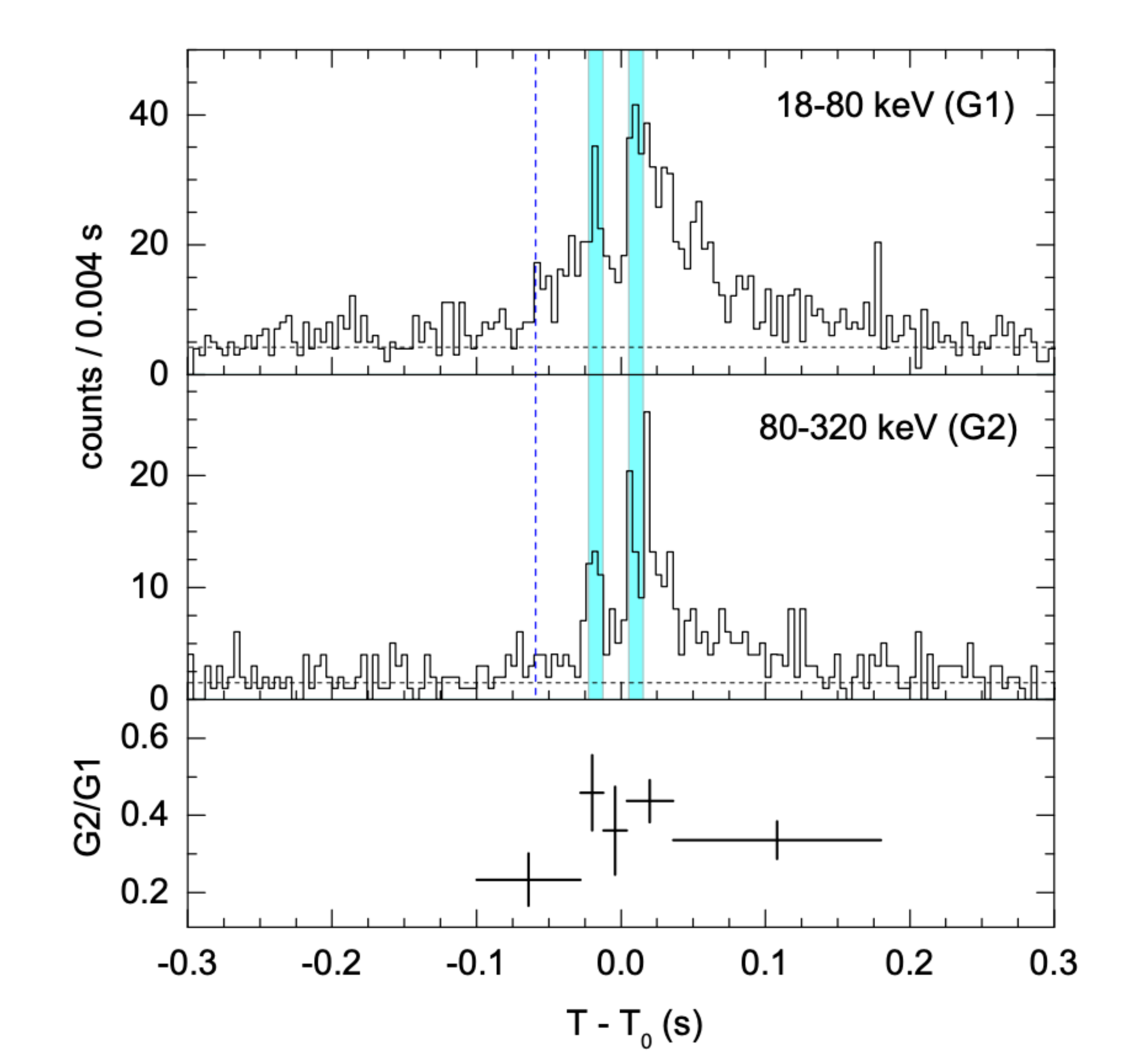

Ridnaia et al. 2020, NatAstro

- SGR 1935+2154 emitted 1.4×10^{39} erg in the INTEGRAL band on April 28th, 2020
- $$\frac{E_X}{E_{radio}} \sim 10^5$$

SGR 1806-20

For the 2004 December 27 magnetar giant flare of SGR 1806-20, Tendulkar et al. (2016) placed upper limits on the possible radio fluence at the time of the 1.4 erg cm−2 X-ray flare **given the nondetection with the Parkes radio telescope, which was observing a location 35.6° away from the source at the time** (Hurley et al. 2005; Palmer et al. 2005; Terasawa et al. 2005). **This corresponds to a lower limit on the X-ray-to-radio fluence ratio**, given it is an upper limit on the radio fluence, which is the denominator, **of 4 × 10^{10} for X-ray counterparts of FRBs if they can be attributed to magnetar giant flares like that observed for SGR 1806-20.** However, the majority of upper limits placed in that paper are incompatible with our limits and all published limits on ηx/r to date.

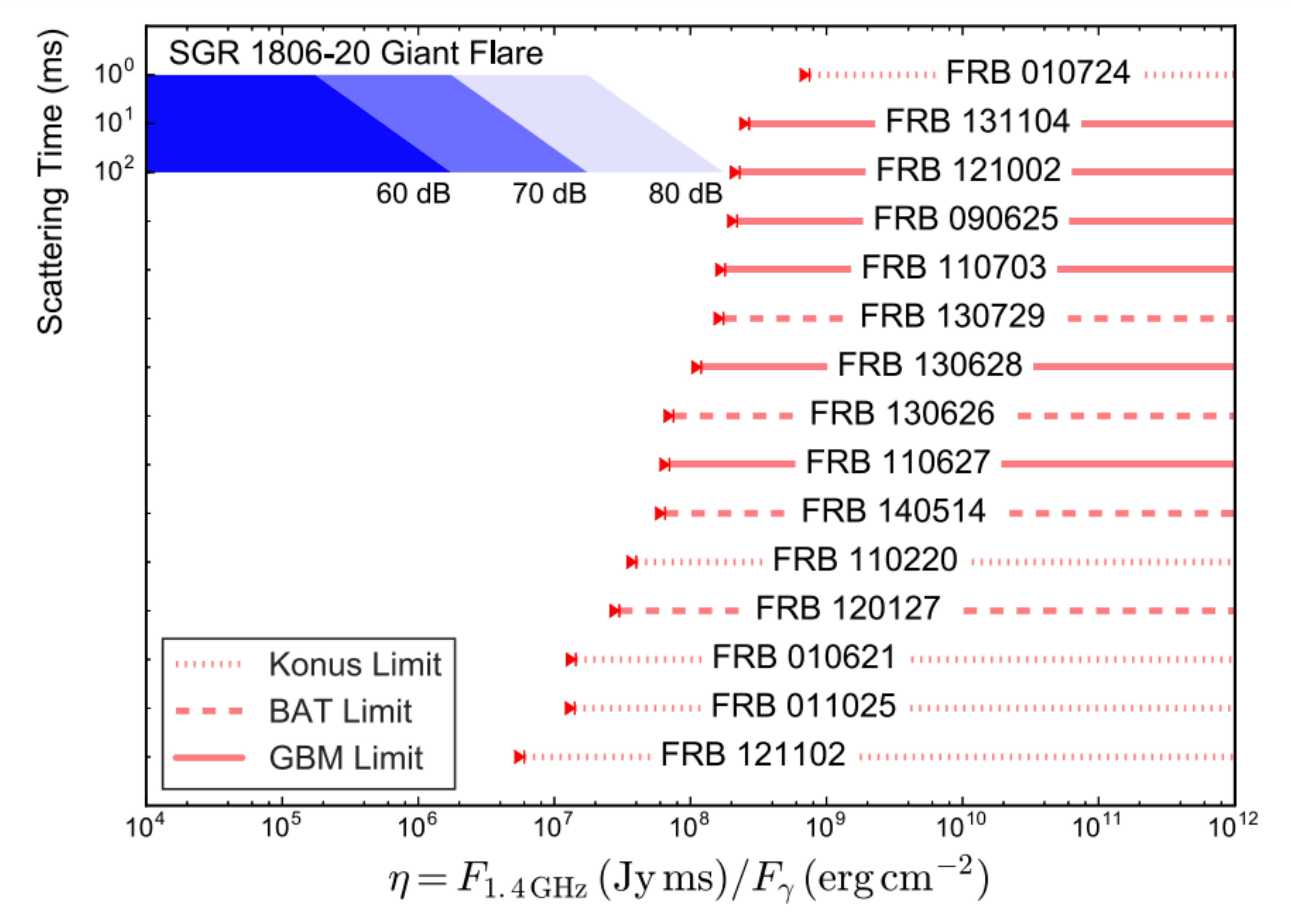

Tendulkar et al. 2016

The second round

Table 2. Properties of the detected bursts.

Burst ID	TOA [MJD]	ϕ	Δt [ms]	S_ν [Jy]	F_ν [Jy ms]	E [10^{37} erg]	$\dot{\nu}$ [MHz ms^{-1}]
SRT-P-01	59162.8253243218	0.5870	19 ± 2	3.1 ± 0.8	48 ± 16	8 ± 2.5	N.A.
SRT-P-02	59162.8343320911	0.5875	14.0 ± 0.5	12.2 ± 3.0	139 ± 43	24 ± 7	-9.7 ± 0.6
SRT-P-03	59162.8567440946	0.5889	13.2 ± 0.5	11.7 ± 2.9	125 ± 39	21 ± 6	-11.4 ± 0.6
SRT-P-04	59162.8665428914	0.5895	23 ± 2	3.2 ± 0.8	61 ± 20	10 ± 2	N.A.
SRT-P-05	59162.8752448474	0.5900	18 ± 2	5.3 ± 1.5	77 ± 29	13 ± 3	N.A.
	59162.8752449374	0.5900	23 ± 1	5.3 ± 1.5	98 ± 27	17 ± 3	N.A.
SRT-P-06	59162.9481096844	0.5945	14 ± 2	5.5 ± 1.4	62 ± 23	10 ± 6	N.A.
SRT-P-07	59162.9513861530	0.5947	23 ± 4	2.7 ± 0.7	50 ± 20	8 ± 1	N.A.
SRT-P-08	59162.9515615864	0.5947	20 ± 2	3.0 ± 0.7	49 ± 17	8 ± 1	N.A.
SRT-P-09	59162.9661486339	0.5956	12 ± 2	2.3 ± 0.6	22 ± 9	4 ± 3	N.A.
SRT-P-10	59194.7961833830	0.5448	9 ± 2	2.1 ± 0.6	15 ± 7	3 ± 1	N.A.
SRT-P-11	59244.9407380909	0.6155	22 ± 2	5.2 ± 1.3	92 ± 21	16 ± 2	-11.3 ± 0.6
SRT-P-12	59244.9503715983	0.6160	18.1 ± 0.9	11.8 ± 2.9	172 ± 55	29 ± 6	-10.7 ± 0.6
SRT-P-13	59244.9559004303	0.6164	12 ± 1	7.3 ± 1.9	70 ± 27	12 ± 3	N.A.
SRT-P-14	59258.8293625230	0.4660	16 ± 2	4.9 ± 1.3	64 ± 23	10 ± 2	N.A.
uGMRT-01	59441.0257263218	0.6231	20 ± 2	0.8 ± 0.2	8.9 ± 0.8	2.1 ± 0.2	-5.9 ± 0.5
uGMRT-02	59441.0453208005	0.6243	9.2 ± 0.7	0.6 ± 0.2	2.8 ± 0.9	0.3 ± 0.1	N.A.
uGMRT-03	59441.0575323455	0.6250	20.8 ± 0.6	7.9 ± 0.2	84 ± 3	36 ± 1	-10.5 ± 0.5
uGMRT-04	59441.0622128892	0.6254	7.6 ± 0.8	0.4 ± 0.4	2.5 ± 0.7	0.6 ± 0.1	N.A.
uGMRT-05	59441.0665624511	0.6256	6 ± 1	0.4 ± 0.1	0.6 ± 0.1	0.06 ± 0.01	N.A.
uGMRT-06	59441.0944839544	0.6273	16 ± 4	1.3 ± 1.2	7.9 ± 2.3	0.8 ± 0.2	N.A.
uGMRT-07	59441.1011067833	0.6277	15 ± 8	0.2 ± 0.1	0.9 ± 0.8	0.2 ± 0.2	N.A.

Trudu et al. 2023, A&A

The second round

Asiago reports an optical peak within a window of ±15 s around the second radio burst detected by the SRT on the night of 2020/11/09. The peak is above the threshold of the aforementioned window of 30 s of 15 counts bin−1 . However, it is slightly below the 19-count bin−1 threshold obtained considering the statistics of the entire observation, so it is not possible to robustly tag it as the optical counterpart of the radio burst.

We constrained the optical/radio efficiency ξ setting a punctual upper limit thanks to a radio detection with the uGMRT and a simultaneous observation with SiFAP2. We set a constraint of **$\xi < 1.3 \times 10^2$.**

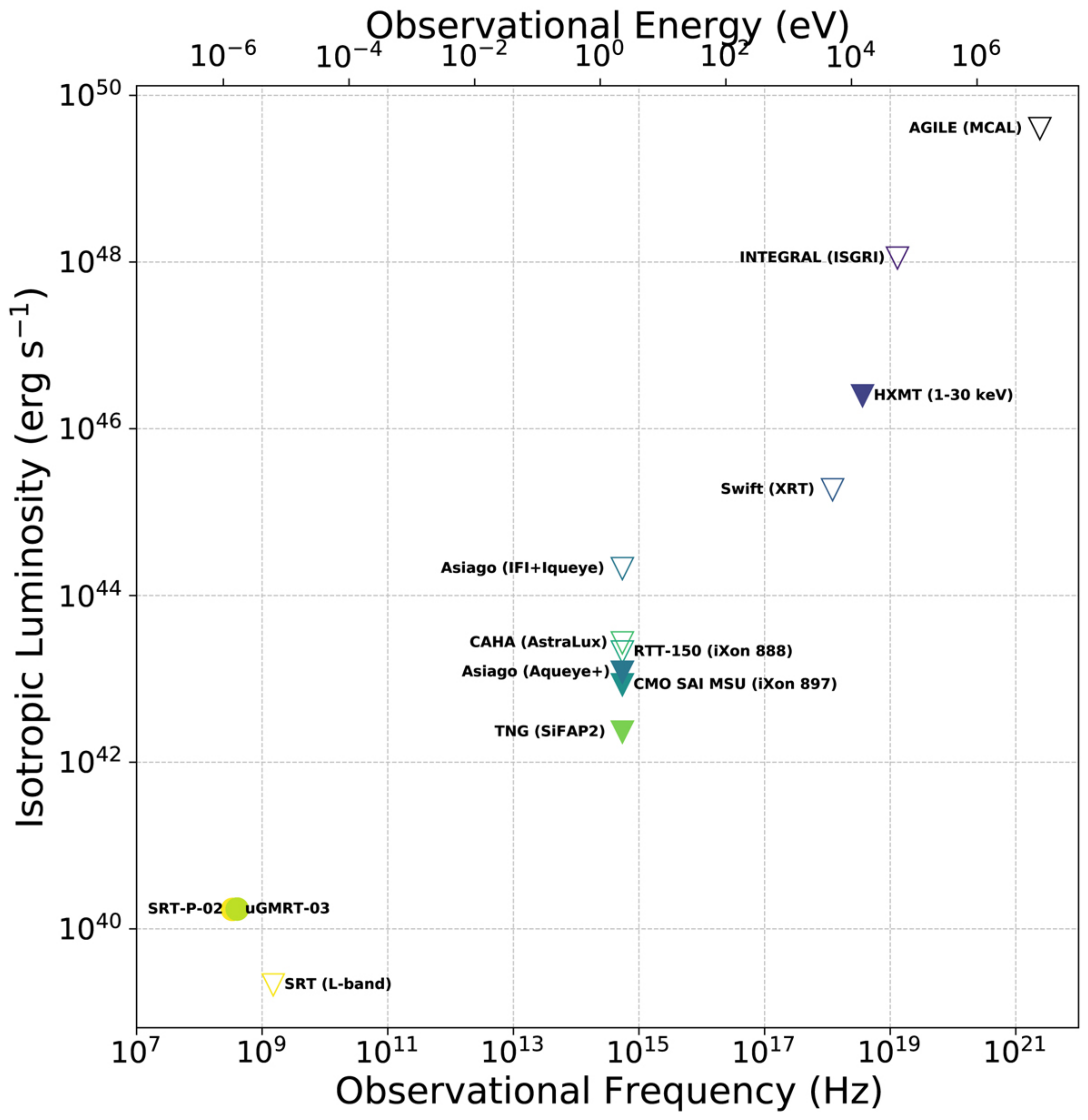

Trudu et al. 2023, A&A

The optical counterpart

‘Alopeke highspeed camera on the 8.1 m Gemini-North.

Similar efforts targeting millisecond-timescale optical emission from FRBs have been conducted with the Tomo-e Gozen high-speed CMOS camera, observing 11 bursts of FRB 20190520B (Niino et al. 2022), and the photomultiplier SiFAP2 and fast optical cameras Aqueye+ and IFI/Iqueye+, targeting FRB 20180916B (Pilia et al. 2020).Our limits on energy are significantly more constraining on similar timescales, yielding the best constraints to date on millisecond-timescale optical emission contemporaneous with a FRB.

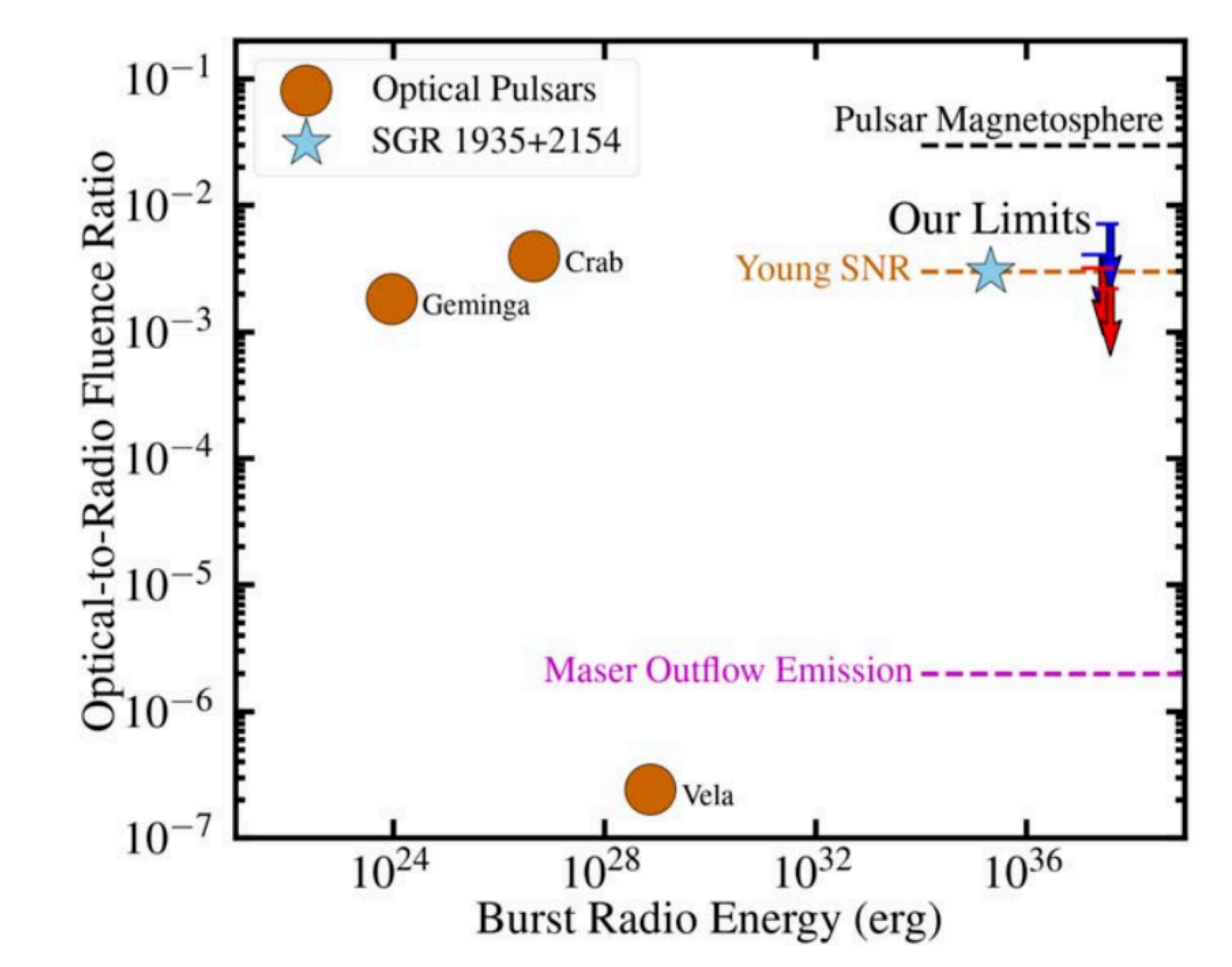

Kilpatrick et al. 2024

The optical counterpart

'Alopeke highspeed camera on the 8.1 m Gemini-North.

Similar efforts targeting millisecond-timescale optical emission from FRBs have been conducted with the Tomo-e Gozen high-speed CMOS camera, observing 11 bursts of FRB 20190520B (Niino et al. 2022), and the photomultiplier SiFAP2 and fast optical cameras Aqueye+ and IFI/Iqueye+, targeting FRB 20180916B (Pilia et al. 2020).Our limits on energy are significantly more constraining on similar timescales, yielding the best constraints to date on millisecond-timescale optical emission contemporaneous with a FRB.

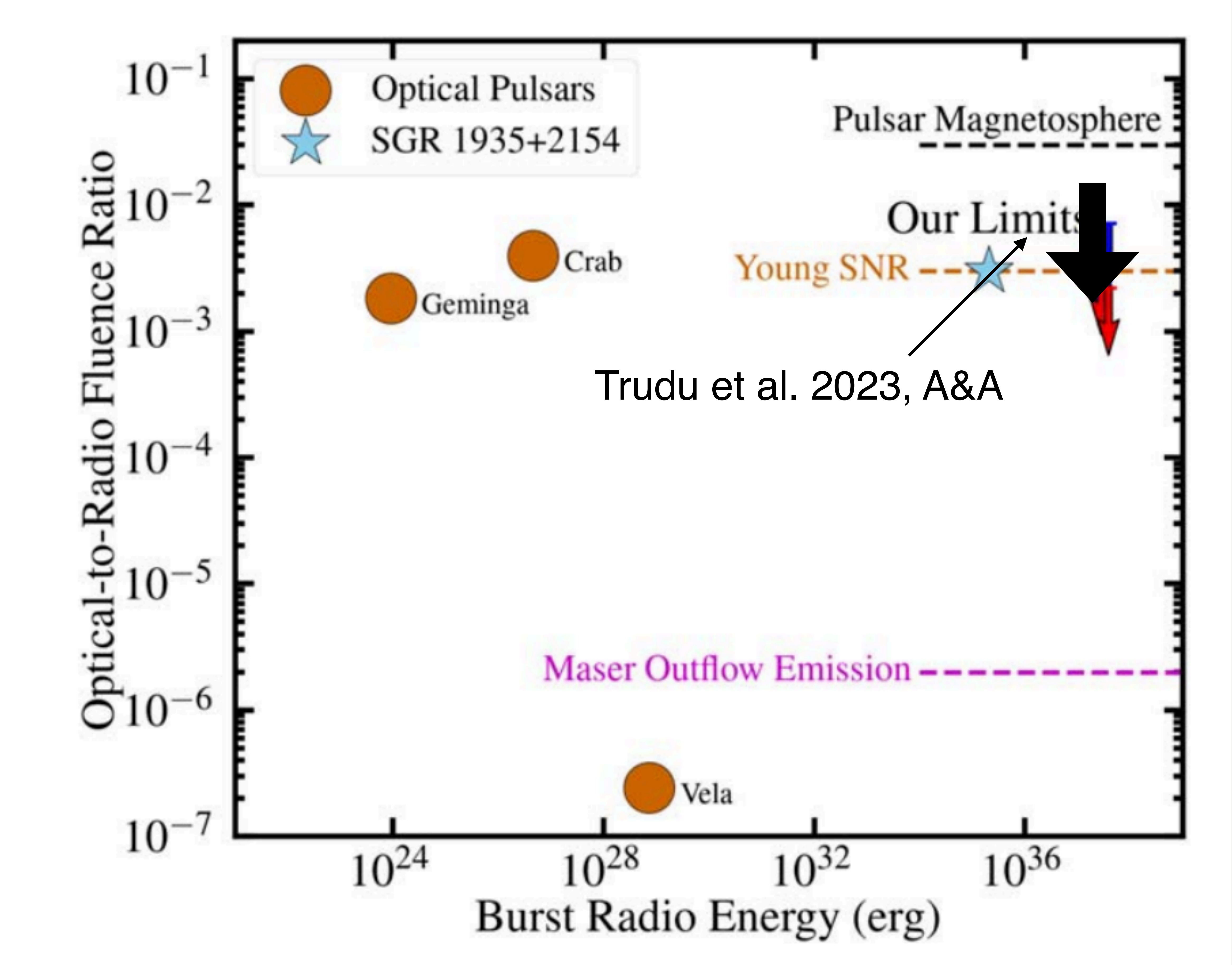

Kilpatrick et al. 2024

The optical counterpart

‘Alopeke highspeed camera on the 8.1 m Gemini-North.

Similar efforts targeting millisecond-timescale optical emission from FRBs have been conducted with the Tomo-e Gozen high-speed CMOS camera, observing 11 bursts of FRB 20190520B (Niino et al. 2022), and the photomultiplier SiFAP2 and fast optical cameras Aqueye+ and IFI/Iqueye+, targeting FRB 20180916B (Pilia et al. 2020).Our limits on energy are significantly more constraining on similar timescales, yielding the best constraints to date on millisecond-timescale optical emission contemporaneous with a FRB.

See upcoming talks!

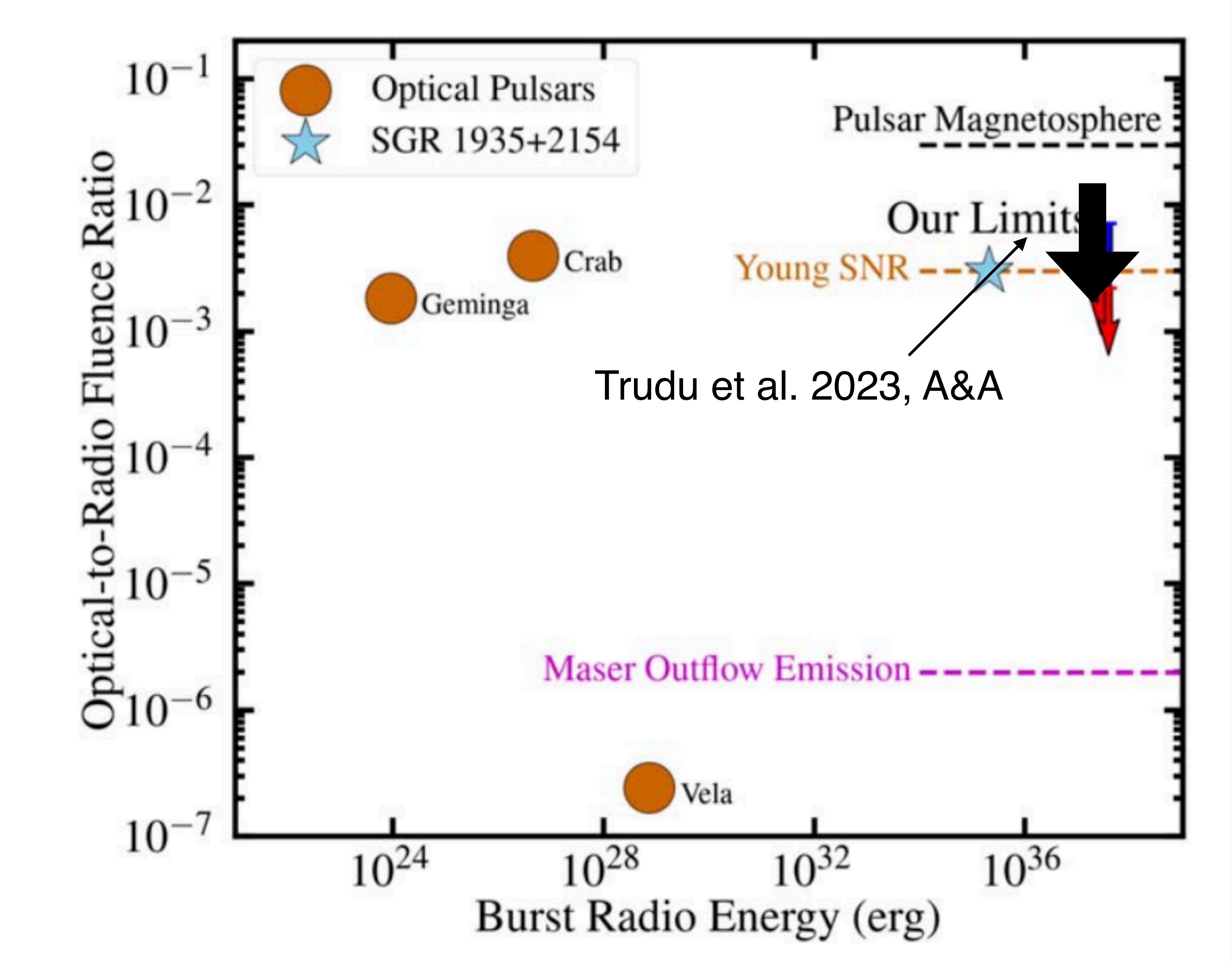

Kilpatrick et al. 2024

The second round

The Insight–HXMT observations, occurring simultaneously with a radio burst detected by the SRT, set a punctual UL on the X-ray-and-radio efficiency η in the range of **$\eta < (0.9–1.3) \times 10^7$ (1–30 keV band),** depending on which emission model is used for the X-ray emission.

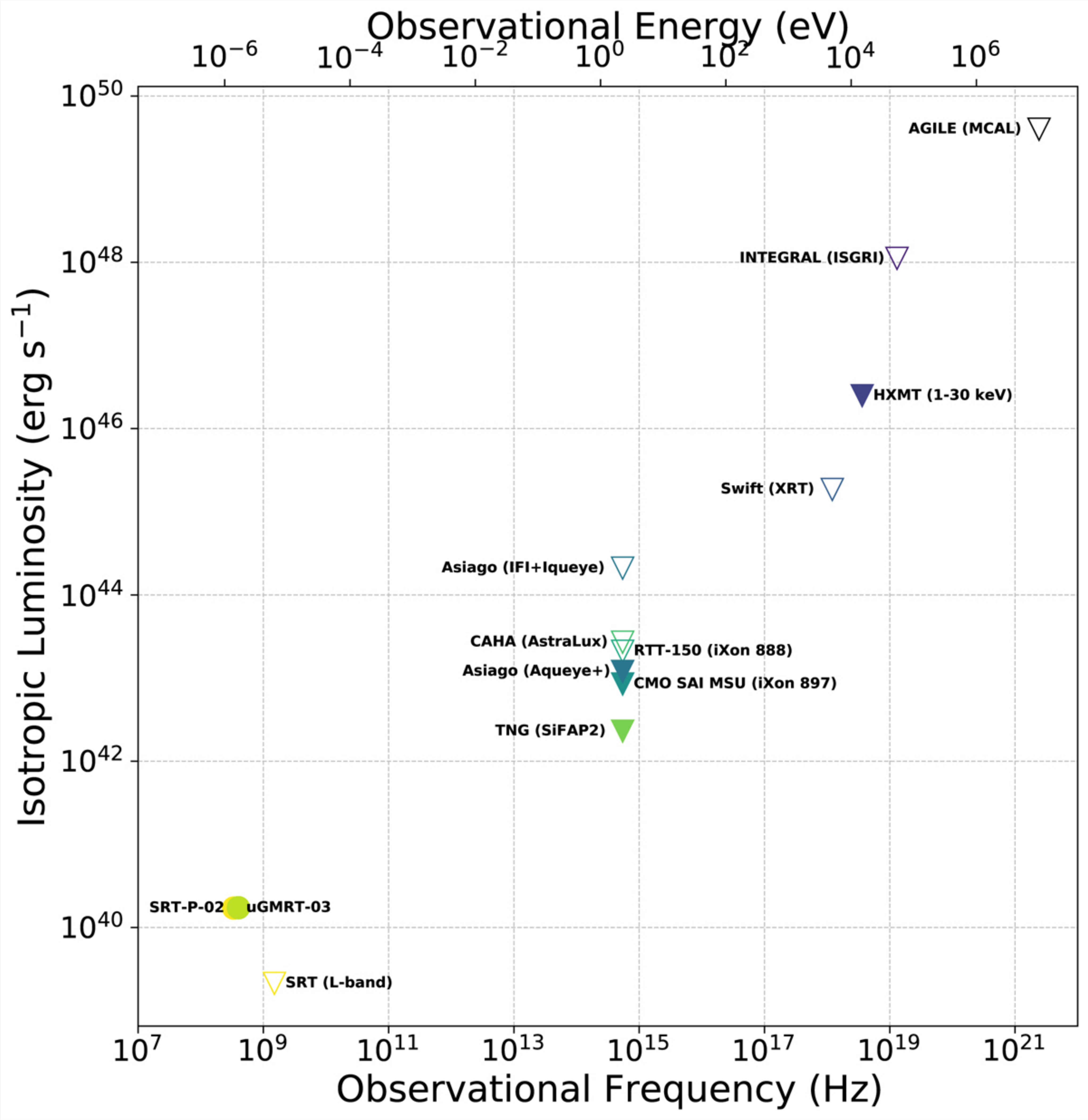

Trudu et al. 2023, A&A

The chances of detecting an X-ray counterpart

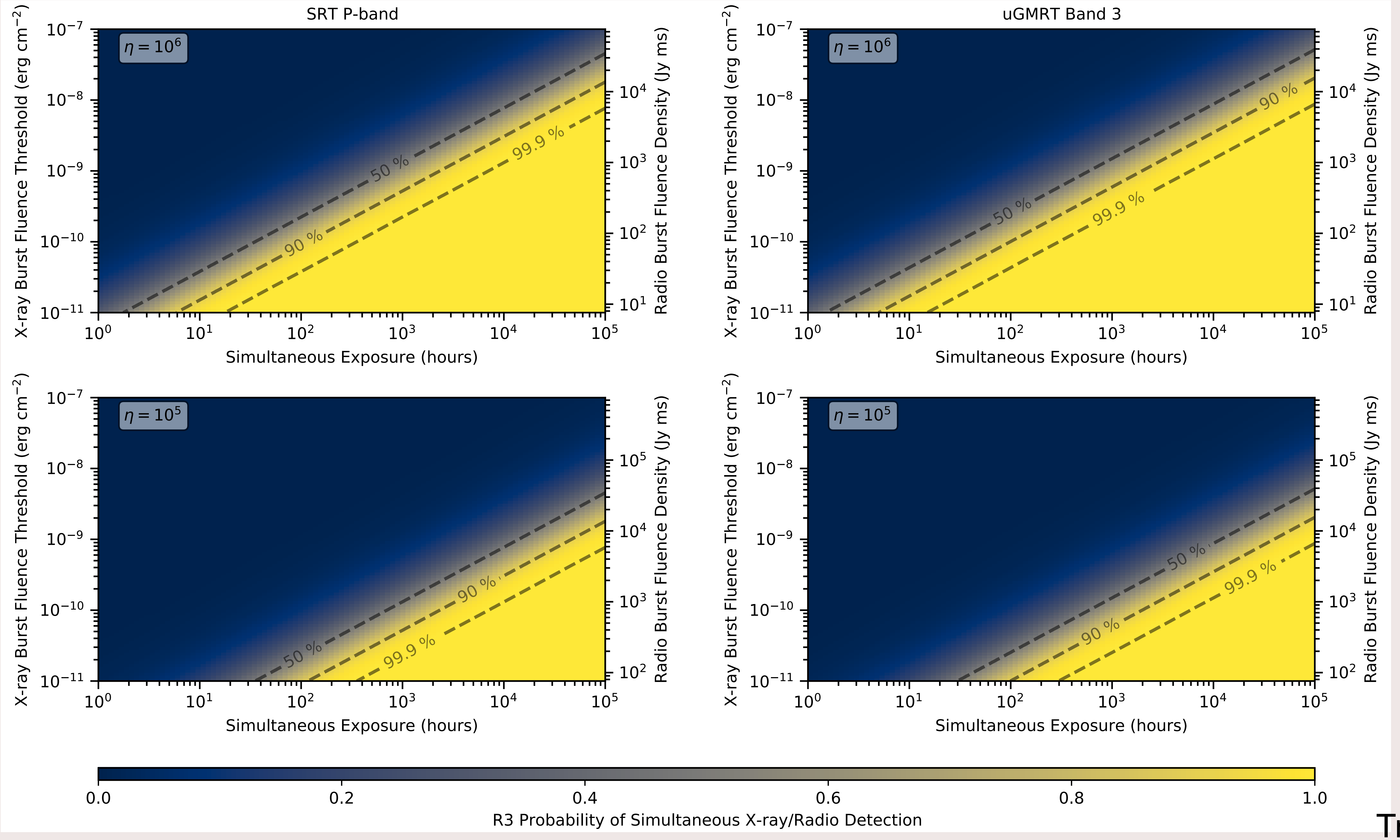

Trudu et al. 2023, A&A

The new players in the field

Table 1
Properties of the R-FRBs Considered in This Work

FRB Name (1)	DM_{exc} ($pc\ cm^{-3}$) (2)	l, b (deg) (3)	N_b (4)	Width (ms) (5)	f (Jy ms) (6)	z_s (Mpc) (7)
FRB 20200120E	18.0 (88.0)	142°.19, +41°.22	80	0.01–0.70	0.04–2.40	0.0008 (3.6)
FRB 20181030A	33.5 (103.7)	133°.40, +40°.92	9	0.59–1.43	4.50–7.30	0.004 (17.3)
FRB 20220912A	67.1 (222.1)	155°.41, +61°.81	1529	0.09–32.9	0.002–37.7	0.077 (343)
FRB 20180814A	72.4 (189.4)	136°.42, +16°.60	22	7.90–63.0	3.40–66.0	0.078 (347)
FRB 20190107B	73.1 (173.1)	127°.14, +21°.75	2	0.98	4.30	0.11 (500)
FRB 20200223B	125.5 (201.5)	118°.07, −33°.88	10	1.26–2.29	1.06–14.4	…
FRB 20180908B	127.8 (195.8)	124°.74, +42°.86	4	1.60–9.00	1.10–2.90	0.17 (800)
FRB 20180916B	150.7 (349.4)	129°.71, +3°.74	290	0.06–158	0.08–318	0.033 (150)
FRB 20181226F	152.1 (240.1)	129°.79, +26°.20	3	…	…	…
FRB 20190905A	153.3 (240.4)	124°.64, +26°.25	6	0.75–1.13	1.79–18.0	…
FRB 20190110C	156.3 (222.0)	65°.56, +42°.15	3	2.95	1.40	0.22 (1050)
FRB 20190303A	164.1 (223.1)	97°.48, +68°.94	38	0.89–7.20	0.78–10.4	0.064 (285)
FRB 20190812A	170.7 (249.1)	78°.05, +29°.83	2	0.42–0.60	0.65–13.0	…
FRB 20201130A	202.3 (288.3)	185°.33, −29°.15	12	0.47–6.55	1.31–20.4	…
FRB 20210323C	204.7 (285.2)	142°.59, +31°.54	11	0.83–5.00	2.32–7.60	…
FRB 20191105B	210.3 (313.8)	140°.59, +20°.40	2	0.55–0.71	2.70–19.7	…
FRB 20190113A	217.6 (426.5)	218°.04, +3°.43	3	1.82–3.03	5.70–9.40	0.29 (1450)
FRB 20190907A	226.8 (309.8)	173°.39, +32°.26	7	0.54–3.00	0.70–6.90	…
FRB 20201114A	253.9 (321.9)	111°.18, +42°.63	2	0.72–1.04	2.45–4.70	…
FRB 20201124A	257.6 (414.1)	177°.60, −8°.50	2883	0.91–316	0.005–640	0.098 (445)
FRB 20200127B	267.0 (351.0)	126°.63, +28°.02	2	0.45–0.61	4.70–7.70	…

Note. Column (1) lists the names of the FRB sources. Column (2) provides DM_{exc}, with the mean DM_{tot} given in parentheses. Column (3) shows the Galactic coordinates of the sources in degrees. Column (4) N_b indicates the total number of bursts observed to date for each source. Columns (5) and (6) give for each source the minimum and maximum burst widths in milliseconds and the minimum and maximum radio fluence values in Jy ms, respectively. Column (7) lists the spectroscopic redshift z_s associated with each source (where available), with the estimated luminosity distance (D_L) in Mpc in parentheses.

Casentini et al. 2025

FRB 20180301

FAST & NICER

The host of FRB 180301 is located at a redshift of z = 0.334, implying a luminosity distance of ~ 1.7 Gpc.

The bursts detected from FRB 180301 had peak flux densities ranging from **5.3 – 94.1 mJy**

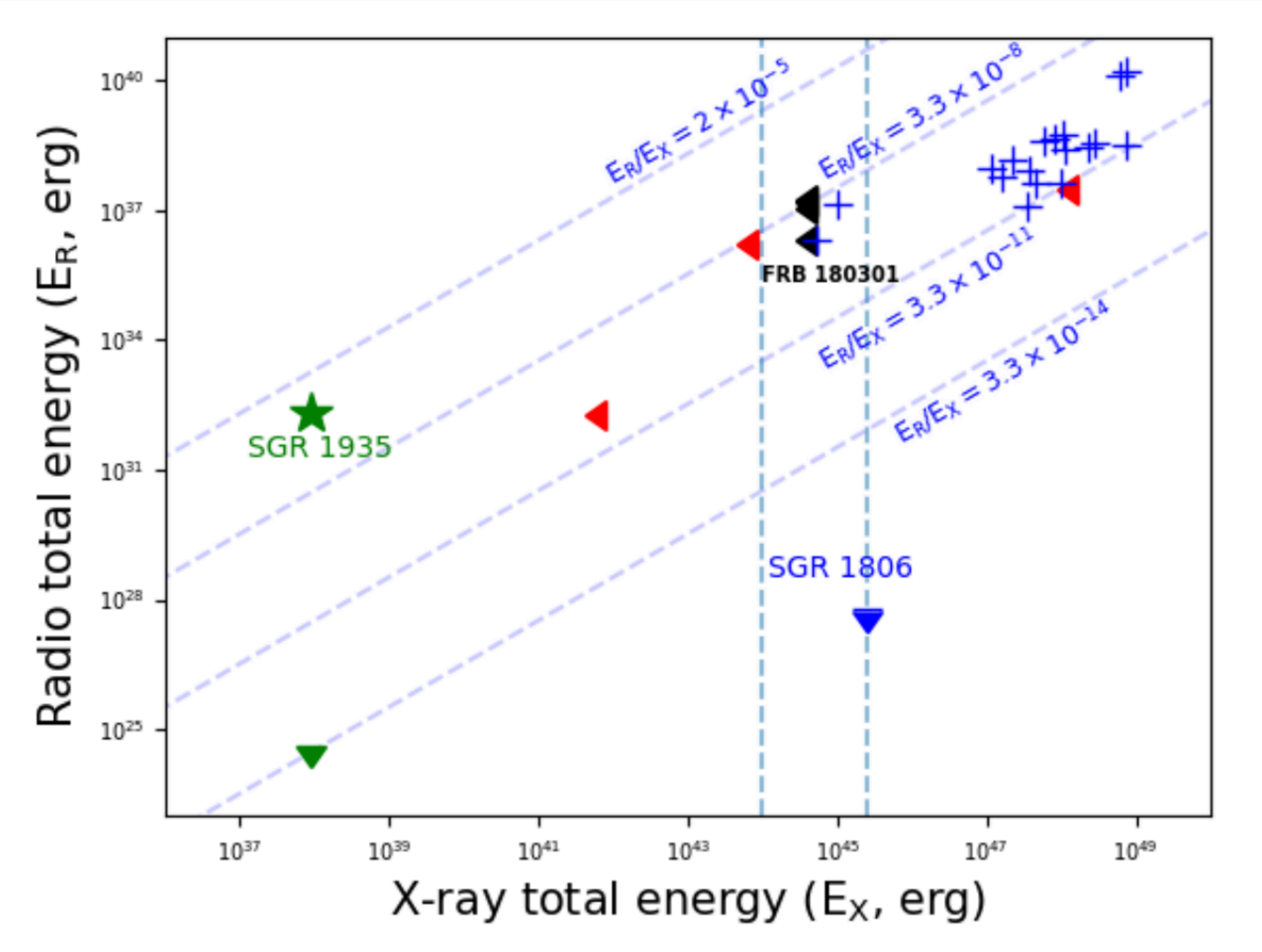

Laha et al. 2022

FRB 20190520B

FAST & Swift

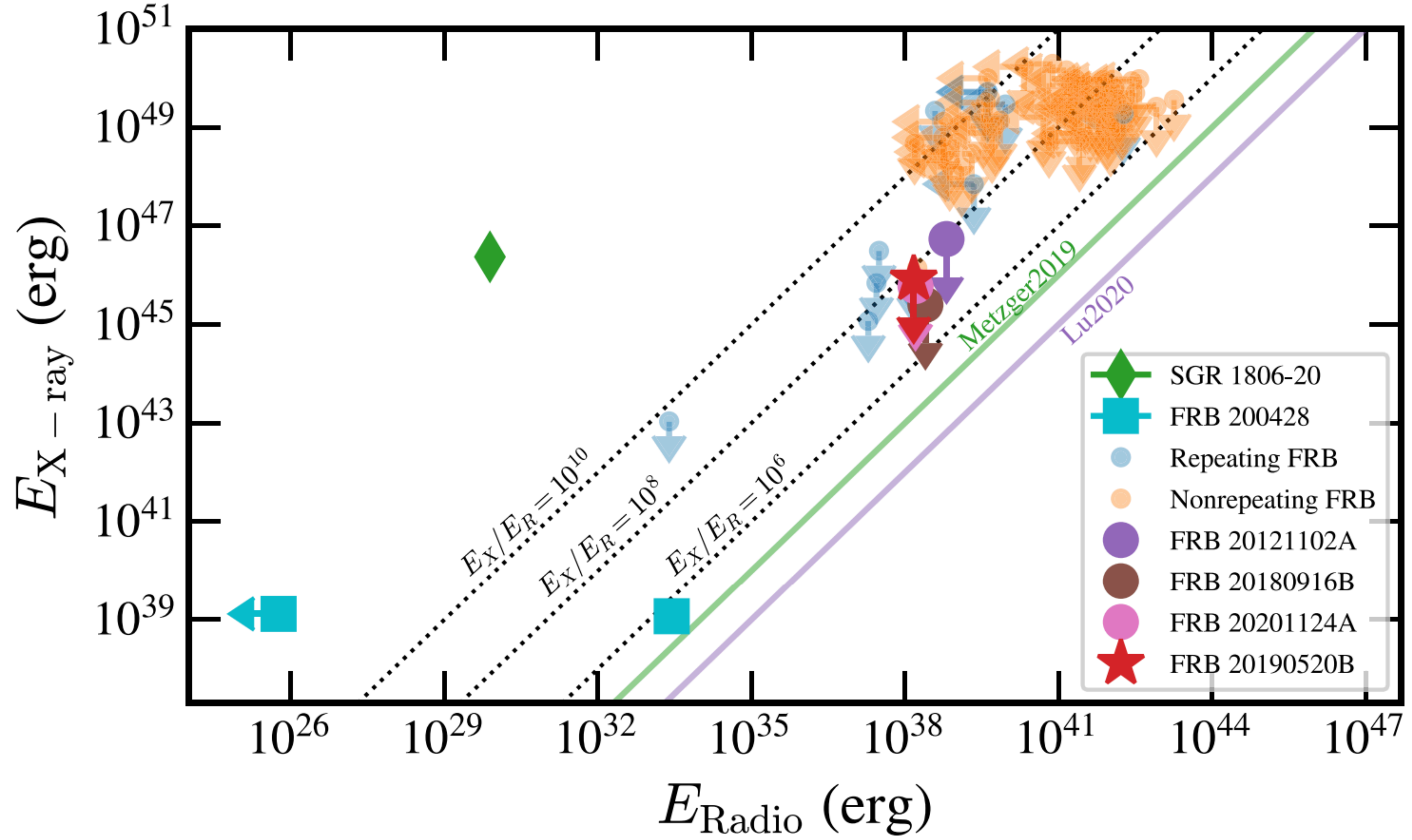

Figure 2. The relationship between X-ray and radio energy of bursts in the FRBs. The data, except for FRB 20190520B, are taken from P. Scholz et al. (2017), C. Guidorzi et al. (2020a), S. Laha et al. (2022). The green and purple lines are the model prediction from B. D. Metzger et al. (2019) and W. Lu et al. (2020), respectively. For many FRBs, the distances are constrained as upper limits, so the burst energy in both X-ray and radio bands is also an upper limit.

Yan et al. 2025

Table 1
Properties of the R-FRBs Considered in This Work

FRB Name (1)	DM_{exc} (pc cm^{-3}) (2)	l, b (deg) (3)	N_b (4)	Width (ms) (5)	f (Jy ms) (6)	z_s (Mpc) (7)
FRB 20200120E	18.0 (88.0)	142°.19, +41°.22	80	0.01–0.70	0.04–2.40	0.0008 (3.6)
FRB 20181030A	33.5 (103.7)	133°.40, +40°.92	9	0.59–1.43	4.50–7.30	0.004 (17.3)
FRB 20220912A	67.1 (222.1)	155°.41, +61°.81	1529	0.09–32.9	0.002–37.7	0.077 (343)
FRB 20180814A	72.4 (189.4)	136°.42, +16°.60	22	7.90–63.0	3.40–66.0	0.078 (347)
FRB 20190107B	73.1 (173.1)	127°.14, +21°.75	2	0.98	4.30	0.11 (500)
FRB 20200223B	125.5 (201.5)	118°.07, −33°.88	10	1.26–2.29	1.06–14.4	…
FRB 20180908B	127.8 (195.8)	124°.74, +42°.86	4	1.60–9.00	1.10–2.90	0.17 (800)
FRB 20180916B	150.7 (349.4)	129°.71, +3°.74	290	0.06–158	0.08–318	0.033 (150)
FRB 20181226F	152.1 (240.1)	129°.79, +26°.20	3	…	…	…
FRB 20190905A	153.3 (240.4)	124°.64, +26°.25	6	0.75–1.13	1.79–18.0	…
FRB 20190110C	156.3 (222.0)	65°.56, +42°.15	3	2.95	1.40	0.22 (1050)
FRB 20190303A	164.1 (223.1)	97°.48, +68°.94	38	0.89–7.20	0.78–10.4	0.064 (285)
FRB 20190812A	170.7 (249.1)	78°.05, +29°.83	2	0.42–0.60	0.65–13.0	…
FRB 20201130A	202.3 (288.3)	185°.33, −29°.15	12	0.47–6.55	1.31–20.4	…
FRB 20210323C	204.7 (285.2)	142°.59, +31°.54	11	0.83–5.00	2.32–7.60	…
FRB 20191105B	210.3 (313.8)	140°.59, +20°.40	2	0.55–0.71	2.70–19.7	…
FRB 20190113A	217.6 (426.5)	218°.04, +3°.43	3	1.82–3.03	5.70–9.40	0.29 (1450)
FRB 20190907A	226.8 (309.8)	173°.39, +32°.26	7	0.54–3.00	0.70–6.90	…
FRB 20201114A	253.9 (321.9)	111°.18, +42°.63	2	0.72–1.04	2.45–4.70	…
FRB 20201124A	257.6 (414.1)	177°.60, −8°.50	2883	0.91–316	0.005–640	0.098 (445)
FRB 20200127B	267.0 (351.0)	126°.63, +28°.02	2	0.45–0.61	4.70–7.70	…

Note. Column (1) lists the names of the FRB sources. Column (2) provides DM_{exc}, with the mean DM_{tot} given in parentheses. Column (3) shows the Galactic coordinates of the sources in degrees. Column (4) N_b indicates the total number of bursts observed to date for each source. Columns (5) and (6) give for each source the minimum and maximum burst widths in milliseconds and the minimum and maximum radio fluence values in Jy ms, respectively. Column (7) lists the spectroscopic redshift z_s associated with each source (where available), with the estimated luminosity distance (D_L) in Mpc in parentheses.

Casentini et al. 2025

Table 1
Properties of the R-FRBs Considered in This Work

FRB Name (1)	DM_{exc} ($pc\ cm^{-3}$) (2)	l, b (deg) (3)	N_b (4)	Width (ms) (5)	f (Jy ms) (6)	z_s (Mpc) (7)
FRB 20200120E	18.0 (88.0)	142°.19, +41°.22	80	0.01–0.70	0.04–2.40	0.0008 (3.6)
FRB 20181030A	33.5 (103.7)	133°.40, +40°.92	9	0.59–1.43	4.50–7.30	0.004 (17.3)
FRB 20220912A	67.1 (222.1)	155°.41, +61°.81	1529	0.09–32.9	0.002–37.7	0.077 (343)
FRB 20180814A	72.4 (189.4)	136°.42, +16°.60	22	7.90–63.0	3.40–66.0	0.078 (347)
FRB 20190107B	73.1 (173.1)	127°.14, +21°.75	2	0.98	4.30	0.11 (500)
FRB 20200223B	125.5 (201.5)	118°.07, −33°.88	10	1.26–2.29	1.06–14.4	…
FRB 20180908B	127.8 (195.8)	124°.74, +42°.86	4	1.60–9.00	1.10–2.90	0.17 (800)
FRB 20180916B	150.7 (349.4)	129°.71, +3°.74	290	0.06–158	0.08–318	0.033 (150)
FRB 20181226F	152.1 (240.1)	129°.79, +26°.20	3	…	…	…
FRB 20190905A	153.3 (240.4)	124°.64, +26°.25	6	0.75–1.13	1.79–18.0	…
FRB 20190110C	156.3 (222.0)	65°.56, +42°.15	3	2.95	1.40	0.22 (1050)
FRB 20190303A	164.1 (223.1)	97°.48, +68°.94	38	0.89–7.20	0.78–10.4	0.064 (285)
FRB 20190812A	170.7 (249.1)	78°.05, +29°.83	2	0.42–0.60	0.65–13.0	…
FRB 20201130A	202.3 (288.3)	185°.33, −29°.15	12	0.47–6.55	1.31–20.4	…
FRB 20210323C	204.7 (285.2)	142°.59, +31°.54	11	0.83–5.00	2.32–7.60	…
FRB 20191105B	210.3 (313.8)	140°.59, +20°.40	2	0.55–0.71	2.70–19.7	…
FRB 20190113A	217.6 (426.5)	218°.04, +3°.43	3	1.82–3.03	5.70–9.40	0.29 (1450)
FRB 20190907A	226.8 (309.8)	173°.39, +32°.26	7	0.54–3.00	0.70–6.90	…
FRB 20201114A	253.9 (321.9)	111°.18, +42°.63	2	0.72–1.04	2.45–4.70	…
FRB 20201124A	257.6 (414.1)	177°.60, −8°.50	2883	0.91–316	0.005–640	0.098 (445)
FRB 20200127B	267.0 (351.0)	126°.63, +28°.02	2	0.45–0.61	4.70–7.70	…

Note. Column (1) lists the names of the FRB sources. Column (2) provides DM_{exc}, with the mean DM_{tot} given in parentheses. Column (3) shows the Galactic coordinates of the sources in degrees. Column (4) N_b indicates the total number of bursts observed to date for each source. Columns (5) and (6) give for each source the minimum and maximum burst widths in milliseconds and the minimum and maximum radio fluence values in Jy ms, respectively. Column (7) lists the spectroscopic redshift z_s associated with each source (where available), with the estimated luminosity distance (D_L) in Mpc in parentheses.

Casentini et al. 2025

FRB 181030

Table 2

AGILE/GRID Flux ULs for the Radio Burst F, G of Source 1 and Burst A of Source 2, as a Function of Integration Timescales

Name	$T_0 + 10^1$ s[a]	$T_0 + 10^2$ s[a]	$T_0 + 10^3$ s[a]	$T_0 + 10^0$ day[a]	$T_0 + 10^1$ day[a]	$T_0 + 10^2$ day[a]
Source 1-F	4.0×10^{-7}	3.6×10^{-8}	1.5×10^{-8}	4.1×10^{-10}	1.1×10^{-10}	3.9×10^{-11}
Source 1-G	1.7×10^{-6}	3.4×10^{-8}	1.6×10^{-8}	4.1×10^{-10}	1.1×10^{-10}	4.0×10^{-11}
Source 2-A	2.7×10^{-7}[b]	4.7×10^{-8}[b]	1.0×10^{-8}	7.3×10^{-10}	5.3×10^{-11}	1.8×10^{-11}

Notes.

[a] 3σ flux ULs (erg cm^{-2} s^{-1}) obtained for emission in the range 50 MeV–10 GeV for the short integration timescales and 100 MeV–10 GeV for the long ones, at each source position.

[b] The first two ULs of Source 2 are evaluated on intervals [+390, +400] s and [+390, +490] s, respectively. These two intervals start as the source enters the exposed region during the *AGILE* spinning revolution.

Casentini et al. 2020

Table 1
Properties of the R-FRBs Considered in This Work

FRB Name (1)	DM_{exc} (pc cm^{-3}) (2)	l, b (deg) (3)	N_b (4)	Width (ms) (5)	f (Jy ms) (6)	z_s (Mpc) (7)
FRB 20200120E	18.0 (88.0)	142°.19, +41°.22	80	0.01–0.70	0.04–2.40	0.0008 (3.6)
FRB 20181030A	33.5 (103.7)	133°.40, +40°.92	9	0.59–1.43	4.50–7.30	0.004 (17.3)
FRB 20220912A	67.1 (222.1)	155°.41, +61°.81	1529	0.09–32.9	0.002–37.7	0.077 (343)
FRB 20180814A	72.4 (189.4)	136°.42, +16°.60	22	7.90–63.0	3.40–66.0	0.078 (347)
FRB 20190107B	73.1 (173.1)	127°.14, +21°.75	2	0.98	4.30	0.11 (500)
FRB 20200223B	125.5 (201.5)	118°.07, −33°.88	10	1.26–2.29	1.06–14.4	⋯
FRB 20180908B	127.8 (195.8)	124°.74, +42°.86	4	1.60–9.00	1.10–2.90	0.17 (800)
FRB 20180916B	150.7 (349.4)	129°.71, +3°.74	290	0.06–158	0.08–318	0.033 (150)
FRB 20181226F	152.1 (240.1)	129°.79, +26°.20	3	⋯	⋯	⋯
FRB 20190905A	153.3 (240.4)	124°.64, +26°.25	6	0.75–1.13	1.79–18.0	⋯
FRB 20190110C	156.3 (222.0)	65°.56, +42°.15	3	2.95	1.40	0.22 (1050)
FRB 20190303A	164.1 (223.1)	97°.48, +68°.94	38	0.89–7.20	0.78–10.4	0.064 (285)
FRB 20190812A	170.7 (249.1)	78°.05, +29°.83	2	0.42–0.60	0.65–13.0	⋯
FRB 20201130A	202.3 (288.3)	185°.33, −29°.15	12	0.47–6.55	1.31–20.4	⋯
FRB 20210323C	204.7 (285.2)	142°.59, +31°.54	11	0.83–5.00	2.32–7.60	⋯
FRB 20191105B	210.3 (313.8)	140°.59, +20°.40	2	0.55–0.71	2.70–19.7	⋯
FRB 20190113A	217.6 (426.5)	218°.04, +3°.43	3	1.82–3.03	5.70–9.40	0.29 (1450)
FRB 20190907A	226.8 (309.8)	173°.39, +32°.26	7	0.54–3.00	0.70–6.90	⋯
FRB 20201114A	253.9 (321.9)	111°.18, +42°.63	2	0.72–1.04	2.45–4.70	⋯
FRB 20201124A	257.6 (414.1)	177°.60, −8°.50	2883	0.91–316	0.005–640	0.098 (445)
FRB 20200127B	267.0 (351.0)	126°.63, +28°.02	2	0.45–0.61	4.70–7.70	⋯

Note. Column (1) lists the names of the FRB sources. Column (2) provides DM_{exc}, with the mean DM_{tot} given in parentheses. Column (3) shows the Galactic coordinates of the sources in degrees. Column (4) N_b indicates the total number of bursts observed to date for each source. Columns (5) and (6) give for each source the minimum and maximum burst widths in milliseconds and the minimum and maximum radio fluence values in Jy ms, respectively. Column (7) lists the spectroscopic redshift z_s associated with each source (where available), with the estimated luminosity distance (D_L) in Mpc in parentheses.

Casentini et al. 2025

FRB 20220912A

AGILE, Swift

Table 4. *AGILE* FRB 20220912A bursts coverage and MCAL ULs.

Burst ID	MCAL FoV	MCAL D.A.	GRID FoV	UL (3σ) [erg cm^{-2}]	MCAL trigger FAR [evt/hour]	UL 1 ms [erg cm^{-2}]
B01				Idle mode		
B02	Yes	No	No	–	–	3.22×10^{-8}
B03				Idle mode		
B04	Yes	No	No	–	–	2.59×10^{-8}
B05	Yes	No	Yes	–	–	1.84×10^{-8}
B06	Yes	No	No	–	–	5.15×10^{-8}
B07				No data		
B08	Yes	No	No	–	–	4.22×10^{-8}
B09	Yes	Yes	No	2.06×10^{-7}	~4.0	–
B10	Yes	Yes	No	2.04×10^{-7}	~4.0	–
B11	Yes	Yes	No	2.00×10^{-7}	~4.0	–
B12	Yes	No	No	–	–	2.17×10^{-8}
B13				Idle mode		
B14				Idle mode		
B15	Yes	No	Yes	–	–	1.83×10^{-8}
B16				No data		

Table 5. Swift exposures and flux ULs (0.3 – 10 keV).

Start time	Stop time (UTC)	UL [erg cm^{-2} s^{-1}]
2022-11-11 19:26:15	2022-11-20 18:29:56	2.3×10^{-13}
2023-07-25 00:09:32	2023-07-30 02:47:55	2.5×10^{-13}
2023-08-29 21:26:07	2023-09-09 21:01:56	2.1×10^{-13}
2023-09-29 22:27:14	2023-10-05 21:30:56	4.9×10^{-13}

Pelliciari et al. 2024

FRB 20220912A

XMM, NICER, Swift

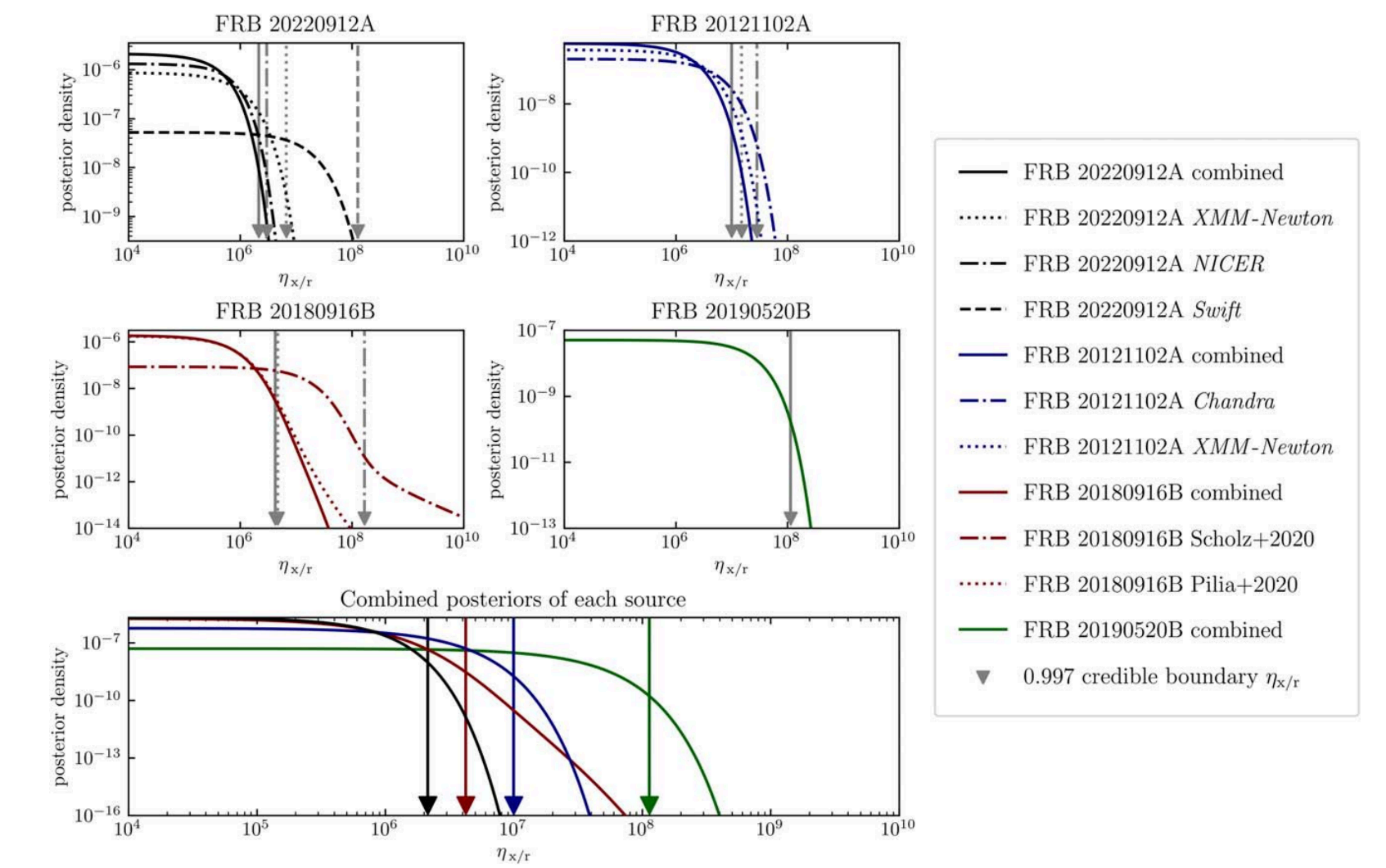

Cook et al. 2024

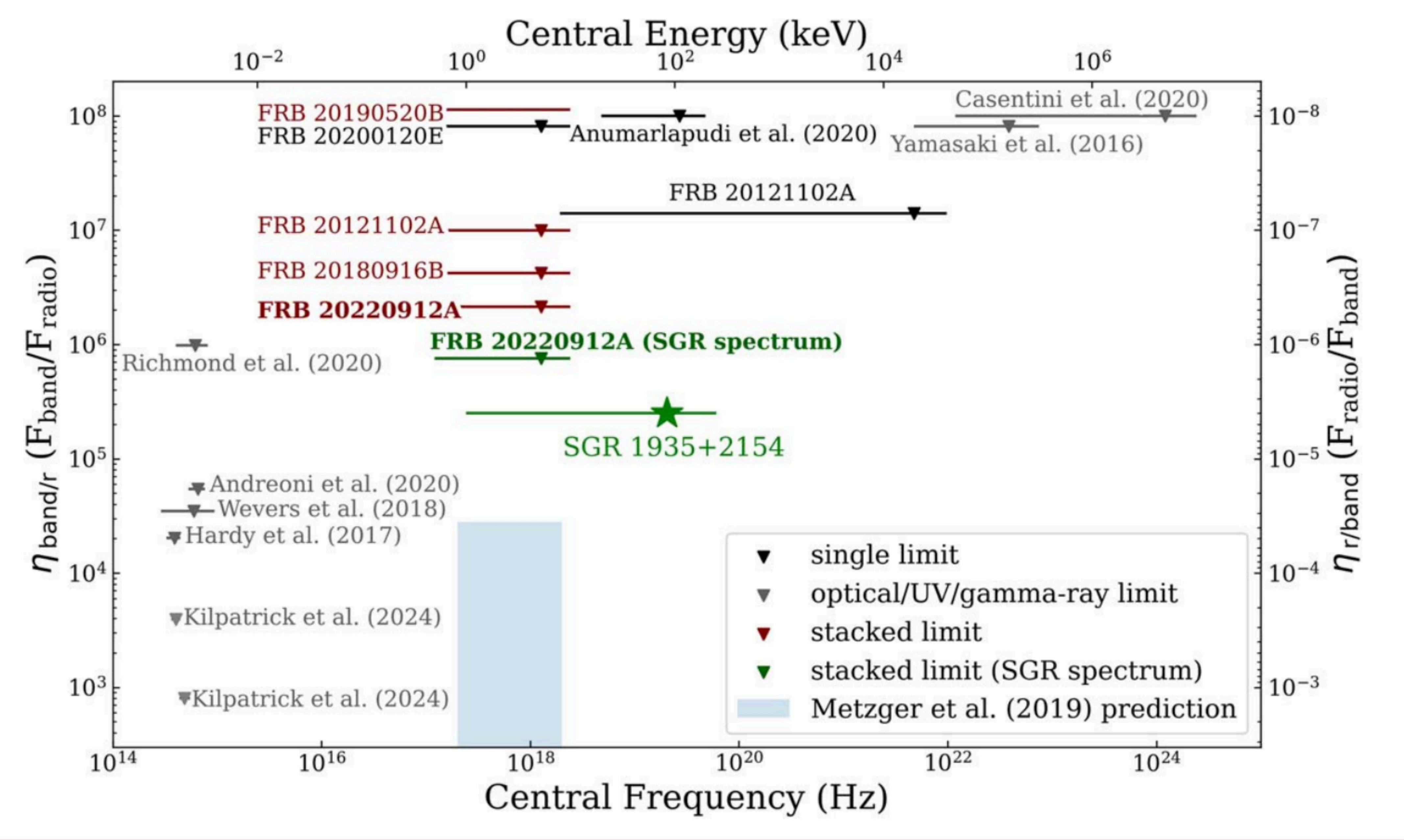

We detect no significant X-ray emission at the time of 30 radio bursts with upper limits on a 0.5–10.0 keV X-ray fluence of (1.5–14.5) × 10−10 erg cm−2 (99.7% credible interval, unabsorbed) on a timescale of 100 ms. Translated into a fluence ratio $\eta_{x/r} = F_{X\text{-ray}}/F_{radio}$, this corresponds to **$\eta_{x/r} < 7 \times 10^6$** . We derive a hierarchical extension to the standard Bayesian treatment of low-count and background contaminated X-ray data, which allows the robust combination of multiple observations. **This methodology allows us to place the best (lowest) 99.7% credible interval upper limit on an FRB $\eta_{x/r}$ to date, $\eta_{x/r} < 2 \times 10^6$** , assuming that all 30 detected radio bursts are associated with X-ray bursts with the same fluence ratio.

Table 1
Properties of the R-FRBs Considered in This Work

FRB Name (1)	DM_{exc} (pc cm^{-3}) (2)	l, b (deg) (3)	N_b (4)	Width (ms) (5)	f (Jy ms) (6)	z_s (Mpc) (7)
FRB 20200120E	18.0 (88.0)	142°19, +41°22	80	0.01–0.70	0.04–2.40	0.0008 (3.6)
FRB 20181030A	33.5 (103.7)	133°40, +40°92	9	0.59–1.43	4.50–7.30	0.004 (17.3)
FRB 20220912A	67.1 (222.1)	155°41, +61°81	1529	0.09–32.9	0.002–37.7	0.077 (343)
FRB 20180814A	72.4 (189.4)	136°42, +16°60	22	7.90–63.0	3.40–66.0	0.078 (347)
FRB 20190107B	73.1 (173.1)	127°14, +21°75	2	0.98	4.30	0.11 (500)
FRB 20200223B	125.5 (201.5)	118°07, −33°88	10	1.26–2.29	1.06–14.4	…
FRB 20180908B	127.8 (195.8)	124°74, +42°86	4	1.60–9.00	1.10–2.90	0.17 (800)
FRB 20180916B	150.7 (349.4)	129°71, +3°74	290	0.06–158	0.08–318	0.033 (150)
FRB 20181226F	152.1 (240.1)	129°79, +26°20	3	…	…	…
FRB 20190905A	153.3 (240.4)	124°64, +26°25	6	0.75–1.13	1.79–18.0	…
FRB 20190110C	156.3 (222.0)	65°56, +42°15	3	2.95	1.40	0.22 (1050)
FRB 20190303A	164.1 (223.1)	97°48, +68°94	38	0.89–7.20	0.78–10.4	0.064 (285)
FRB 20190812A	170.7 (249.1)	78°05, +29°83	2	0.42–0.60	0.65–13.0	…
FRB 20201130A	202.3 (288.3)	185°33, −29°15	12	0.47–6.55	1.31–20.4	…
FRB 20210323C	204.7 (285.2)	142°59, +31°54	11	0.83–5.00	2.32–7.60	…
FRB 20191105B	210.3 (313.8)	140°59, +20°40	2	0.55–0.71	2.70–19.7	…
FRB 20190113A	217.6 (426.5)	218°04, +3°43	3	1.82–3.03	5.70–9.40	0.29 (1450)
FRB 20190907A	226.8 (309.8)	173°39, +32°26	7	0.54–3.00	0.70–6.90	…
FRB 20201114A	253.9 (321.9)	111°18, +42°63	2	0.72–1.04	2.45–4.70	…
FRB 20201124A	257.6 (414.1)	177°60, −8°50	2883	0.91–316	0.005–640	0.098 (445)
FRB 20200127B	267.0 (351.0)	126°63, +28°02	2	0.45–0.61	4.70–7.70	…

Note. Column (1) lists the names of the FRB sources. Column (2) provides DM_{exc}, with the mean DM_{tot} given in parentheses. Column (3) shows the Galactic coordinates of the sources in degrees. Column (4) N_b indicates the total number of bursts observed to date for each source. Columns (5) and (6) give for each source the minimum and maximum burst widths in milliseconds and the minimum and maximum radio fluence values in Jy ms, respectively. Column (7) lists the spectroscopic redshift z_s associated with each source (where available), with the estimated luminosity distance (D_L) in Mpc in parentheses.

Casentini et al. 2025

FRB 20201124A

Table H.1. Limits on X-ray burst energy associated with FRBs.

FRB	E_{XRB} [erg]	$E_{XRB,N}$ [erg]	N_{FRB}	Ref.
20121102A	$\lesssim 4 \times 10^{46}$	$\lesssim 4 \times 10^{45}$	10	1
20180916B	$\lesssim 1.6 \times 10^{45}$	$\lesssim 1.6 \times 10^{45}$	1	2
20201124A	$\lesssim 6 \times 10^{45}$	$\lesssim 1.1 \times 10^{44}$	49	3

References. (1) Scholz et al. (2017); (2) Scholz et al. (2020); (3) this work

Piro et al. 2021

Table 1. Overview of the three brightest bursts detected within our MWL campaign.

Burst-ID	TOA [a] [MJD]	Fluence [b] [Jy ms]	Bandwidth [c] [MHz]	Radio burst [d] Fluence [erg cm^{-2}]	Radio burst [e] Energy [erg]	X-ray burst [f] Fluence [erg cm^{-2}]	Fluence ratio [g] $\eta_{x/r}$
B1	60453.093476719	1.55	881	1.4×10^{-17}	5.8×10^{38}	$<3.4 \times 10^{-11}$	$<2.4 \times 10^{6}$
B2	60453.103822424	0.38	2015	7.6×10^{-18}	3.2×10^{38}	$<3.4 \times 10^{-11}$	$<4.5 \times 10^{6}$
B3	60453.186311513	0.63	830	5.2×10^{-18}	2.2×10^{38}	$<3.4 \times 10^{-11}$	$<6.5 \times 10^{6}$

Eppel et al. 2025

Using a blackbody model like Cook et al. (2024), the limit from burst B1 transforms to $\eta x/r < 8.5\times10^{6}$ at 0.5–10 keV. This is comparable to the lowest single burst limits found for FRB 20220912A and FRB 20180916B.

Coincident gamma-ray emission in the direction of the active repeater FRB 20240114A

ATel #16594; *Yi Xing, Wenfei Yu (Shanghai Astronomical Observatory)*
on **19 Apr 2024; 02:56 UT**
Credential Certification: Wenfei Yu (wenfei@shao.ac.cn)

Subjects: Radio, Gamma Ray, Transient, Fast Radio Burst

Referred to by ATel #: 16602, 16630, 16695

1. The 2024 Fermi LAT light curve (5 day averaged)

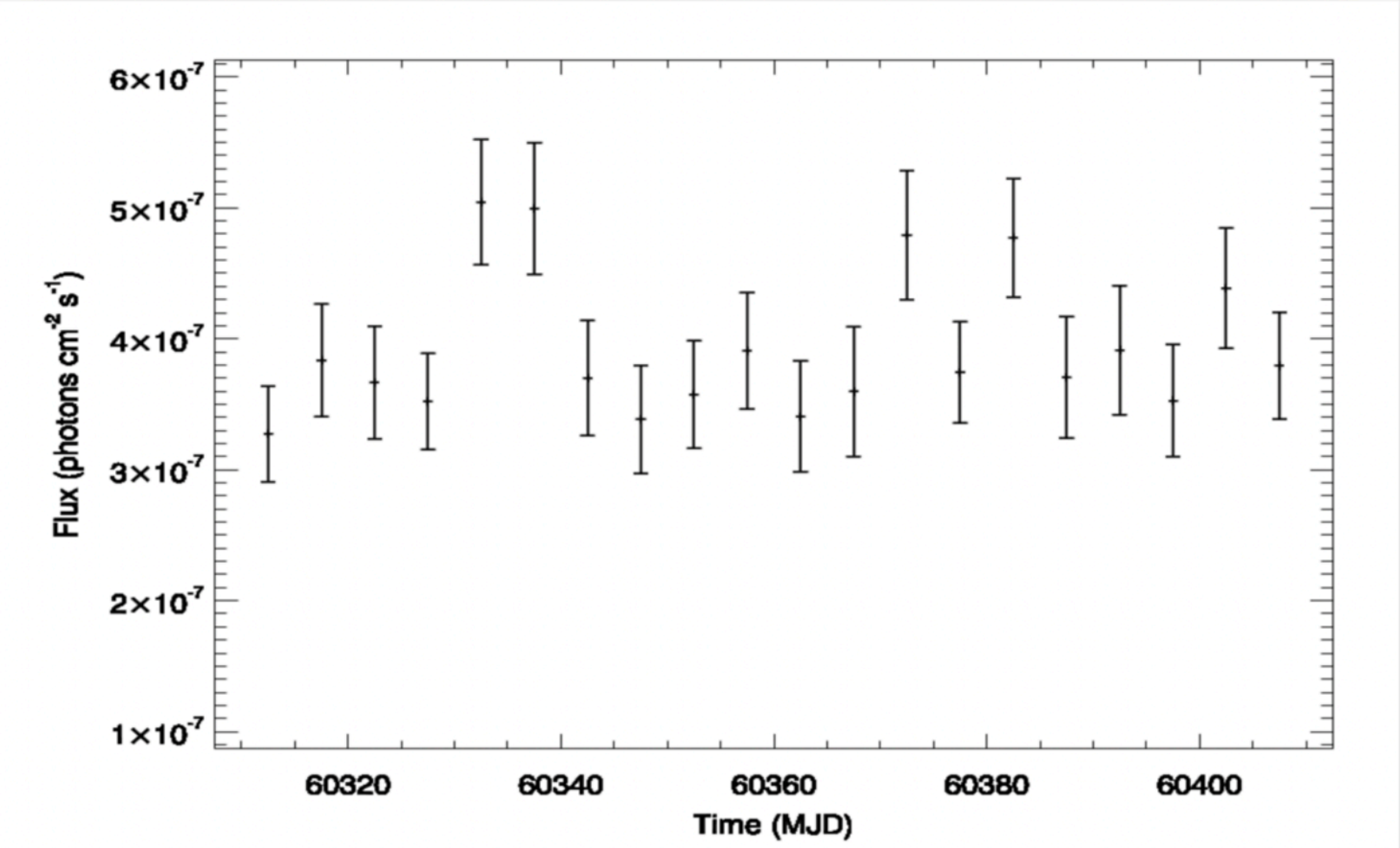

2. The 2023 Fermi LAT light curve (5 day averaged)

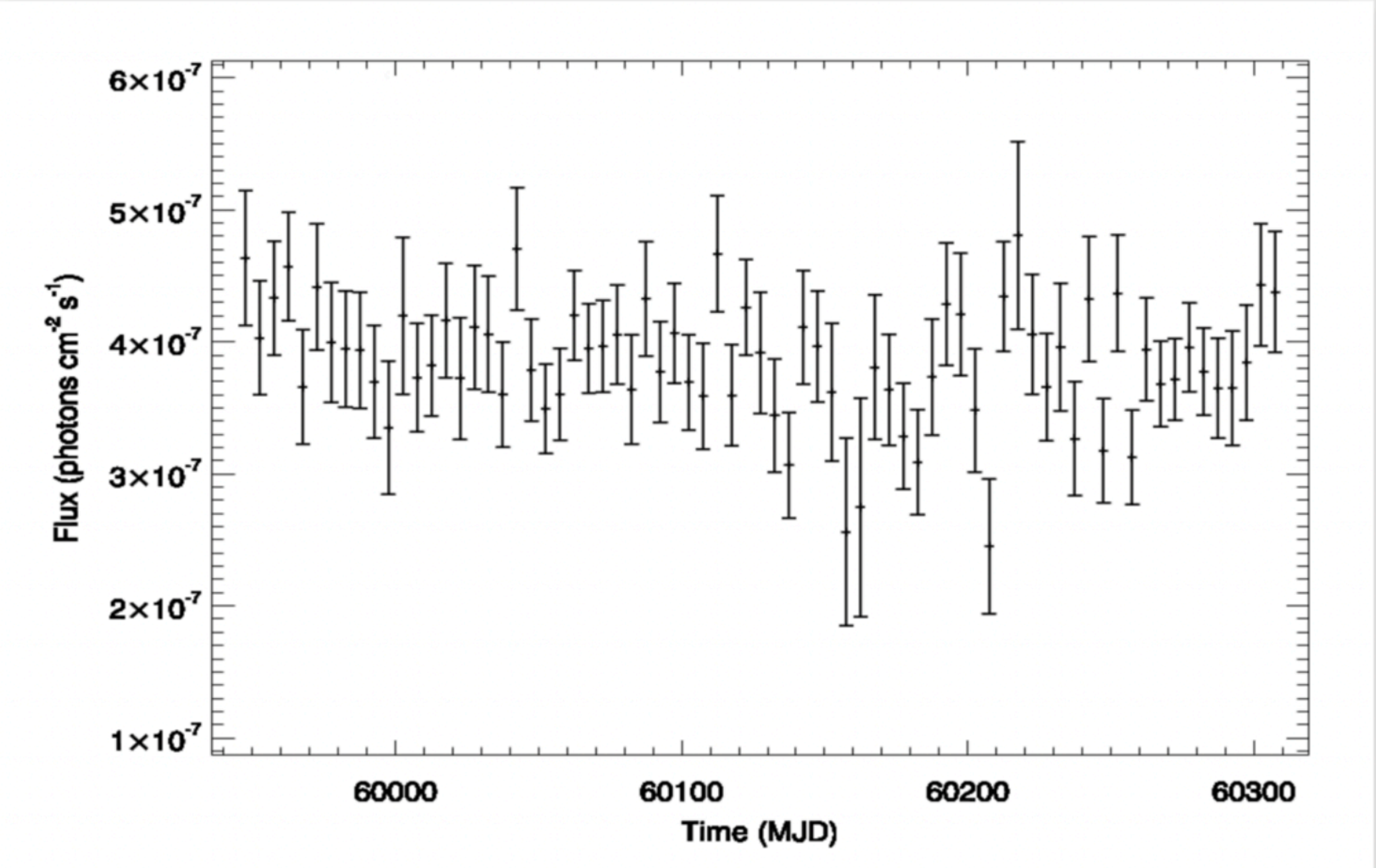

The Fermi Team does not confirm the detection

FRB 20240114A: No counterpart candidate in Fermi-LAT observations

ATel #16602; *G. Principe (University and INFN Trieste), M. Negro (Louisiana State University) N. Di Lalla (Stanford University), N. Omodei (Stanford University), G. Marti-Devesa (University and INFN Trieste), Z. Wadiasingh (University of Maryland College Park, NASA/GSFC), F. Longo (University and INFN Trieste), report on behalf of the Fermi-LAT Collaboration*

*on **26 Apr 2024; 18:15 UT***

Credential Certification: Giacomo Principe (giacomo.principe@inaf.it)

Subjects: Radio, Gamma Ray, Fast Radio Burst

X Post

We have searched data collected by the Fermi Large Area Telescope (LAT) from January to March 2024, for possible high-energy (E > 100 MeV) gamma-ray emission in spatial/temporal coincidence with the repeating FRB 20240114A (ATel #16420) and its extreme radio burst activity (bright bursts - ATel #16432; burst storm - ATel #16505; more than a hundred bright bursts - ATel #16565, GCN 27388).

We performed a search for transient gamma-ray emission from the precise FRB position reported by the EVN (ATel #16542). We used different time windows (from tens of seconds up to few months) around all the events reported so far for the repeating FRB 20240114A. Contrary to what was reported in ATel #16594, we found no significance gamma-ray emission.

Table 1
Properties of the R-FRBs Considered in This Work

FRB Name (1)	DM_{exc} ($pc\ cm^{-3}$) (2)	l, b (deg) (3)	N_b (4)	Width (ms) (5)	f (Jy ms) (6)	z_s (Mpc) (7)
FRB 20200120E	18.0 (88.0)	142°19, +41°22	80	0.01–0.70	0.04–2.40	0.0008 (3.6)
FRB 20181030A	33.5 (103.7)	133°40, +40°92	9	0.59–1.43	4.50–7.30	0.004 (17.3)
FRB 20220912A	67.1 (222.1)	155°41, +61°81	1529	0.09–32.9	0.002–37.7	0.077 (343)
FRB 20180814A	72.4 (189.4)	136°42, +16°60	22	7.90–63.0	3.40–66.0	0.078 (347)
FRB 20190107B	73.1 (173.1)	127°14, +21°75	2	0.98	4.30	0.11 (500)
FRB 20200223B	125.5 (201.5)	118°07, −33°88	10	1.26–2.29	1.06–14.4	…
FRB 20180908B	127.8 (195.8)	124°74, +42°86	4	1.60–9.00	1.10–2.90	0.17 (800)
FRB 20180916B	150.7 (349.4)	129°71, +3°74	290	0.06–158	0.08–318	0.033 (150)
FRB 20181226F	152.1 (240.1)	129°79, +26°20	3	…	…	…
FRB 20190905A	153.3 (240.4)	124°64, +26°25	6	0.75–1.13	1.79–18.0	…
FRB 20190110C	156.3 (222.0)	65°56, +42°15	3	2.95	1.40	0.22 (1050)
FRB 20190303A	164.1 (223.1)	97°48, +68°94	38	0.89–7.20	0.78–10.4	0.064 (285)
FRB 20190812A	170.7 (249.1)	78°05, +29°83	2	0.42–0.60	0.65–13.0	…
FRB 20201130A	202.3 (288.3)	185°33, −29°15	12	0.47–6.55	1.31–20.4	…
FRB 20210323C	204.7 (285.2)	142°59, +31°54	11	0.83–5.00	2.32–7.60	…
FRB 20191105B	210.3 (313.8)	140°59, +20°40	2	0.55–0.71	2.70–19.7	…
FRB 20190113A	217.6 (426.5)	218°04, +3°43	3	1.82–3.03	5.70–9.40	0.29 (1450)
FRB 20190907A	226.8 (309.8)	173°39, +32°26	7	0.54–3.00	0.70–6.90	…
FRB 20201114A	253.9 (321.9)	111°18, +42°63	2	0.72–1.04	2.45–4.70	…
FRB 20201124A	257.6 (414.1)	177°60, −8°50	2883	0.91–316	0.005–640	0.098 (445)
FRB 20200127B	267.0 (351.0)	126°63, +28°02	2	0.45–0.61	4.70–7.70	…

Note. Column (1) lists the names of the FRB sources. Column (2) provides DM_{exc}, with the mean DM_{tot} given in parentheses. Column (3) shows the Galactic coordinates of the sources in degrees. Column (4) N_b indicates the total number of bursts observed to date for each source. Columns (5) and (6) give for each source the minimum and maximum burst widths in milliseconds and the minimum and maximum radio fluence values in Jy ms, respectively. Column (7) lists the spectroscopic redshift z_s associated with each source (where available), with the estimated luminosity distance (D_L) in Mpc in parentheses.

Casentini et al. 2025

FRB 20200120E

XMM & Nicer

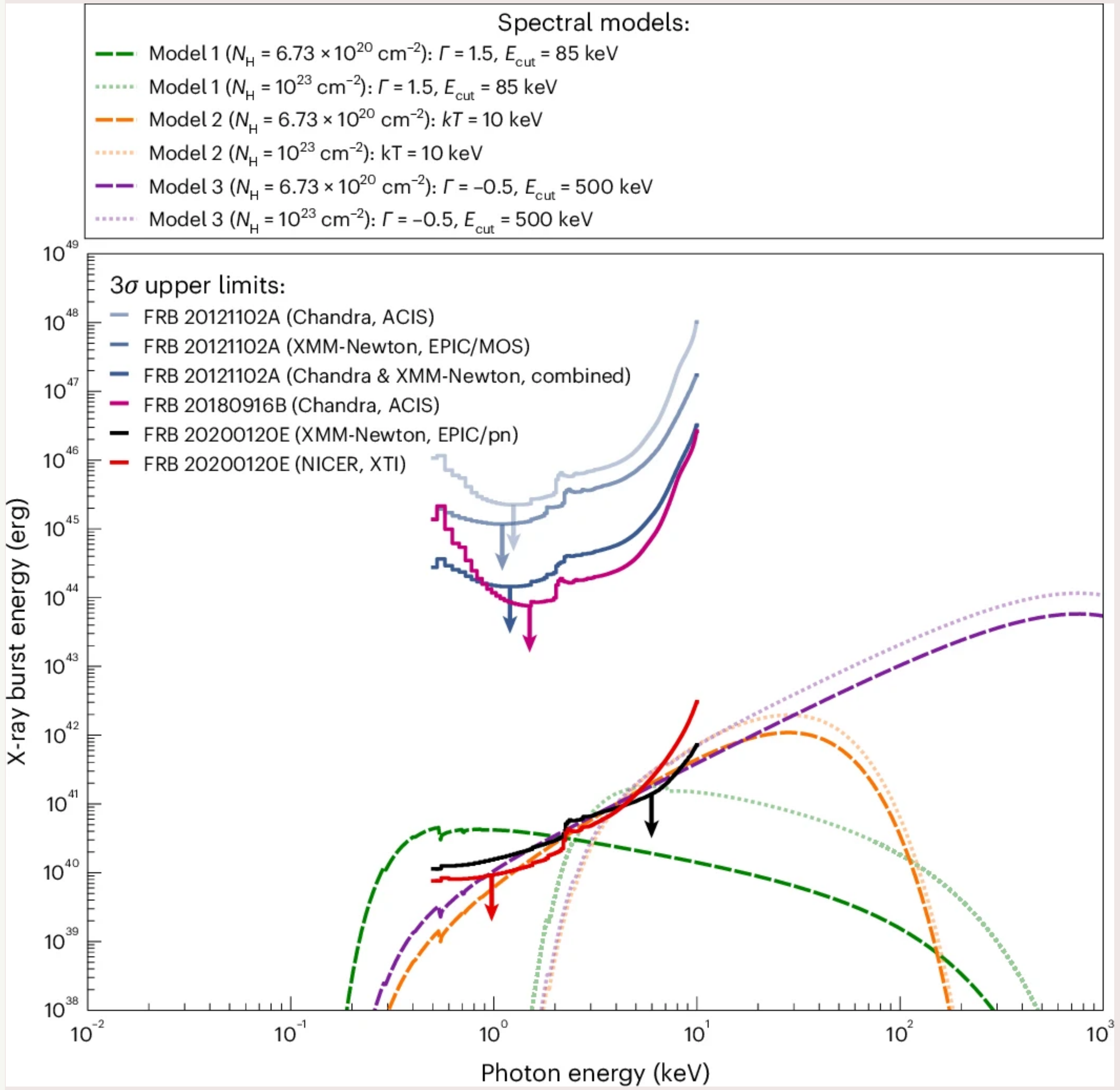

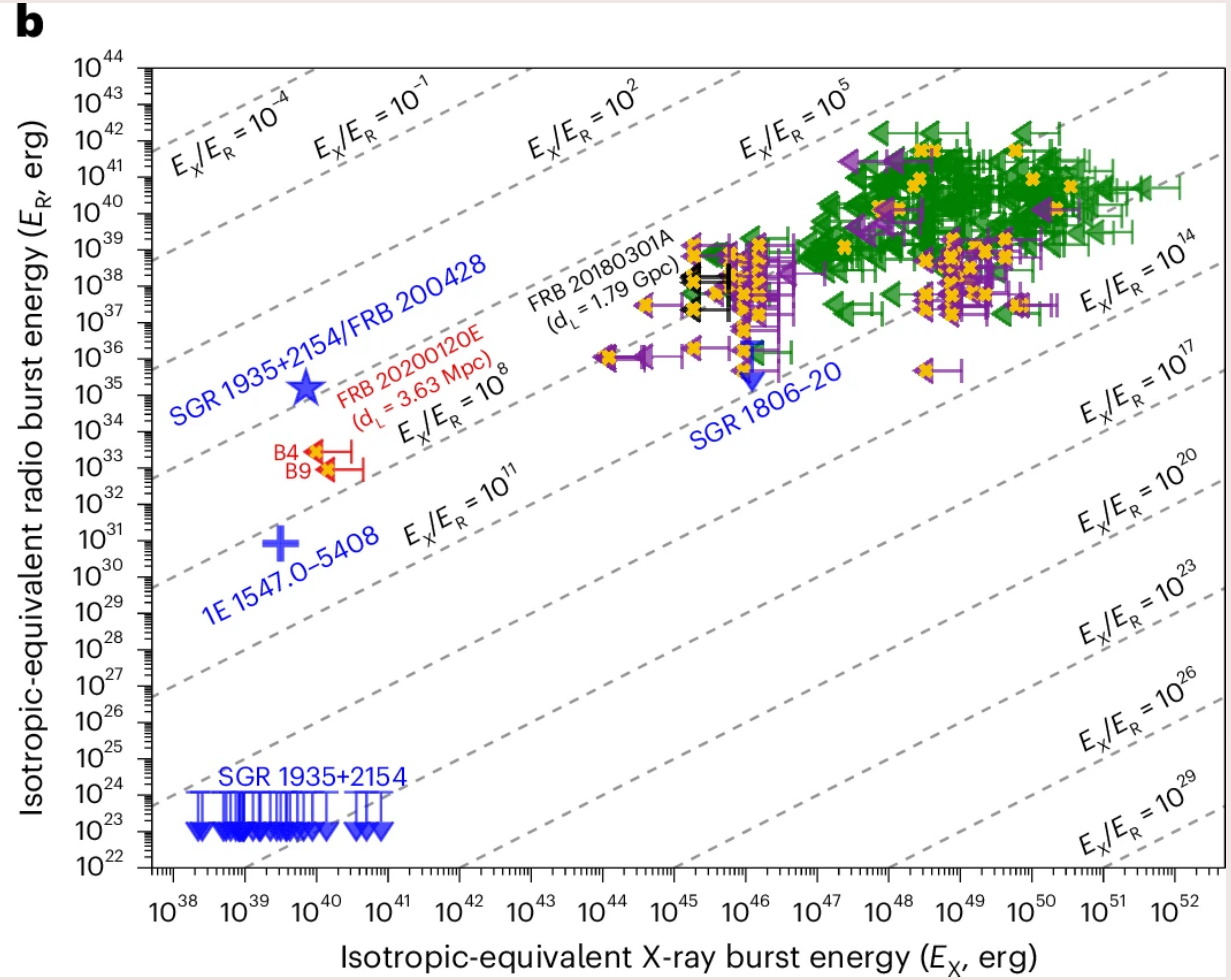

Pearlman et al. 2024

Untargeted searches

Archival X-ray and gamma-ray searches

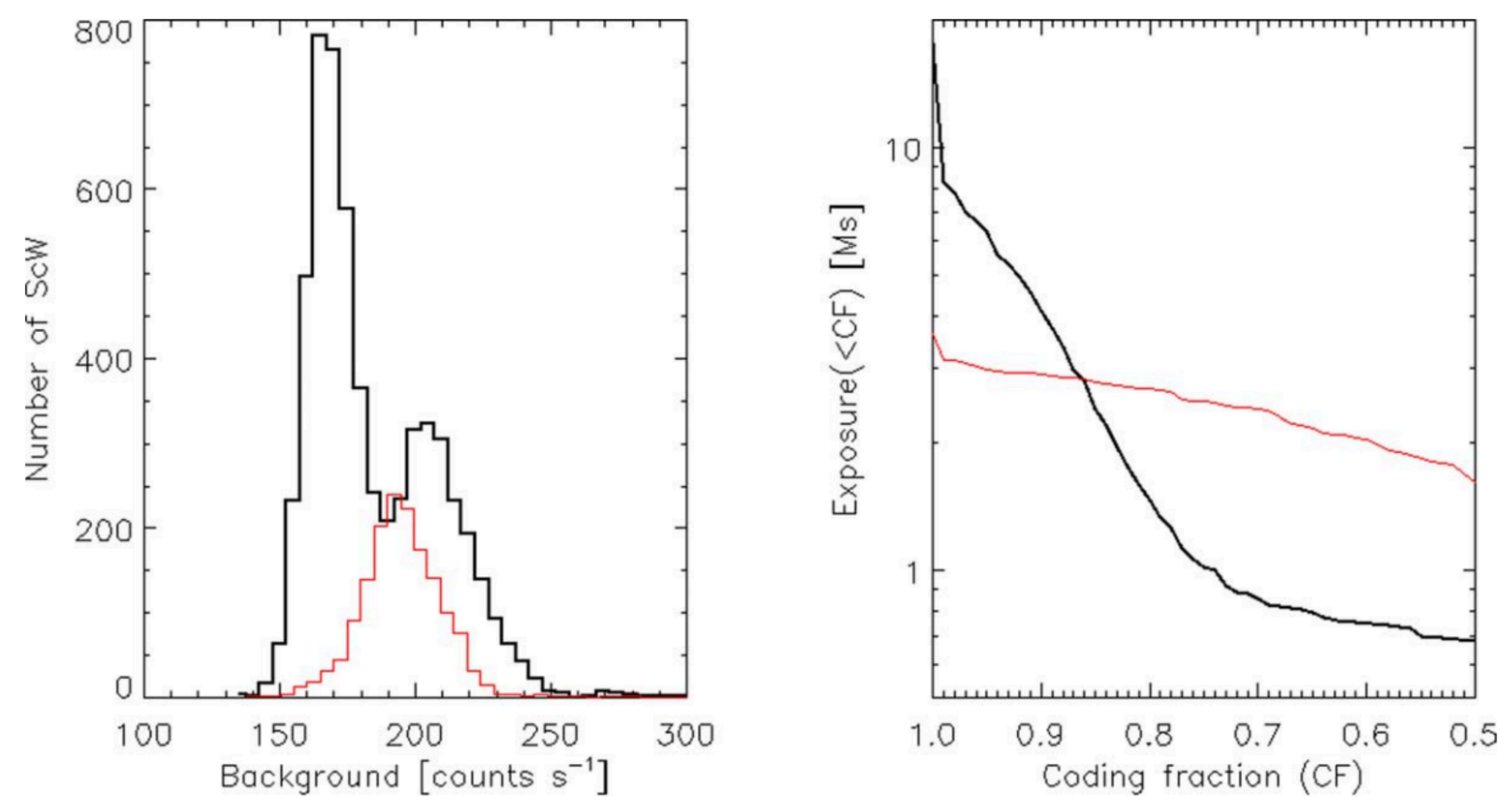

Figure 1. Left: distribution of background count rates (20–200 keV) of the ScW used in the search for bursts from FRB 20200120E (black) and in the observations of SGR 1806–20 used for comparison (red). The count rates have been corrected for the coding fraction (i.e., the fraction of detector area over which the photons coming from the source direction are modulated by the coded mask aperture pattern). Right: distribution of net exposure time as a function of coding fraction for FRB 20200120E (black) and for SGR 1806–20 (red).

Mereghetti et al. 2021

Archival X-ray and gamma-ray searches

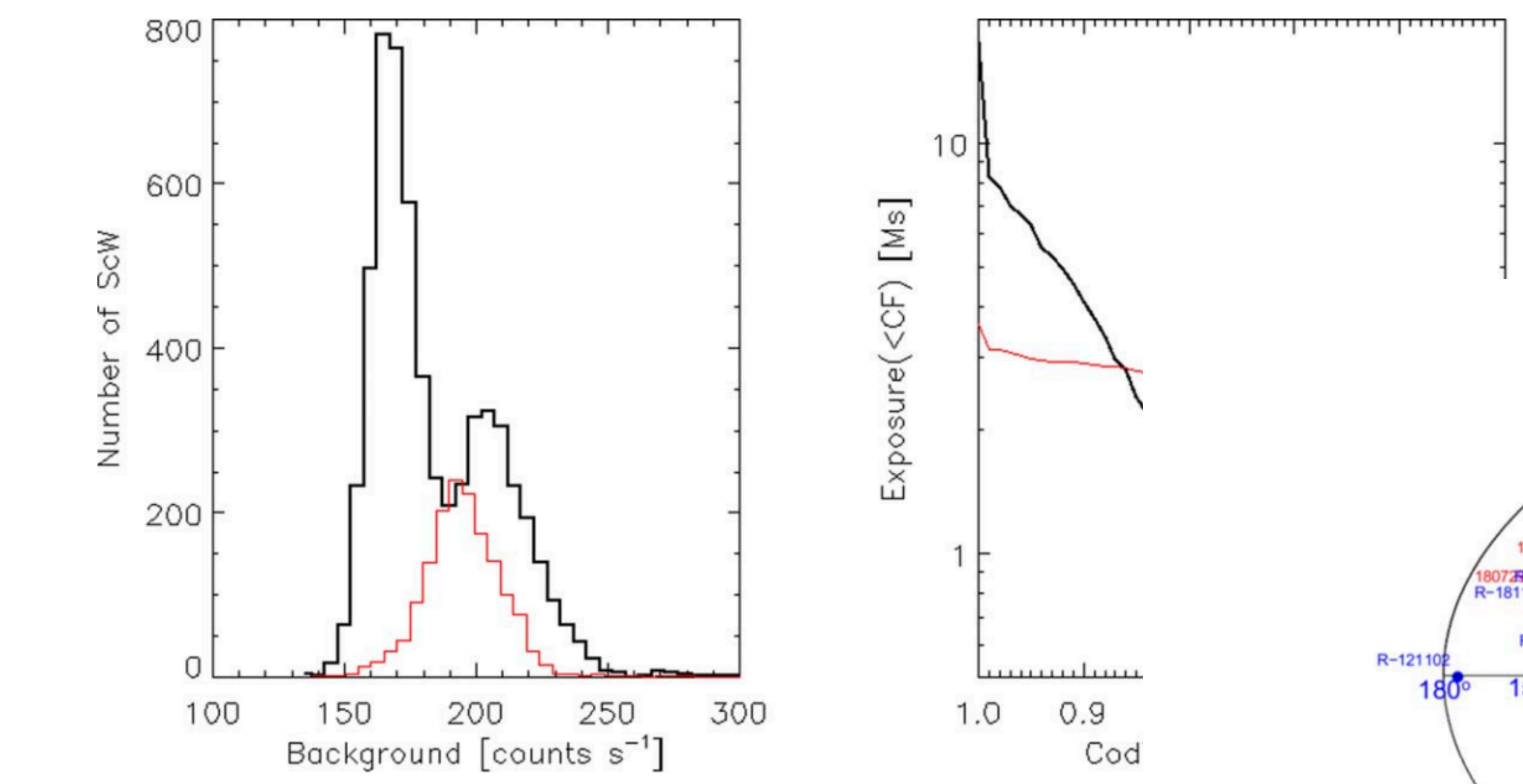

Figure 1. Left: distribution of background count rates (20–200 keV) of the ScW used in the search for bursts from SGR 1806–20 used for comparison (red). The count rates have been corrected for the coding fraction (i.e., the fract from the source direction are modulated by the coded mask aperture pattern). Right: distribution of net ex FRB 20200120E (black) and for SGR 1806–20 (red).

Mereghetti et al. 2021

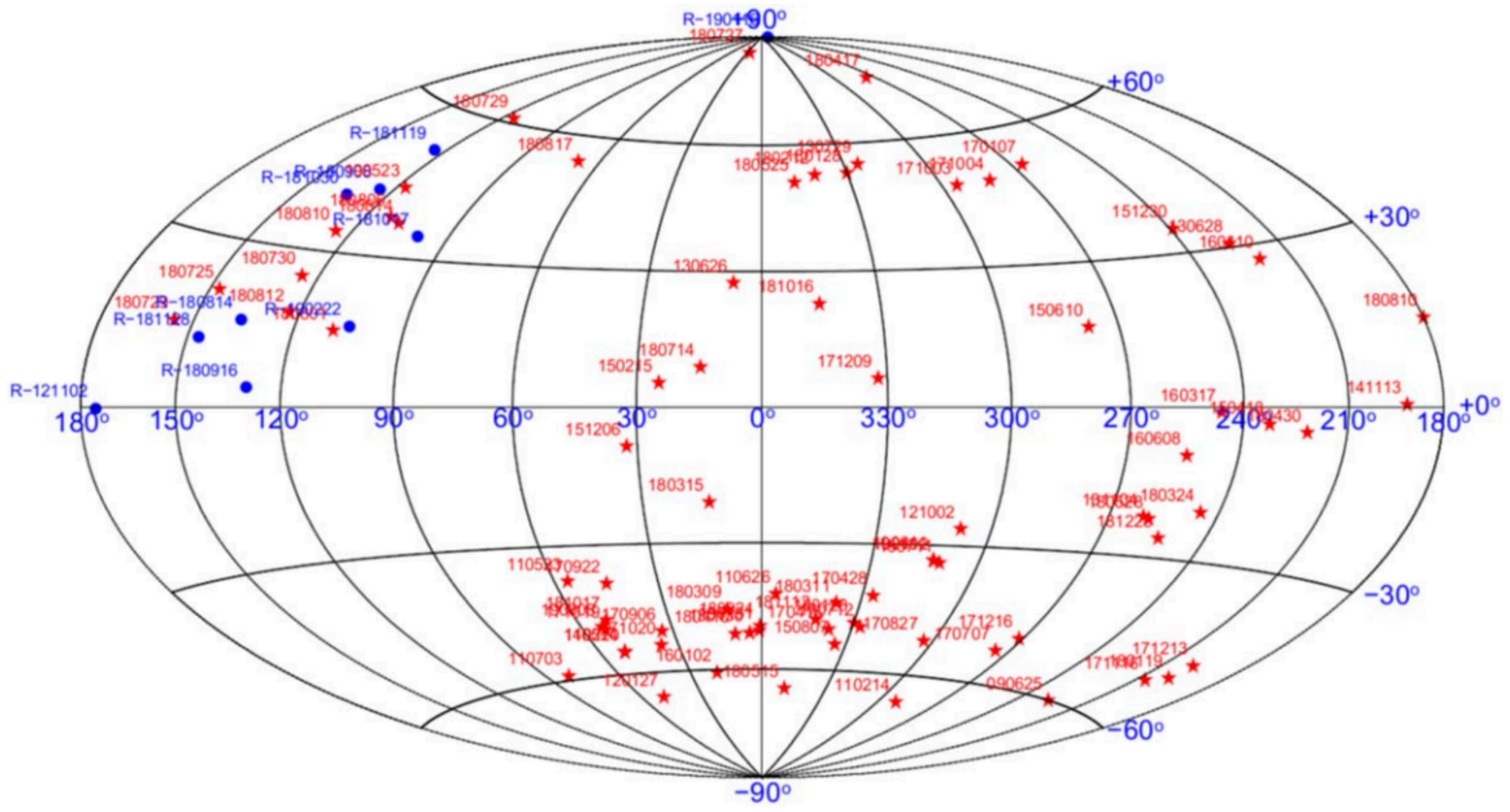

Figure 1. The Aitoff plot of the source positions (in Galactic coordinates) included in the FRB sample selected. Nonrepeating source positions are marked with red stars, while those of R-FRBs are marked with blue circles.

Verrecchia et al. 2021

Casentini et al. 2025

Archival X-ray and gamma-ray searches

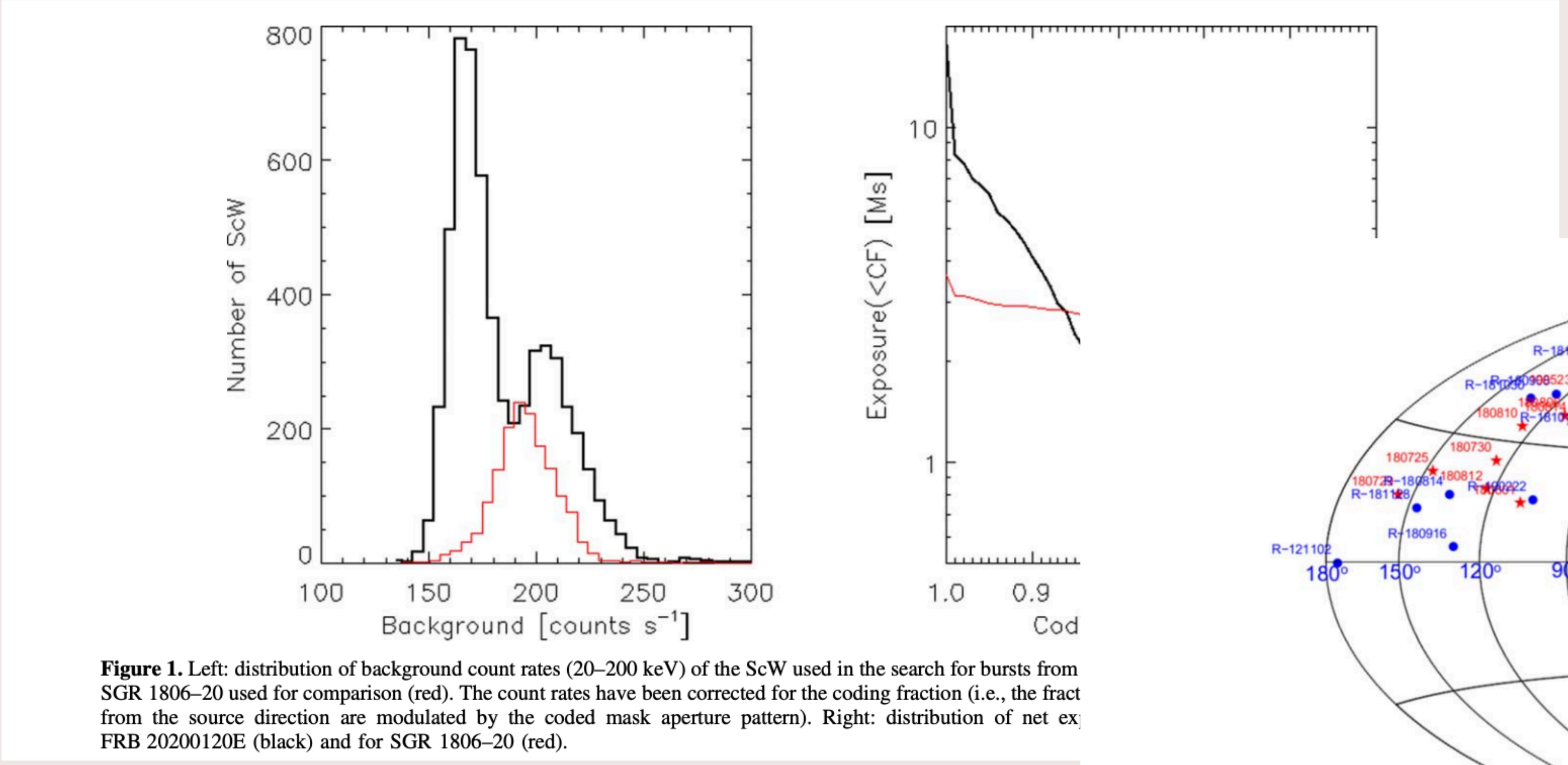

Mereghetti et al. 2021

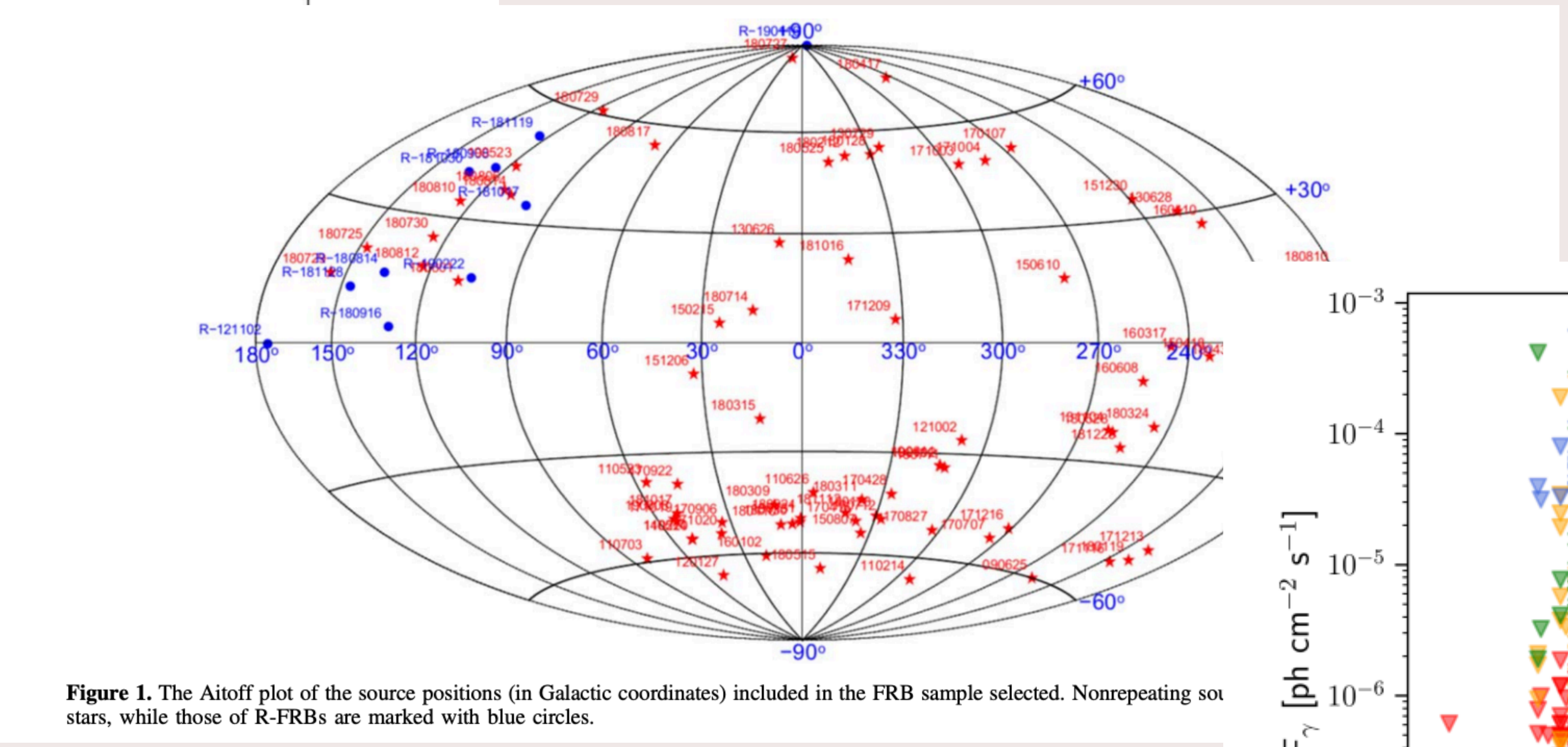

Verrecchia et al. 2021

Casentini et al. 2025

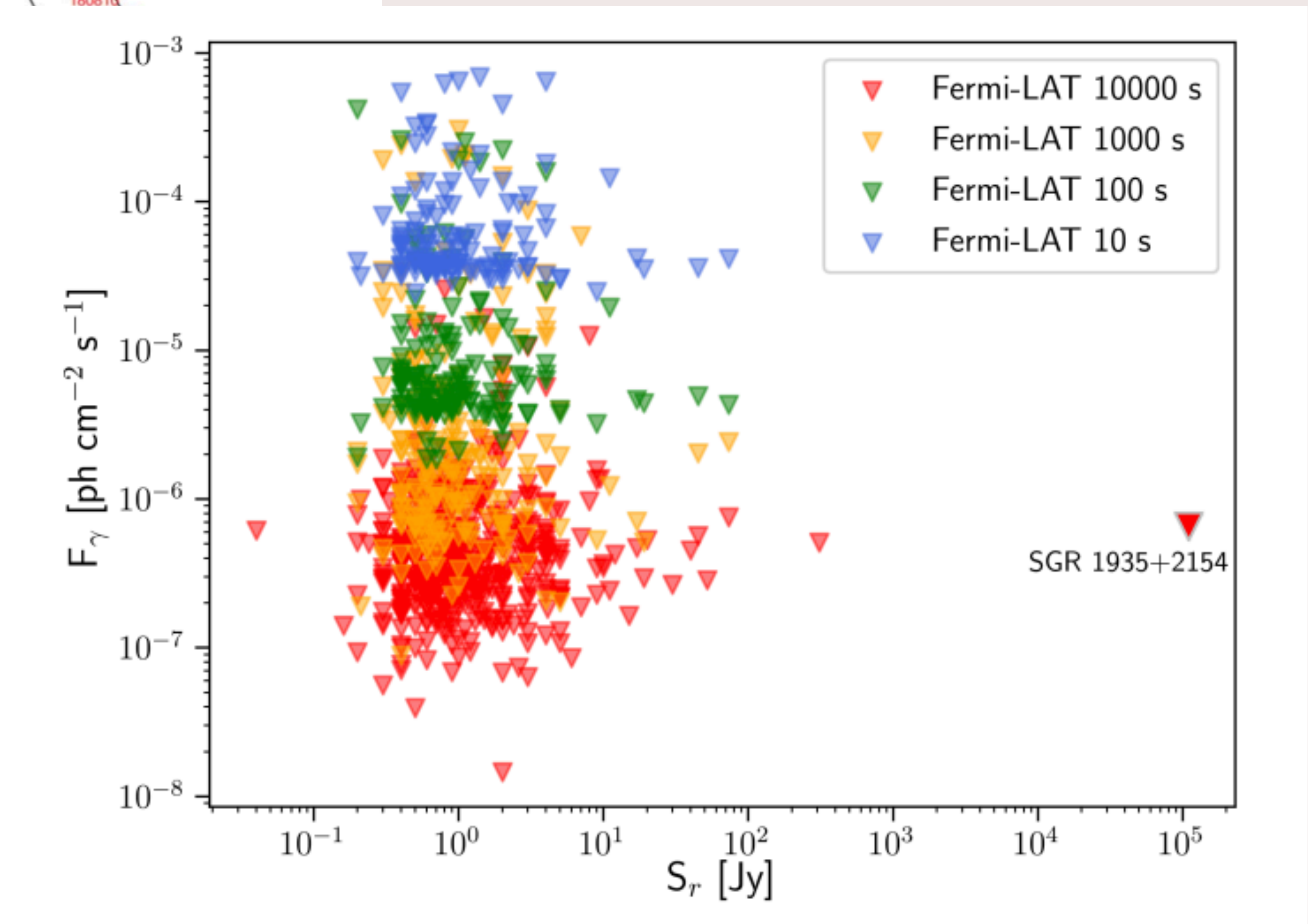

Principe et al. 2023

Archival X-ray and gamma-ray searches

- We have developed and demonstrated a technique to estimate η—the ratio between the energy emitted by the multiwavelength counterparts of FRBs and FRBs themselves— by combining existing multiwavelength fast transient surveys with the fluence distribution of the FRB population. The extremely large FOVs and observation durations of surveys from the optical to the TeV bands, combined with the high allsky rate of FRBs, mean that the locations of several FRBs undetected by radio telescopes have likely been observed by telescopes across the electromagnetic spectrum. We use the properties of several multiwavelength surveys (listed in Table 1) to constrain η under the assumption that no FRB counterparts have been detected and, in some cases, to estimate η under the assumption that all unclassified transient events are FRB counterparts

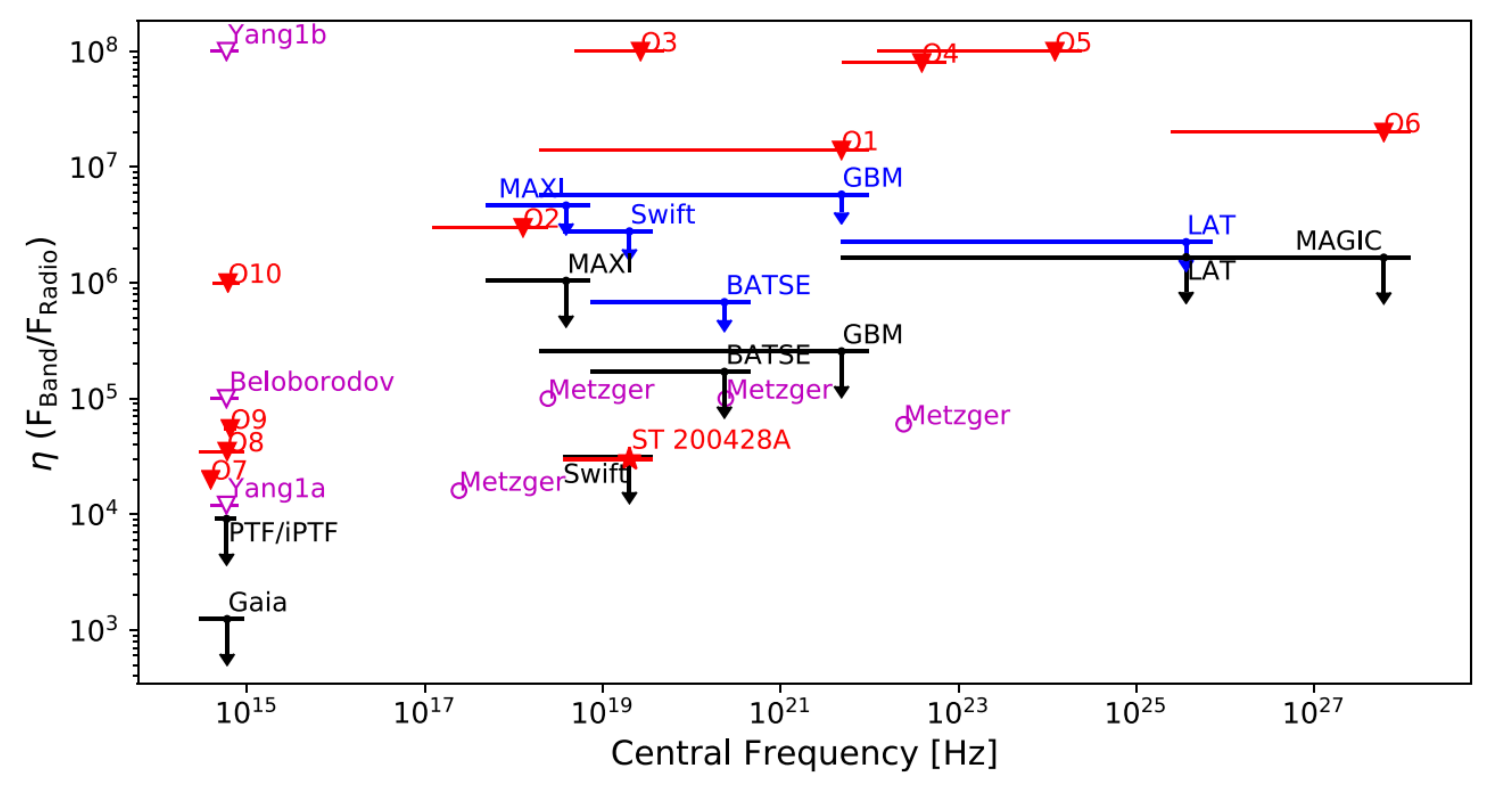

Chen, Ravi & Lu 2020

Optical searches

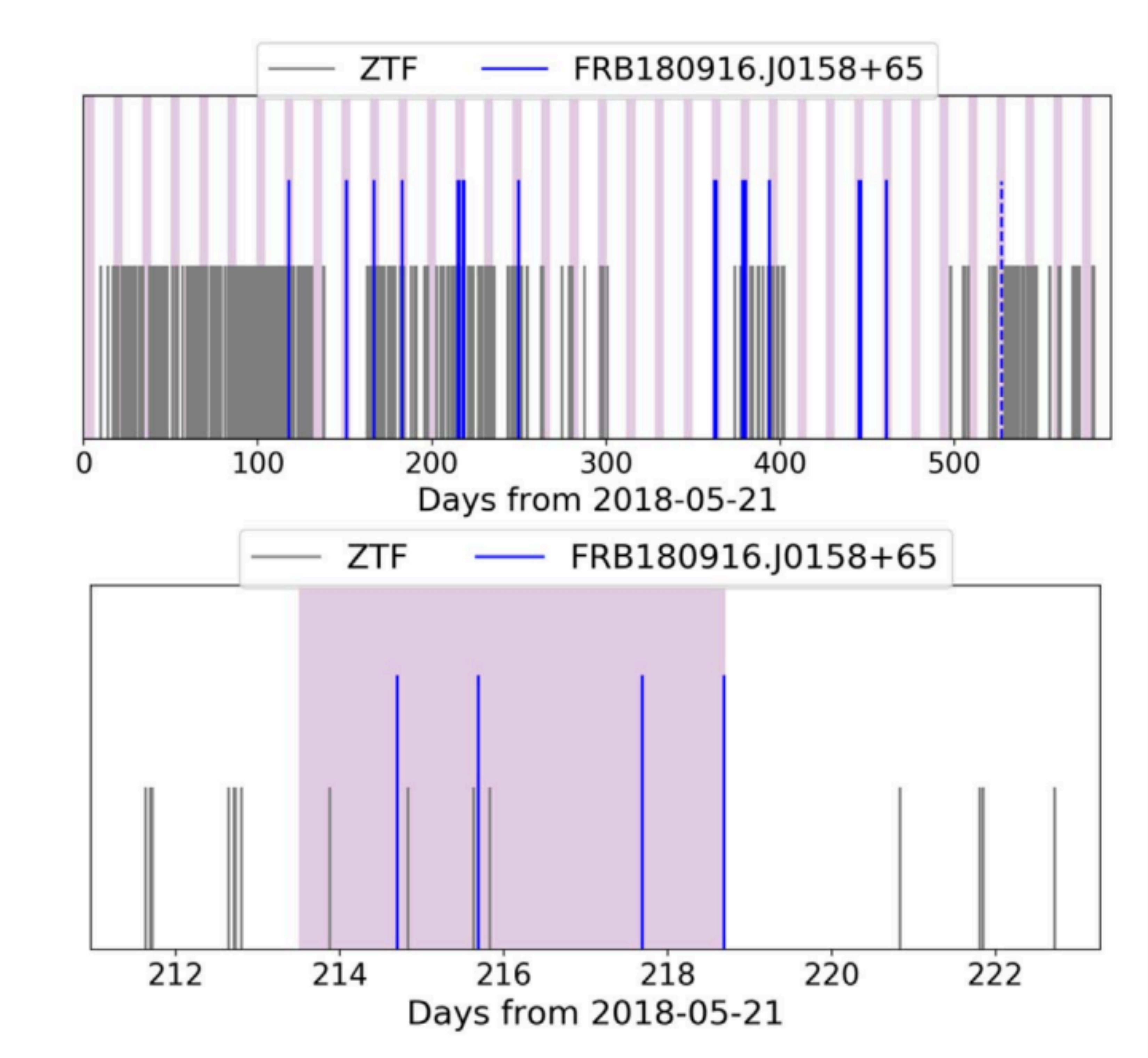

Andreoni et al. 2020

Counterparts

Afterglows

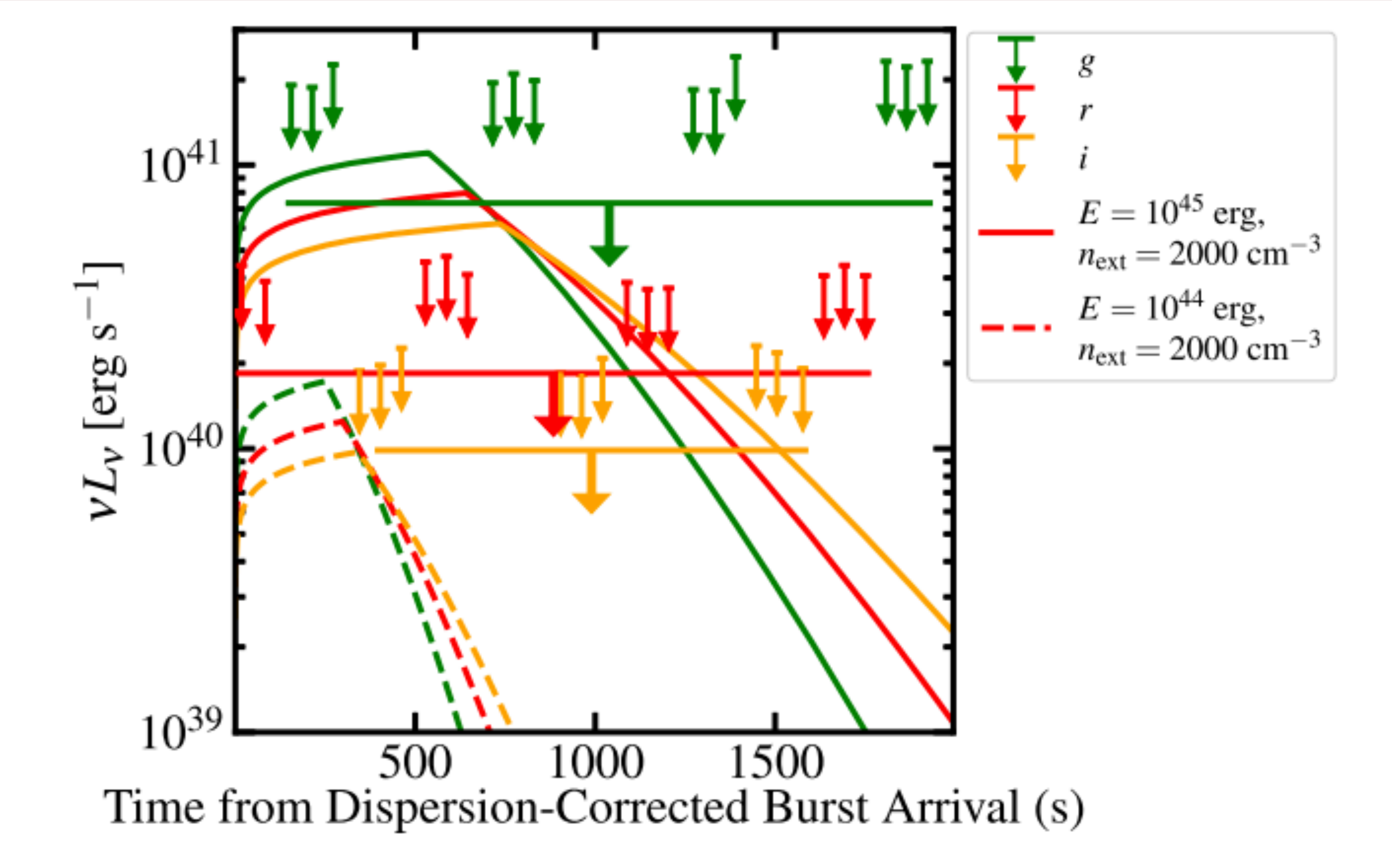

Kilpatrick et al. 2021

Gamma-ray bursts

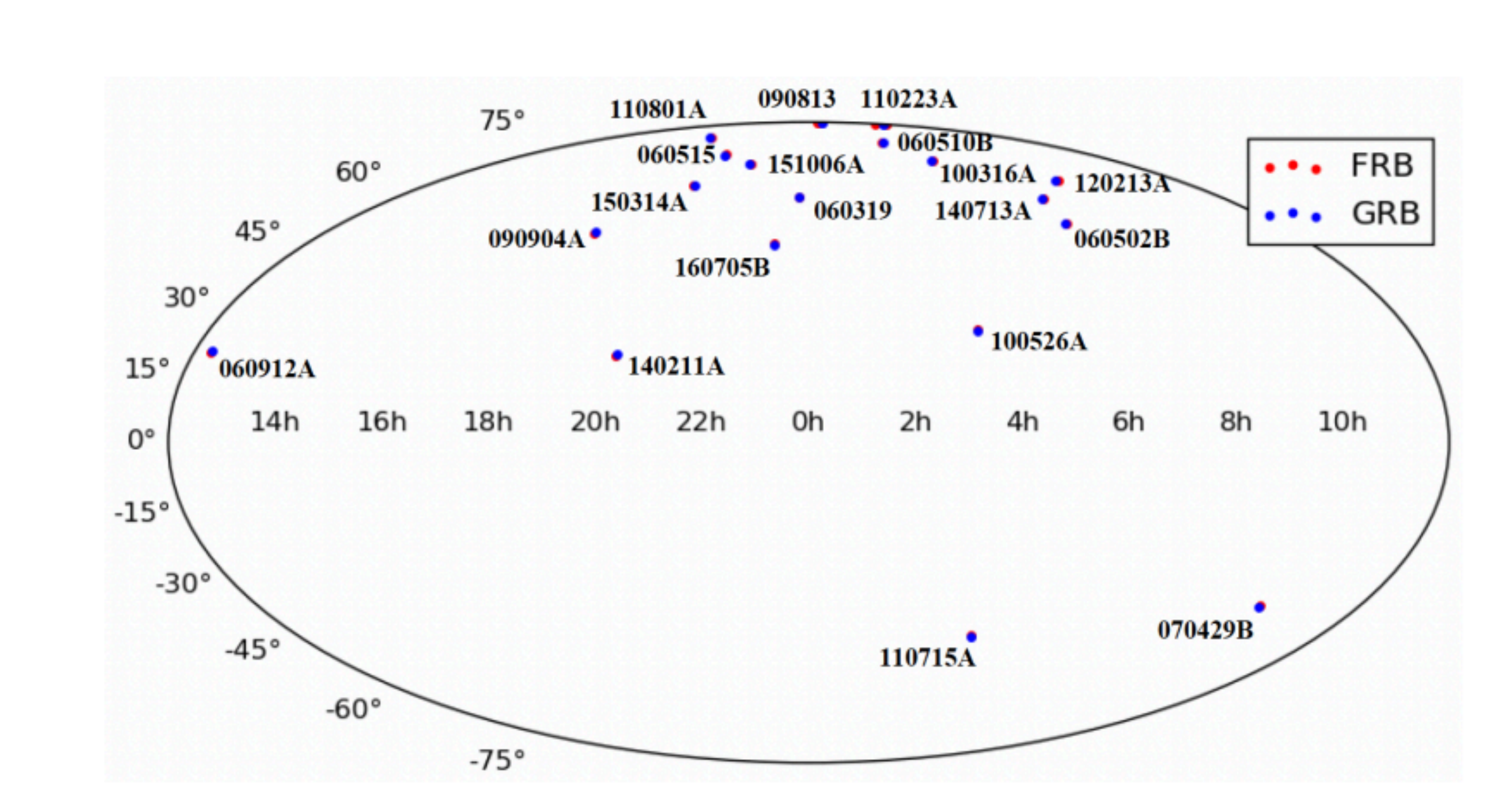

Patricelli, Bernardini. & Ferro 2024

Take home messages

What has worked

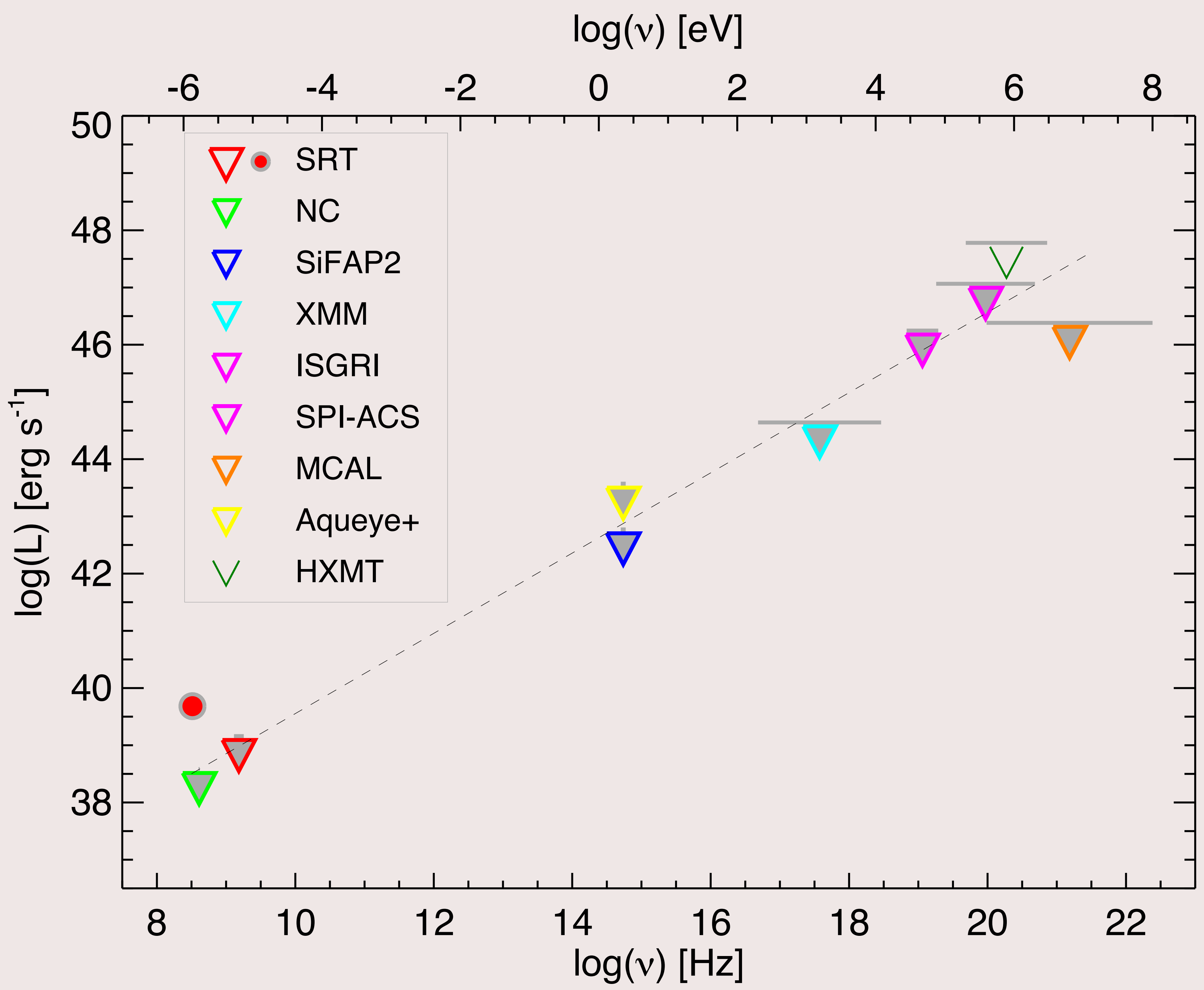

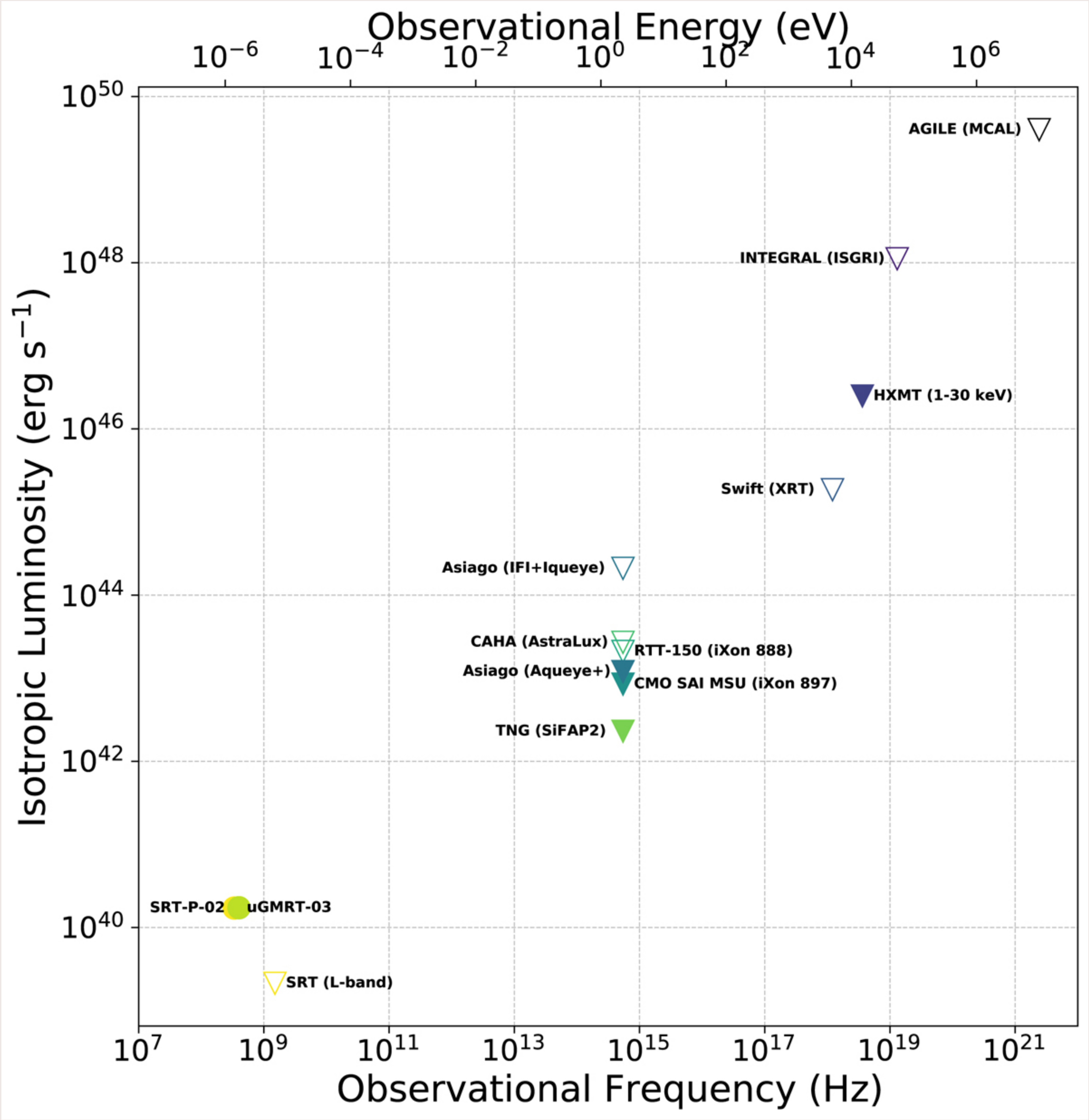

The challenges

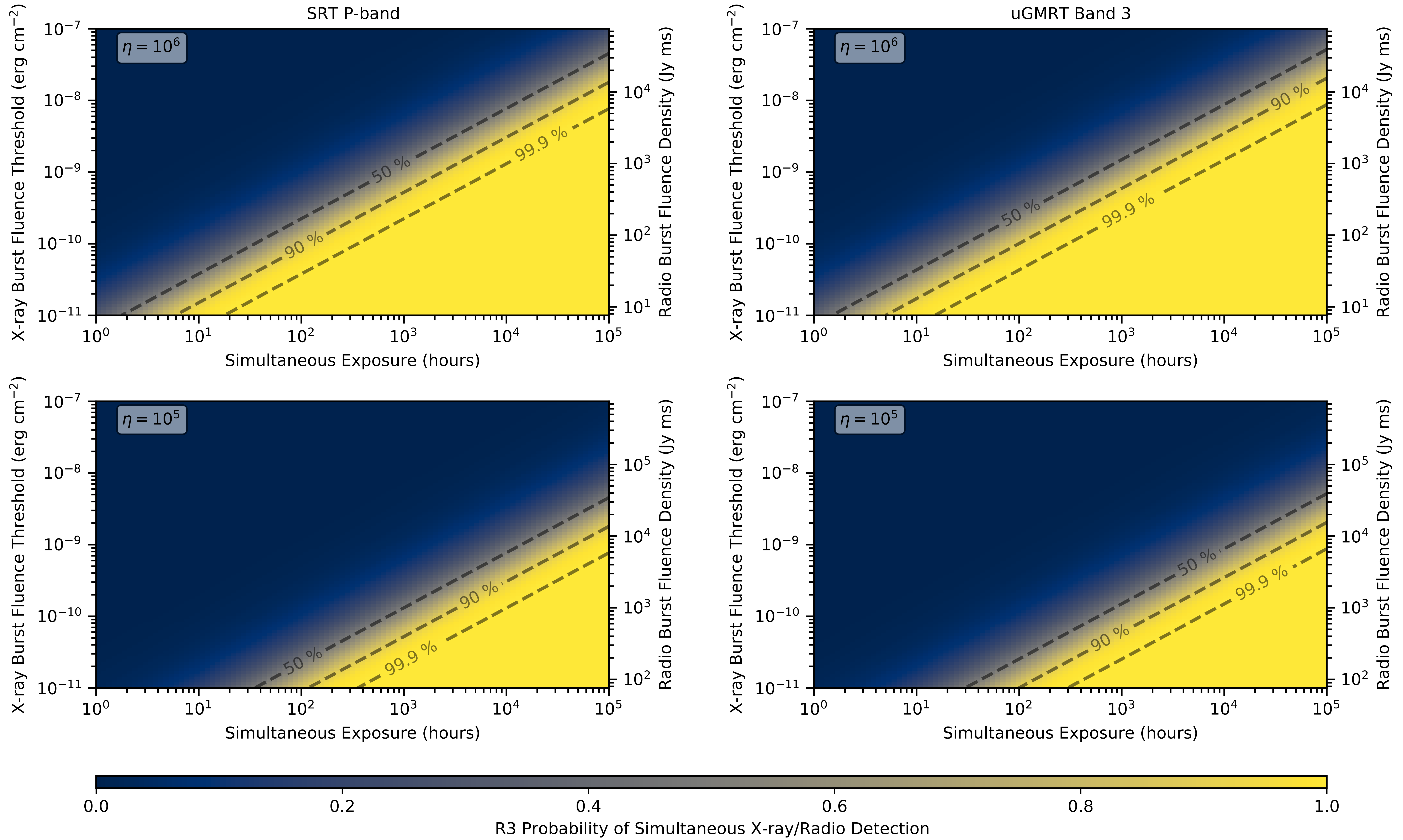

The best candidates

or lack thereof

Table 1
Properties of the R-FRBs Considered in This Work

FRB Name (1)	DM_{exc} (pc cm^{-3}) (2)	l, b (deg) (3)	N_b (4)	Width (ms) (5)	f (Jy ms) (6)	z_s (Mpc) (7)
FRB 20200120E	18.0 (88.0)	142°.19, +41°.22	80	0.01–0.70	0.04–2.40	0.0008 (3.6)
FRB 20181030A	33.5 (103.7)	133°.40, +40°.92	9	0.59–1.43	4.50–7.30	0.004 (17.3)
FRB 20220912A	67.1 (222.1)	155°.41, +61°.81	1529	0.09–32.9	0.002–37.7	0.077 (343)
FRB 20180814A	72.4 (189.4)	136°.42, +16°.60	22	7.90–63.0	3.40–66.0	0.078 (347)
FRB 20190107B	73.1 (173.1)	127°.14, +21°.75	2	0.98	4.30	0.11 (500)
FRB 20200223B	125.5 (201.5)	118°.07, −33°.88	10	1.26–2.29	1.06–14.4	…
FRB 20180908B	127.8 (195.8)	124°.74, +42°.86	4	1.60–9.00	1.10–2.90	0.17 (800)
FRB 20180916B	150.7 (349.4)	129°.71, +3°.74	290	0.06–158	0.08–318	0.033 (150)
FRB 20181226F	152.1 (240.1)	129°.79, +26°.20	3	…	…	…
FRB 20190905A	153.3 (240.4)	124°.64, +26°.25	6	0.75–1.13	1.79–18.0	…
FRB 20190110C	156.3 (222.0)	65°.56, +42°.15	3	2.95	1.40	0.22 (1050)
FRB 20190303A	164.1 (223.1)	97°.48, +68°.94	38	0.89–7.20	0.78–10.4	0.064 (285)
FRB 20190812A	170.7 (249.1)	78°.05, +29°.83	2	0.42–0.60	0.65–13.0	…
FRB 20201130A	202.3 (288.3)	185°.33, −29°.15	12	0.47–6.55	1.31–20.4	…
FRB 20210323C	204.7 (285.2)	142°.59, +31°.54	11	0.83–5.00	2.32–7.60	…
FRB 20191105B	210.3 (313.8)	140°.59, +20°.40	2	0.55–0.71	2.70–19.7	…
FRB 20190113A	217.6 (426.5)	218°.04, +3°.43	3	1.82–3.03	5.70–9.40	0.29 (1450)
FRB 20190907A	226.8 (309.8)	173°.39, +32°.26	7	0.54–3.00	0.70–6.90	…
FRB 20201114A	253.9 (321.9)	111°.18, +42°.63	2	0.72–1.04	2.45–4.70	…
FRB 20201124A	257.6 (414.1)	177°.60, −8°.50	2883	0.91–316	0.005–640	0.098 (445)
FRB 20200127B	267.0 (351.0)	126°.63, +28°.02	2	0.45–0.61	4.70–7.70	…

Note. Column (1) lists the names of the FRB sources. Column (2) provides DM_{exc}, with the mean DM_{tot} given in parentheses. Column (3) shows the Galactic coordinates of the sources in degrees. Column (4) N_b indicates the total number of bursts observed to date for each source. Columns (5) and (6) give for each source the minimum and maximum burst widths in milliseconds and the minimum and maximum radio fluence values in Jy ms, respectively. Column (7) lists the spectroscopic redshift z_s associated with each source (where available), with the estimated luminosity distance (D_L) in Mpc in parentheses.

The challenges

The challenges

The challenges

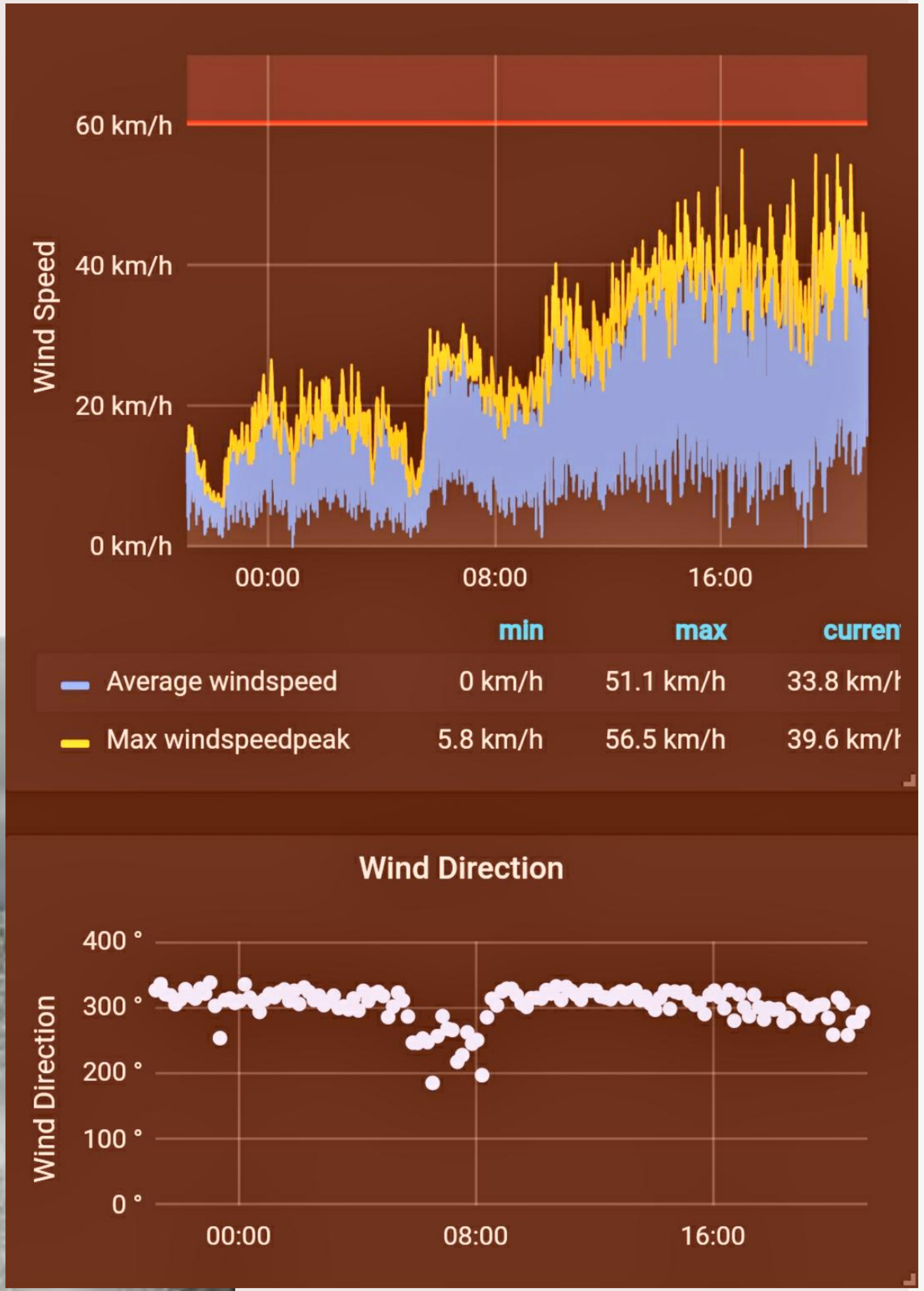

The challenges

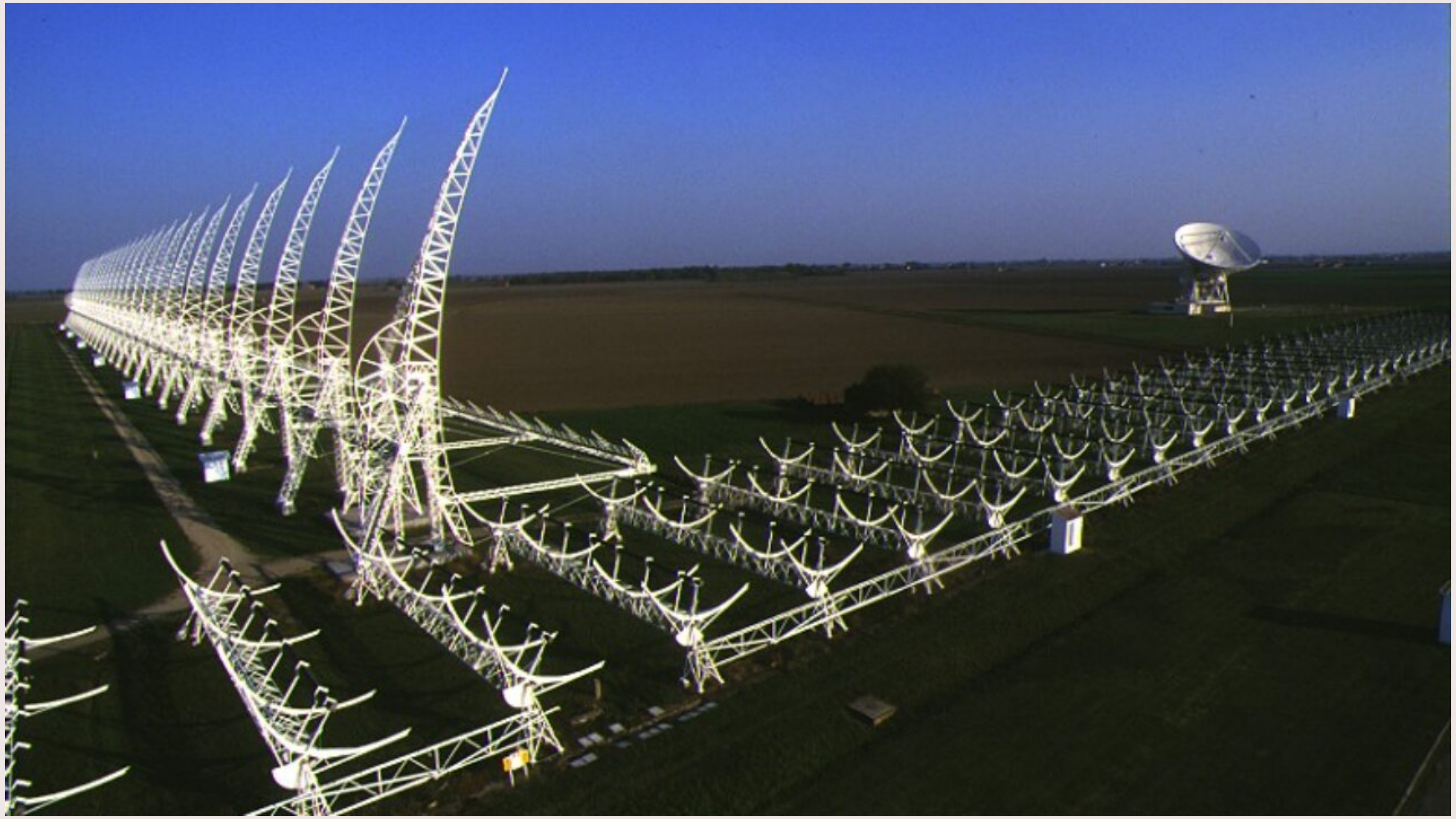

The challenges

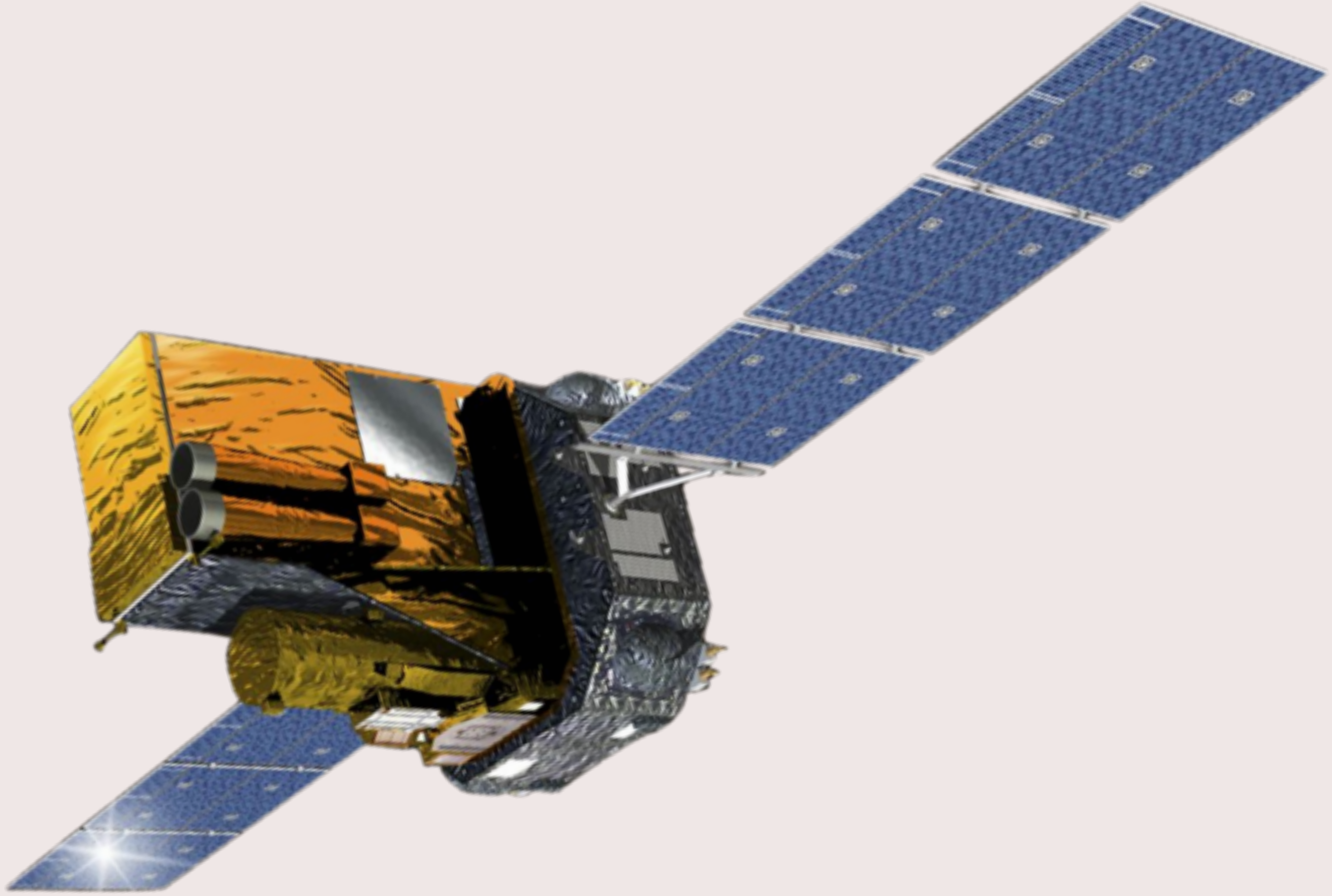

On a positive note..

Radio

On a positive note..

COMEFAR

Table 1. Facilities accessible from the participants to the project and type of usage.

	Facility	Receiver/Camera/Detector	Observation Type	Used for Goals
Radio	SRT-VLBI	0.3 / 1.4 / 7.0 / 18 GHz	Tracking-filterbank; VLBI	MWL Campaigns; Burst Detection. (I.1,I.2,II.1,III.1)
	Medicina-NC	0.408 GHz	Transit	Monitoring. (I.1,I.2)
	Medicina-VLBI	1.4 GHz	VLBI	VLBI Detection. (III.1)
	Noto-VLBI	1.4 GHz	VLBI	VLBI Detection. (III.1)
	EVN	5 GHZ	VLBI	VLBI Detection; PRS Characterization (III.1)
	e-Merlin	5 GHz	VLBI	PRS Characterization (III.1)
	ATCA	2.1 / 5.5 / 9 / 18 GHz	Local Interferometry	PRS Characterization (III.1)
	VLA	6 / 8 / 15 / 22 GHz	Local Interferometry	PRS Characterization (III.1)
	Parkes/MeerKAT/GMRT	0.3 / 0.8 / 1.4 GHz	Tracking-filterbank; Local Interferometry	Radio Characterization (I.1,I.2)
Optical/Infrared	Copernicus	Aqueye+	Fast-photometry	MWL campaigns; Burst detection (I.2, II.1)
	Galileo	IFI-Iqueye	Fast-photometry	MWL campaigns; Burst detection (I.2, II.1)
	TNG	SiFAP 2	Fast-photometry; Polarimetry	MWL campaigns; Burst detection (I.2, II.1)
	LBT	LBC/Lucifer/MODS	Multi-filter photometry; Spectroscopy	Deep photometry; Host Galaxy studies (II.1)
	CAHA-2.2	AstraLux	Fast-photometry	MWL campaigns; Burst detection (I.2, II.1)
	REM	ROS2/REMIR	Sub-s multi-filter monitoring	MWL campaigns (II.1)
	VST	OMEGACAM	Multi-filter; Deep photometry	MWL campaigns; Host galaxies photo-z (II.1)
	NTT	EFOSC2/SOX	Deep photometry; Spectroscopy	MWL campaigns; Burst detection (II.1)
	Schmidt 67/92	CCD	Wild field photometric monitoring; Calibration for fast-	MWL campaigns (II.1)
	Savelli	CCD	Multi-filter	Deep photometry; Host Galaxy studies (III.1)
	NOT	CCD	Multi-filter	Deep photometry; Host Galaxy studies (III.1)
	HST	WFC3/ACS	High spatial resolution	Photometry in crowded environments (III.1)
	JWST	NIRCAM	High spatial resolution	Photometry in crowded environments (III.1)
	ESO-VLT	MUSE (NFM)	IFU high spatial resolution spectroscopy	Spectroscopy in crowded environments (III.1)
X-Gamma	Insight-HXMT	LE / ME / HE	Event mode (timing accuracy < 10 μs)	MWL campaigns; Burst detection (I.2, II.1)
	AGILE	GRID / MCAL / SA	Event mode (MC 4 μs,GR 2 μs); ratemeters (MC/GR 1s, SA	MWL campaigns; Burst and persistent emission detection (I.2, II.1)
	INTEGRAL	IBIS/ISGRI/SPI-ACS/JEM-X	High time resolution (~10 ms) ISGRI lightcurve; Spectral	MWL campaigns; Burst and persistent emission detection (I.2, II.1)
	Swift	BAT / XRT / UVOT	Event mode (~ 2 ms)	MWL campaigns; Burst detection (I.2, II.1)
	XMM-Newton/Chandra/NICER	EPIC / ACIS / XTI	Soft X-ray imaging for spectral and timing studies	MWL campaigns; Burst detection (I.2, II.1)
	Fermi	LAT / GBM	FRB counterparts; High time resolution lightcurve (~ 1 ms)	MWL campaigns; Burst and persistent emission detection (I.2, II.1)

Legend: Italian Facility; International Facility; = Archival data; ✓= Accepted proposals; = Full-time accessibility; = Future proposals and ToO that build on previous successful proposals and well established international collaborations; = Guaranteed time for the Italian scientific community; = Members of our team are part of commissioning/developing teams; = Specific instrumentation developed by us and with granted time.

Thank you!